ACTIVE NEURO-ADAPTIVE CONTROL OF A SMART BEAM HAVING
UNCERTAINTIES IN STRUCTURAL DYNAMICS

A THESIS SUBMITTED TO
THE GRADUATE SCHOOL OF NATURAL AND APPLIED SCIENCES
OF
MIDDLE EAST TECHNICAL UNIVERSITY

BY

ONUR AKIN

IN PARTIAL FULFILLMENT OF THE REQUIREMENTS
FOR
THE DEGREE OF MASTER OF SCIENCE
IN
AEROSPACE ENGINEERING

SEPTEMBER 2015

Approval of the thesis:

ACTIVE NEURO-ADAPTIVE CONTROL OF A SMART BEAM HAVING UNCERTAINTIES IN STRUCTURAL DYNAMICS

submitted by **ONUR AKIN** in partial fulfillment of the requirements for the degree of **Master of Science in Aerospace Engineering Department, Middle East Technical University** by,

Prof. Dr. Gülbin Dural Ünver _____
Director, Graduate School of **Natural and Applied Sciences**

Prof. Dr. Ozan Tekinalp _____
Head of Department, **Aerospace Engineering**

Assoc. Prof. Dr. Melin Şahin _____
Supervisor, **Aerospace Engineering Dept., METU**

Examining Committee Members:

Prof. Dr. Yavuz Yaman _____
Aerospace Engineering Dept., METU

Assoc. Prof. Dr. Melin Şahin _____
Aerospace Engineering Dept., METU

Asst. Prof. Dr. Ercan Gürses _____
Aerospace Engineering Dept., METU

Asst. Prof. Dr. Ali Türker Kutay _____
Aerospace Engineering Dept., METU

Prof. Dr. Metin Uymaz Salamcı _____
Mechanical Engineering Dept., Gazi University

Date: 02.09.2015

I hereby declare that all the information in this document has been obtained and presented in accordance with academic rules and ethical conduct. I also declare that, as required by these rules and conduct, I have fully cited and referenced all material and results that are not original to this work.

Name, Last Name:

Signature:

ABSTRACT

**ACTIVE NEURO-ADAPTIVE CONTROL OF A SMART BEAM HAVING
UNCERTAINTIES IN STRUCTURAL DYNAMICS**

Akın, Onur

M.S., Department of Aerospace Engineering

Supervisor: Assoc. Prof. Dr. Melin Şahin

September 2015, 102 pages

In this thesis, an active vibration suppression of a smart beam having piezoelectric sensor and actuators is investigated by designing separate controllers comprising a linear quadratic regulator and a neural network.

At first, design of a smart beam which consists of a cantilever aluminum beam with surface bonded piezoelectric patches and a designed mechanism having a micro servomotor with a mass attached arm for obtaining variations in the frequency response function are presented. Secondly, the frequency response functions of the smart beam are investigated experimentally by using different piezoelectric patch combinations and the analytical models of the smart beam around its first resonance frequency region for various servomotor arm angle configurations are also obtained. Then, a linear quadratic regulator controller is designed and used to simulate the suppression of free and forced vibrations which are performed both in time and frequency domain. Parallel to simulations, experiments are conducted to observe the closed loop behavior of the smart beam and the results are compared as well. Finally, active vibration suppression of the smart beam is investigated by using a linear

controller with a neural network based adaptive element which is designed for the purpose of overcoming the undesired consequences due to variations in the real system.

This thesis study shows that sufficient vibration suppression levels are reached in the smart beam structure through linear quadratic regulator and an artificial neural network based control algorithms via piezoelectric sensor and actuators in the cases where there are some variations in the frequency response function of the structure around its first resonance frequency region.

Keywords: Vibration Suppression, System Identification, Piezoelectric Patch, Linear Quadratic Regulator, Artificial Neural Network

ÖZ

YAPISAL DİNAMİK ÖZELLİKLERİ BELİRSİZLİKLER İÇEREN AKILLI BİR KİRİŞİN YAPAY SİNİR AĞI TABANLI ADAPTİF AKTİF KONTROLÜ

Akın, Onur

Yüksek Lisans, Havacılık ve Uzay Mühendisliği

Tez Yöneticisi: Assoc. Prof. Dr. Melin Şahin

Eylül 2015, 102 sayfa

Bu çalışmada, piezoelektrik algılayıcı ve uyarıcılara sahip akıllı bir kirişin titreşimlerinin aktif olarak sönümlenmesi doğrusal karesel düzenleyici ve bir sinir ağı yöntemi kullanılarak tasarlanmış denetçiler vasıtasıyla araştırılmıştır.

İlk olarak, yüzeyine piezoelektrik yamalar yapıştırılmış ve frekans yanıt fonksiyonlarının değişimi için kütle bağlanmış kollu bir mikro servo motora sahip düzeneği de içeren, tek ucu tutturulmuş ve diğer ucu serbest olan alüminyum kirişten oluşan akıllı bir kirişin tasarımı yapılmıştır. İkinci olarak, farklı piezoelektrik yama kombinasyonları kullanılarak akıllı kirişin frekans yanıt fonksiyonları deneysel olarak araştırılmıştır ve kirişin farklı servo motor kol açıları durumlarında birinci rezonans frekans bölgesindeki analitik modelleri, deneysel olarak bulunan freakans yanıt fonksiyonları da kullanılarak elde edilmiştir. Akabinde, serbest ve zorlanmış titreşimlerin bastırılması benzetimlerinde kullanılmak üzere, doğrusal karesel düzenleyici kullanan bir denetçi tasarlanmış ve analizler hem zaman hem de frekans alanında gerçekleştirilmiştir. Bu benzetimlere paralel olarak, akıllı kirişin kapalı döngü davranışlarının gözlenmesi için ayrıca deneyler yapılmış ve elde edilen sonuçlar benzetimlerle de karşılaştırılmıştır. Son olarak, gerçek sistemdeki değişimler

nedeniyle oluşan istenmeyen sonuçların üstesinden gelme amaçlı tasarlanmış sinir ağı temelli uyarlanabilir elemanlı doğrusal denetçi ile akıllı kirişin titreşimlerinin sönümlenmesi araştırılmıştır.

Sonuç olarak bu tez çalışması, piezoelektrik algılayıcı ve uyarıcılar içeren akıllı bir kirişin ilk rezonans frekansı etrafındaki frekans yanıt fonksiyonlarında meydana gelen değişimlerinde olduğu durumlardaki titreşimlerinin doğrusal karesel düzenleyici ve yapay sinir ağları temelli denetleyiciler yardımı ile yeterli ölçüde bastırılmasının mümkün olduğunu göstermiştir.

Anahtar Kelimeler: Titreşim Bastırılması, Sistem Modellenmesi, Piezoelektrik Yama, Doğrusal Karesel Düzenleyici, Yapay Sinir Ağları

To My Parents

ACKNOWLEDGEMENTS

TABLE OF CONTENTS

LIST OF TABLES

CHAPTER 1

INTRODUCTION

Vibration is an oscillatory motion around an equilibrium point and it can be divided into two categories. One is desirable vibration like musical instruments, mobile phones, etc. and the other one is undesirable like engine noise, earthquake, etc. Suppression of undesirable vibrations is important because these vibrations can cause flutter, noise, structural failure, damage of equipment and even damage to human body. Suppression of vibrations are widely used in many applications such as in cars [1], hard disc drives [2], telescopes [3], railway vehicles [4], marine applications [5].

Nowadays, being more lightweight, flexible and stiffer has the key importance in design of aerospace structures. But, these criteria lead unwanted oscillatory behavior in case of exposing dynamic loads and this affects the performance and the service life of the structure in a negative way. Other negative effects that occur due to vibration of the aerospace structures are pollution created by the propulsion systems, low fuel efficiency because of increasing drag, less accuracy in satellite applications, unwanted effects on cabin crew and hardware of the aerospace vehicles. Hence, a suitable control mechanism is required to reduce the vibrations in order to preserve structural integrity.

Two types of vibrations namely free and forced exist. Free vibration occurs when a system is moved out of its equilibrium position and then left free to vibrate on its own. Without damping, the system will vibrate indefinitely. However, energy of the system is dissipated and the system returns to its equilibrium position with damping. On the other hand, forced vibration occurs when a force applied to the system continuously at various frequencies which means adding energy to the system. If this energy is not

dissipated by the damper, the vibration becomes greater and may cause a damage on the structure.

In order to suppress vibrations of a structure, either passive or active techniques are used. Passive technique generally uses dampers, masses and springs in order to reduce the structural noise and/or vibrations [6]. But, usage of a passive technique is inefficient below 200 Hz and it increases weight of the structure which is an undesirable solution for the light weight aerospace structures [7]. Active technique has been widely investigated and applied by the engineers for decades. An active structure can sense external disturbances through sensors via transforming mechanical energy to electrical energy and it also has actuators to be excited for obtaining desirable behavior of the structure by transforming electrical energy to mechanical energy. Adding a controller between the sensors and actuators makes the structure controllable actively and this structure is called as a smart structure. In order to control the structure for decided performance criteria, a good analytical model of a smart structure is required. It is possible to obtain this model by using either system identification techniques experimentally or modelling it on a computer platform numerically through simulations.

Recent technological developments on smart materials allow engineers to use them effectively in vibration suppression field. One of them is piezoelectric materials which offer cost effective solutions in the active vibration suppression of structures due to their usage both as actuators and sensors.

Various fixed controllers are designed by using the obtained analytical model of the structures. They are effective solution for the vibration suppression of the modelled structure. However, the frequency response function (FRF) of the structure may change due to various structural changes in structures (i.e. crack, boundary condition, variations in mass and stiffness properties, etc.). In order to make the controller robust, these variations that can occur in the structure are needed to be taken into consideration. Another solution to handle the variation in dynamic characteristics of the structure is making the controller adaptive.

2

1.1 Background of the Study

In this section, first, smarts materials and structures are defined. Then, piezoelectricity and piezoelectric materials are explained. Following that active vibration control strategies are described. Finally, the research studies on smart structure applications performed in the Department of Aerospace Engineering at METU are presented.

1.1.1 Smart Materials and Structures

Smart materials are defined as materials that can sense variations in their environment and respond to those variations. The response may present itself as a change in color, change in volume, change in viscosity etc. in the effect of change in temperature, stress, magnetic field and electrical current. There are several types of smart materials used in variety of technological applications. Piezoelectric materials, shape memory alloys and polymers, magneto-rheological and electro-rheological materials, magnetostrictive materials are examples of the smart materials [8].

A smart structure consists of passive structure, some form of sensor and actuator which may be made of from smart materials embedded or surface bonded and a controller unit. The smart structure senses its environment and sends information to the control hardware system and then the control system applies required signals to the structure by actuators to get a desired change or response of the structure. As an example, the smart structure might be an aircraft wing that changes its shape during flight to increase the aerodynamic efficiency for different flight conditions. In this study, the smart structure is a smart beam and the aim of this smart structure is to suppress its vibrations at the fundamental resonance frequency.

1.1.2 Piezoelectric Materials

Piezoelectric materials are popular smart materials that are used in the field of smart structures. The piezoelectric materials generate voltage in case of exposing mechanical deformation. Reversely, they exhibit deformation when an electric field is applied.

Therefore, they can be used both as sensors and actuators in smart structures. The main advantages of the piezoelectric materials is the almost instantaneous generation of an electrical charge or change in shape.

Generation of electrical charge which is a result of applying mechanical force is called as direct piezoelectric effect. The direct piezoelectric effect first discovered by Jacques and Pierre Curie who conducted experiments using specially prepared crystals (tourmaline, quartz, topaz, cane sugar and Rochelle salt) in 1880. Their experiment consisted of a conclusive measurement of surface charges appearing on the crystals which were subjected to mechanical stress. However the Curies did not predict the converse piezoelectric effect (creating stress as a response to applied electric field). The property was mathematically deduced from fundamental thermodynamic principles by Gabriel Lippmann in 1881 [9]. Details of the direct and converse piezoelectric effect are given in Figure 1.1.
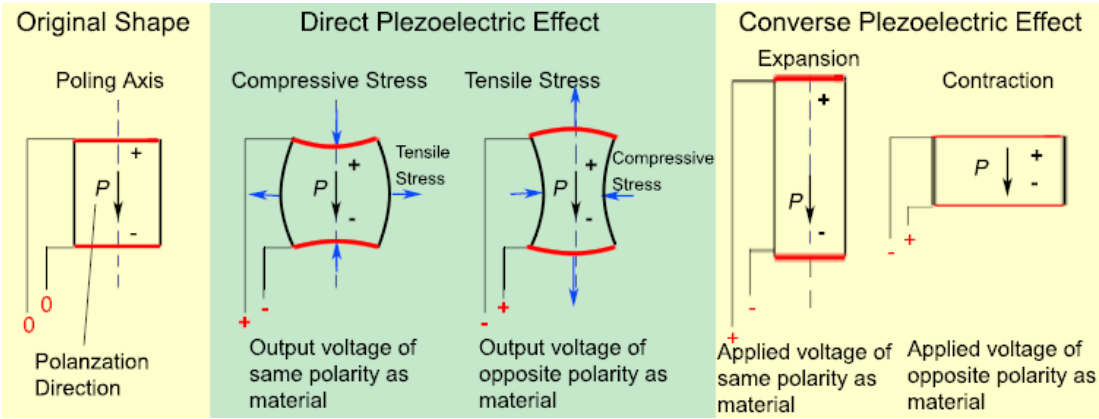
Figure 1.1 Direct and Converse Piezoelectric Effect [10]

Features of the piezoelectric materials make them an effective solution to many applications. Some important features can be listed as follows [11]:

- They have very fast response with high bandwidth.
- They are cheap and commercially available.
- They can be bonded on a surface or embedded into a structure.
- They can be shaped to sense and control individual flexural modes.
- Piezoelectric sensors can be used for both strain and strain rate measurements.

The most popular piezoelectric materials used in vibration control are PZT (Lead-Zirconate-Titanate) and PVDF (Polyvinylidene Fluoride) [12]. PZT is a ceramic and PVDF which is more flexible than PZT and actually is a polymer. There are several forms of piezoelectric materials such as patch, stack, tube and motor.

Piezoelectric materials are used in several applications such as precise frequency control, passive signal processing for wireless communication, identification, sonic alerts, telephone, blood pressure, medical diagnostics, sources and detectors for sound location, cleaning, humidifiers, micro pumps, etc. [13]. As an example in aerospace structure field, the smart material actuated rotor technology can be given. Tests were demonstrated on smart material control of flaps on a full scale rotor in a wind tunnel (Figure 1.2 where rotor, blade and flap are shown) and the effectiveness of the active flap control on noise and vibration was conclusively demonstrated [14].

Figure 1.2 The Smart Rotor, Blade, and Flap in the Tunnel [14]

Consequently, having the capability of usage both ways, suitable features and lightweight of the piezoelectric materials, they are considered to be convenient materials for smart structure applications. In this thesis study, PZT patches are used as surface bonded sensors and actuators.

1.1.3 Active Vibration Control Strategies

The active vibration control has been used as a solution for vibration problems of aerospace structures for decades. Using piezoelectric materials as smart materials to suppress the vibration of a structure is an effective approach. For active vibration of structures, various control strategies have been developed. The research on active vibration suppression of structures was started using piezoelectric materials as sensors and actuators by Bailey and Hubbard [15]. They performed an experiment of the active vibration control on a cantilever beam using constant-gain and constant-amplitude controllers. Crawley and Luis [16] presented a study about interaction between bonded piezoelectric elements and the substructure. They made tests on the first mode of the cantilever beam with distributed piezoelectric elements and with three different test specimens. Fanson and Caughey [17] implemented a positive position feedback (PPF) controller to control the first six bending modes of a cantilever beam by using piezoelectric materials for actuators and sensors. In addition to positive position feedback (PPF) control, Song, Schmidt and Agrawal [18] implemented strain rate feedback (SRF) control and their combinations. Manning, Plummer, and Levesley [19] designed a controller using pole placement to achieve a desired closed loop response and compared it with the velocity feedback controller. Calıskan [20] developed PID and H_∞ controller to suppress the vibration of a cantilever beam and a fin successfully. Singh et al. [21] implemented a controllers based on a method which is an extension of modified independent space control and compared it with the existing methods of independent modal space control (IMSC) and modified independent modal space control (MIMSC). Sahin et al. [22] presented studies with H_∞ and μ-synthesis controllers which are intended to be used in the suppression of free and forced vibrations of the smart structures. In addition to these a sliding mode control (SMC) is also conducted [23]. Vasques and Rodrigues [24] implemented optimal control strategies, linear quadratic regulator (LQR), linear quadratic Gaussian (LQG) and compared them with the classical control strategies having constant gain and amplitude velocity feedback. There are studies which also include novel control algorithms used in vibration suppression field as genetic algorithm [25], fuzzy logic [26], and neural network [27].

1.1.4 Research Studies on Smart Structure Applications in Department of Aerospace Engineering at METU

In the Department of Aerospace Engineering at Middle East Technical University, studies are performed to obtain modal characteristics and to control vibrations of structures actively [22]. In these studies, an aluminium cantilever beam and one side clamped plate are used. In theoretical studies, in order to determine locations of the piezoelectric patches and to investigate the static and dynamic behaviors of the structures, finite element method is used and the models of the structures are obtained [20]. In experimental studies, model of the system is determined either by using laser displacement measurement device or strain gages. It is also shown that piezoelectric patches can be used effectively together with the H_∞ controller in vibration suppression of a smart beam [28,29,30]. A similar study is conducted for a plate [31]. In another study, suppression of vibrations of a smart beam is performed successfully by using μ-synthesis method [32].Various studies are also performed for active vibration control of a smart beam by using a spatial approach [33,34,35]. It is shown that this approach is effective on the first two out of plane bending vibrations.

The purpose of all these studies is to suppress both free and forced vibrations. In these studies, piezoelectric patches are used as actuators and laser displacement measurement device and strain gages are used as sensor [22]. In a later study [30], active vibration suppression is performed by using piezoelectric patches both as sensors and actuators and effectiveness of usage of piezoelectric patches is shown.

Various controllers are designed to suppress vibrations of a smart beam in the Department of Aerospace Engineering at METU. The designed controllers are tested and performances of the controllers are observed. These controllers are: Proportional-Integral-Derivative (PID) [36], Linear Quadratic Gaussian (LQG) [37], Continued Fractional Expansion (CFE) [38],[39], and Linear Quadratic Regulator (LQR) [40]. In addition to these, response of the system by changing mass of the smart beam using Linear Parameter Varying (LPV) controller is also investigated [41].

1.2 Motivation to the Study

Having motivated from the previous research studies, in this particular thesis, a mass variation mechanism is designed and implemented on a smart beam and for a particular mass location, a controller is designed by using Linear Quadratic Regulator. Performance of the designed controller is investigated and effect of variation of the mass on the smart beam is also observed. By designing a neural network based adaptive element, vibration of the smart beam at the fundamental resonance frequency is suppressed even if there is variation between reference model and real system.

1.3 Limitations of the Study

The following list presents the limitations of the study.
- Nonlinear characteristics of piezoelectric patches and their hysteresis effects are neglected.
- The boundary condition of the smart beam is considered to be perfectly fixed.
- Bonding between the PZT patches and the beam is assumed to be perfect and they are structurally fully coupled.
- The frequency range of interest covers only the first out-of-plane bending mode of the smart beam with different arm angle configurations.

1.4 Objectives of the Study

The objectives of the thesis is listed as follows:
- Placement of piezoelectric patches on aluminum beam as actuator/sensor.
- Design of a mass variation mechanism for the smart beam.
- Describing a closed loop experimental setup.
- Investigation of the resonance frequencies of the smart beam at different servomotor arm angle configurations.
- Obtaining frequency response functions of the smart beam with different cases experimentally.

- Obtaining analytical models by using obtained frequency response functions for five different arm angles of the smart beam and a particular sensor-actuator pairs.

- Design of controllers by using Linear Quadratic Regulator (LQR) method.

- Performance evaluation of the controllers for free and forced vibration on a simulation platform.

- Conducting an experiment for the best controller for free and forced vibration suppression.

- Performance evaluation of the controller experimentally.

- Design of an artificial neural network Simulink block.

- Conducting simulations and experiments of the neural network based closed loop design.

1.5 Outline of the Study

In Chapter 2, design of a smart beam which consists of a passive cantilever beam and a mechanism built at the tip of the beam is presented. Details of the smart beam and the hardware and software of the mass variation system are described. Then, the detailed description of the experimental setup is presented.

In Chapter 3, FRFs of the smart beam are investigated by using the piezoelectric patches and the variation of the FRFs are observed by changing the servomotor arm to particular angles. Then, analytical models of the smart beam for different arm angle cases are obtained in the frequency range covering the first resonance frequency by using the experimentally obtained FRFs.

Chapter 4 presents a controller designed by using Linear Quadratic Regulator method to be used in free and forced vibration suppression simulations. Analyses are performed both in time and frequency domain. Then, the controller is adjusted to be used experimentally by transforming it to discrete transfer function. Furthermore, experiments are conducted to observe the closed loop behavior of the smart beam for free and forced vibrations in time domain. The closed loop FRF is obtained

experimentally and compared with the simulation result. The effect of the plant variation on the closed loop system behavior is also investigated.

In Chapter 5, design of a multilayer feedforward neural network with back propagation algorithm is described and a neural network based adaptive element is built and trained. After this, forced and free vibration simulations are investigated to observe the behavior of the closed loop system in case of a plant variation. Moreover, forced and free vibration suppressions of the plant is also achieved experimentally.

Chapter 6 presents the general conclusions and the future work of this research study.

CHAPTER 2

DESIGN OF THE SMART BEAM AND EXPERIMENTAL SETUP

2.1 Introduction

In this chapter, design of a smart beam and experimental setup are presented. The smart beam consists of a cantilever beam and a mechanism built at the tip side. At first, details of the cantilever beam which is made of aluminum and bonded with four piezoelectric patches are described. Then, hardware and software designs of the mechanism which has a micro digital servomotor with a mass attached arm, are explained. Finally, detailed description of the experimental setup is presented.

2.2 Cantilever Beam with Piezoelectric Patches

A beam made of aluminium is used as the passive structure of the smart beam. The aluminum beam has dimensions of 35 [cm] x 3 [cm] with a thickness of 2 [mm]. At one end, the beam is clamped from 5 [cm] which makes the length of the vibrating part of the beam 30 [cm]. Sensor Technology BM500 (PZT - Lead Zirconate Titanate) which is shown in Figure 2.1 is used as the piezoelectric patch. It has dimensions of 25.37 [mm] x 25.38 [mm] with a thickness of 0.57 [mm].

Figure 2.1 Sensor Technology BMP500 (PZT - Lead Zirconate Titanate)

In order to use the piezoelectric patches independently, insulation between aluminium and the piezoelectric patches is needed. The aluminum beam used in this research was grey anodized in production. So, a good insulation layer was provided by this process. The dimensions of the clamped cantilever beam with bonded piezoelectric patches are shown in Figure 2.2. Four piezoelectric patches are bonded on the beam. Two of them are on the front surface, the other two are on the back surface with the same distances from the fixed boundary. The piezoelectric patches are labelled as follows; piezo actuators (named and numbered as A1 & A2), a sensor piezo (named as S), a disturbance piezo (named as D). On the front surface; the piezoelectric patch on the root side is (A1), the other one is (S) and on the back surface; the piezoelectric patch on the root side is (A2) and the other one is (D) as shown in Figure 2.3.
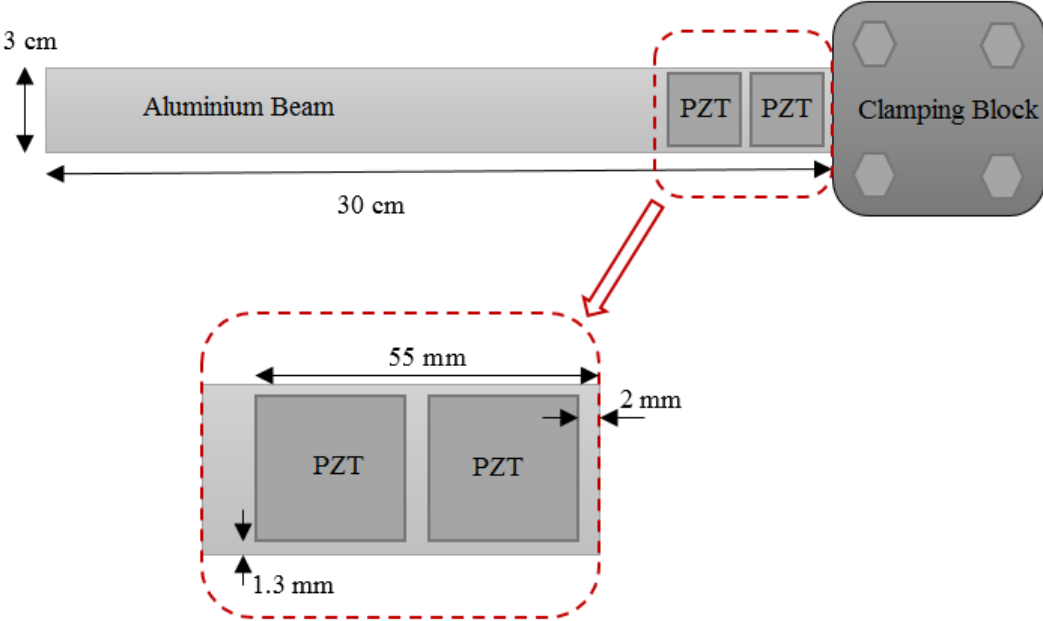
Figure 2.2 Dimensions of the Cantilever Beam with Piezoelectric Patches
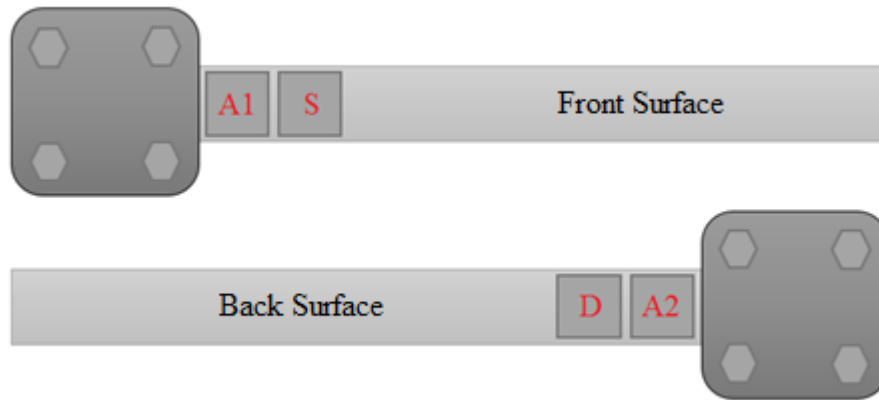
Figure 2.3 Labels of the Piezoelectric Patches

Cables are soldered on each piezoelectric patch after bonding (Figure 2.4). For bimorph configuration of the actuators, the cables which are soldered on (A1) and (A2) are connected with opposite polarization (- of A1 with + of A2, + of A1 with – of A2) so that an applied voltage causes one of the piezoelectric patch to expand and the other to contract. By giving an initial displacement to the tip of the beam, the amplitude and the continuousness of the wave is observed for each piezoelectric patch.
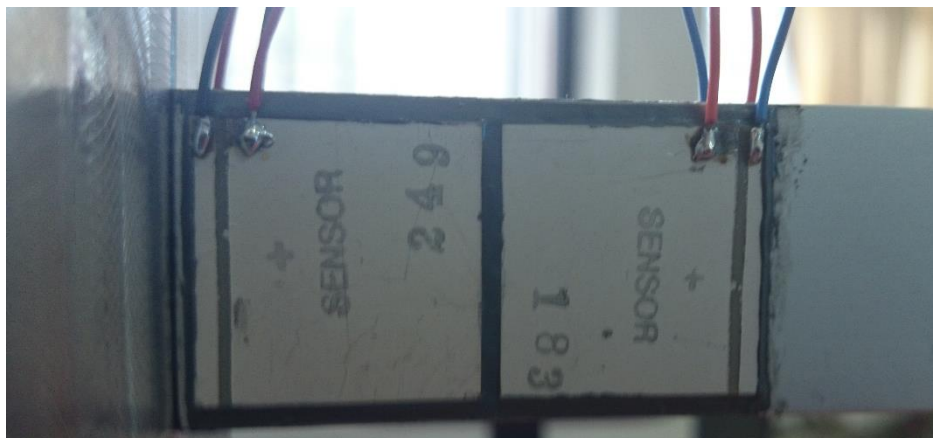
Figure 2.4 Bonded Piezoelectric Patches with Soldered Cables

2.3 Mass Variation Mechanism

Mass variation is considered in order to demonstrate a variation in the frequency response functions (FRF). Before deciding the location of the servomotor on the beam and the arm dimensions, a simple finite element model (FEM) of the aluminum beam

is created. By considering the maximum travel of the servomotor and the different arm lengths, the servomotor and a lumped mass are attached on different locations on the beam. After that, the first out-of-plane bending frequencies are obtained and listed by solving the finite element models. Therefore, location of the servomotor, arm length and lumped mass are decided to create at least 1 Hz difference in the first natural frequencies between the maximum clockwise and counterclockwise angles of the arm. One of the finite element models of the cantilever beam with different elements used for attaching mass, arm and servomotor on its tip shown in Figure 2.5.
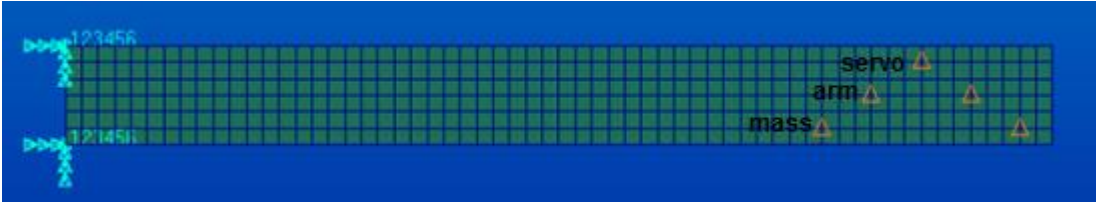
Figure 2.5 Finite Element Model

After deciding the location of the servomotor, by considering the technical drawing of the servomotor (Savöx SH-0253) which is given in Figure 2.6, the aluminum beam is drilled and bolted to the tip of the cantilever beam.
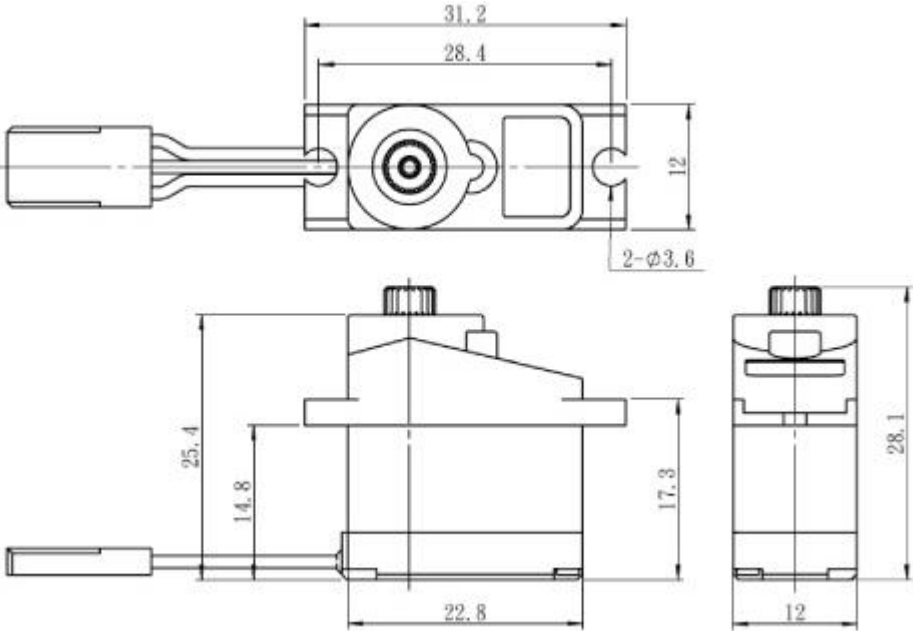
Figure 2.6 Technical Drawings of the Servomotor [42]

A rectangular aluminum beam is decided as a servomotor arm which has dimensions of 50 [mm] x 10 [mm] with a thickness of 2 [mm]. One end of the arm is attached to the servomotor shaft and the other end is drilled in order to attach different masses.

The detailed drawings of the tip of the cantilever beam is also shown in Figure 2.7. As an example, top view of the servomotor with the mass attached servomotor arm is shown in Figure 2.8.
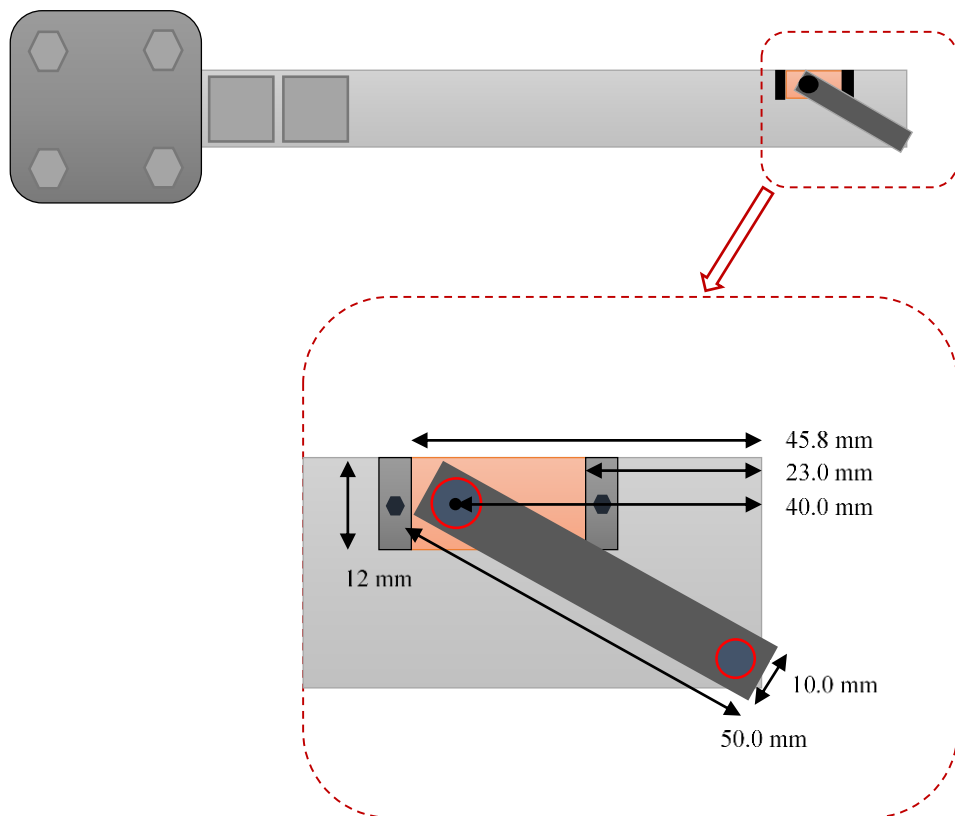
Figure 2.7 Dimensions of the Mass Variation Mechanism

Figure 2.8 Top View of the Mass Variation Mechanism

Maximum value of the attached mass at the tip of the servomotor arm is considered as 20 g. Maximum torque is achieved when the aluminum arm which is shown in Figure 2.9 is parallel to the ground.
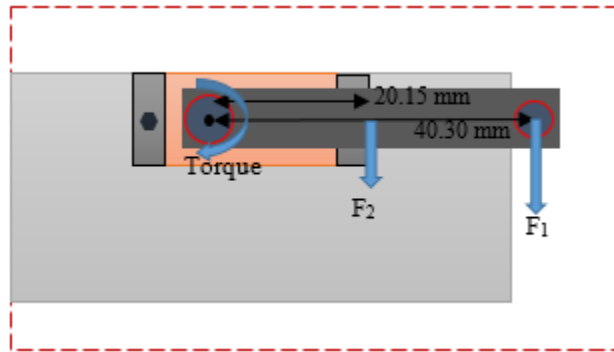
Figure 2.9 Maximum Torque Created by the Forces F_1 and F_2

The distance between the servomotor shaft and the center of the hole that is used for the mass attachment is calculated as $d = 40.30$ [mm]. Mass of the arm (m_{arm}) is calculated as 2.7 gram. So, the following equation gives the maximum torque that is created by the arm and tip mass (m).

$$T = g \times \left(m \times d + m_{arm} \times \frac{d}{2} \right) \qquad (2.1)$$

$$T = 9.81 \left[\frac{m}{s^2} \right] \left(0.0200 \, [kg] \, 0.0403 \, [m] + 0.0027 \, [kg] \, \frac{0.0403}{2} \, [m] \right) \qquad (2.2)$$

16

$$T = 0.0084 \ [N.m] \tag{2.3}$$

From the Table 2.1, minimum torque is at 4.8 [V] and it is 0.176 [Nm]. This value is much greater than the possible maximum torque created by the arm and the tip mass.

Table 2.1 Technical Specifications of the Savöx SH-0253 [42]

Weight [g]:	13.6
Speed [at 4.8V sec/60]:	0.13
Torque [at 4.8V N-m]:	0.176
Speed [at 6.0V sec/60]:	0.09
Torque [at 6.0V N-m]:	0.216

For the control of the Savöx SH-0253 servomotor [42], an Arduino which is a physical computing platform based on simple microcontroller board is used to generate PWM (pulse width modification) signal, a series of repeating pulses of variable width. As it can be seen from Table 2.2, the neutral position pulse width is 1500 microseconds and the maximum travel is around 150° when the signal pulse width is from 700 to 2300 microseconds. So, there are 75° available for both in clockwise and counterclockwise directions.

Table 2.2 Control Specifications of the Savöx SH-0253 [42]

Control system	Pulse width modification
Amplifier type	Digital Controller
Operating Travel	44° (when 1500→2000 μsec)
Neutral position	1500 μsec
Dead band width	5 μsec
Rotating direction	Clockwise (when 1500→2000 μsec)
Pulse width range	700→2300 μsec
Maximum travel	Approx. 150°(when 700→2300 μsec)

Five different configurations of the arm are considered. The angle differences between the configurations are the same and it is chosen as 32°. So, the total travel is 128° which is less than the maximum travel of the servomotor. The midpoint of the servomotor where the arm is perpendicular to the beam is considered as 0°. Therefore, the configurations are +32, +64, -32, and -64 degrees and they are shown in Figure 2.10.
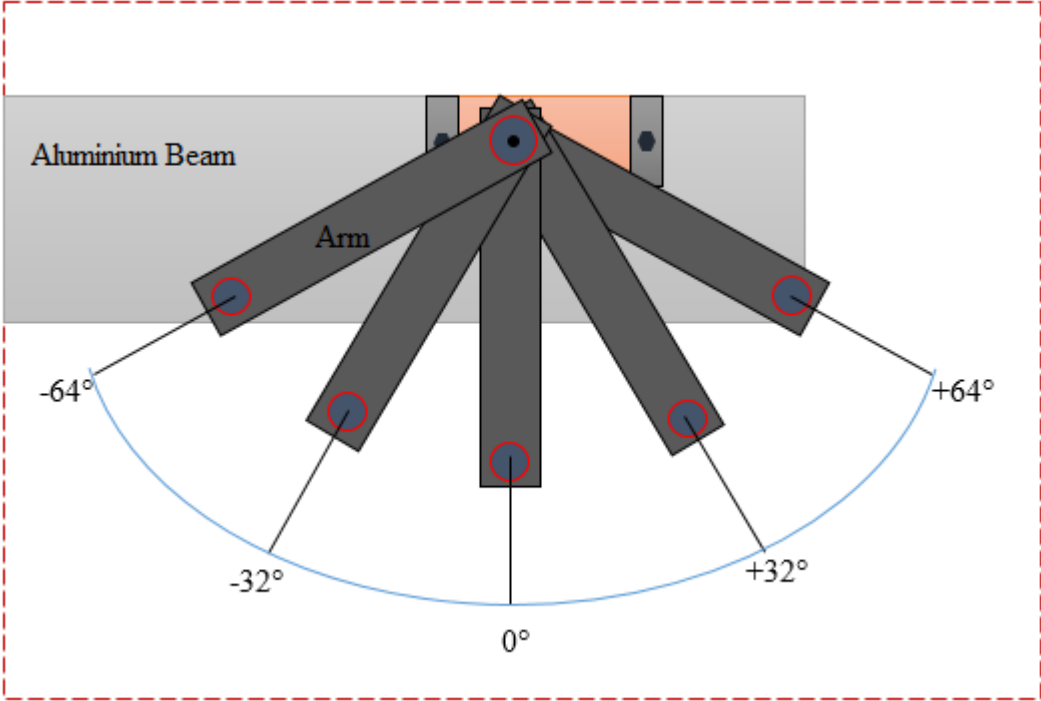
Figure 2.10 Different Arm Configurations

In order to move the servomotor arm to various different locations, 5 different push buttons are connected to the microcontroller (Atmega328p). Each button corresponds to a different angle and when a button is pushed, the arm moves and holds its position at the corresponding angle. In Figure 2.11, the microcontroller board, push buttons, battery and the cables which are connected to the power and signal cables of the servomotor are shown.

18
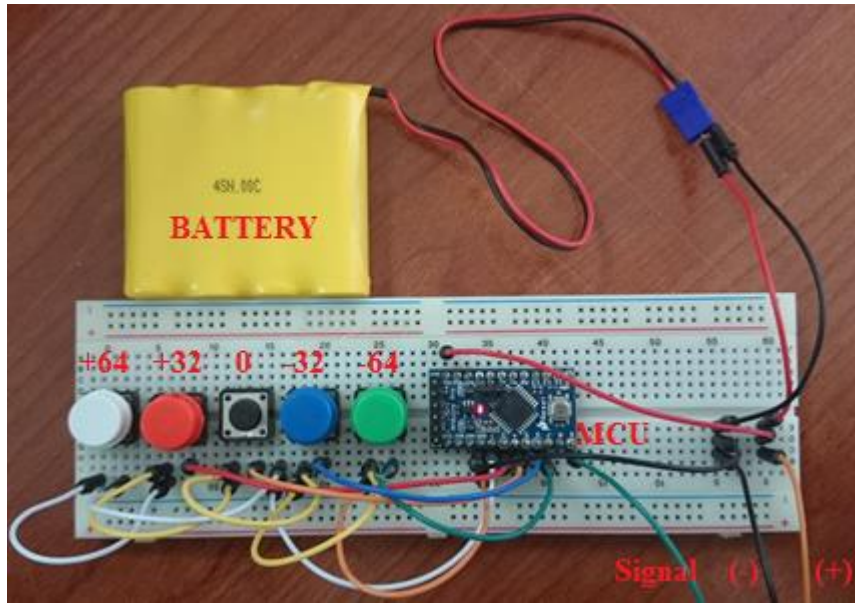
Figure 2.11 Board Setup for Servomotor Control

After that, a simple code is written and uploaded to the MCU board. Also, 10 gr mass is chosen and attached to the tip of the arm. Then, the code is tested for different cases by pushing the corresponding buttons. The following Figure 2.12 shows the different configurations of the arm and the labels as Case 1 (+64°), Case 2 (+32°), Case 3 (0°), Case 4 (-32°), Case 5 (-64°).
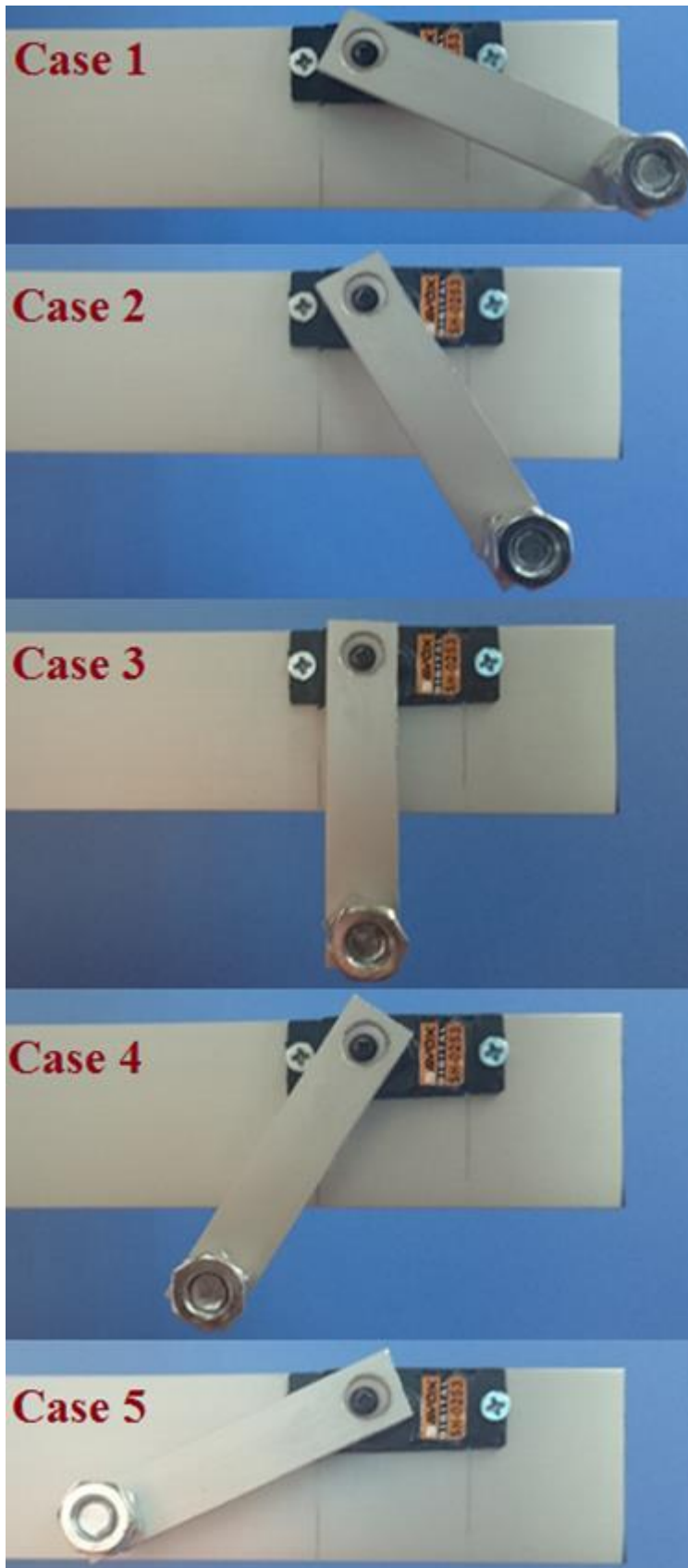
Figure 2.12 Arm Angles (64°, 32°, 0°, -32°, -64° respectively from upper to lower)

2.4 Experimental Setup

Experimental setup consists of the smart beam, a data acquisition system, an amplification system, and a sensor system. A closed loop system is installed and details are also described. There are some peripheral instruments such as a signal generator, a multi-meter, and an oscilloscope that are not used actively in closed loop experiments but are used for checks and preparation purposes.

2.4.1 Smart Beam

In order to add the smart beam (Figure 2.13) to the closed loop system, two connectors which are connected directly to the piezoelectric patches, are used. The connector (1) used for applying signal to the smart beam, has 4 pins. Two of the pins are connected to the disturbance piezoelectric patch (D) and the other two pins are connected to actuator piezoelectric patches (A1) and (A2) as bimorph. The connector (2) used for measuring the vibrations of the smart beam has two pins which are connected to the sensor piezoelectric patch (S).
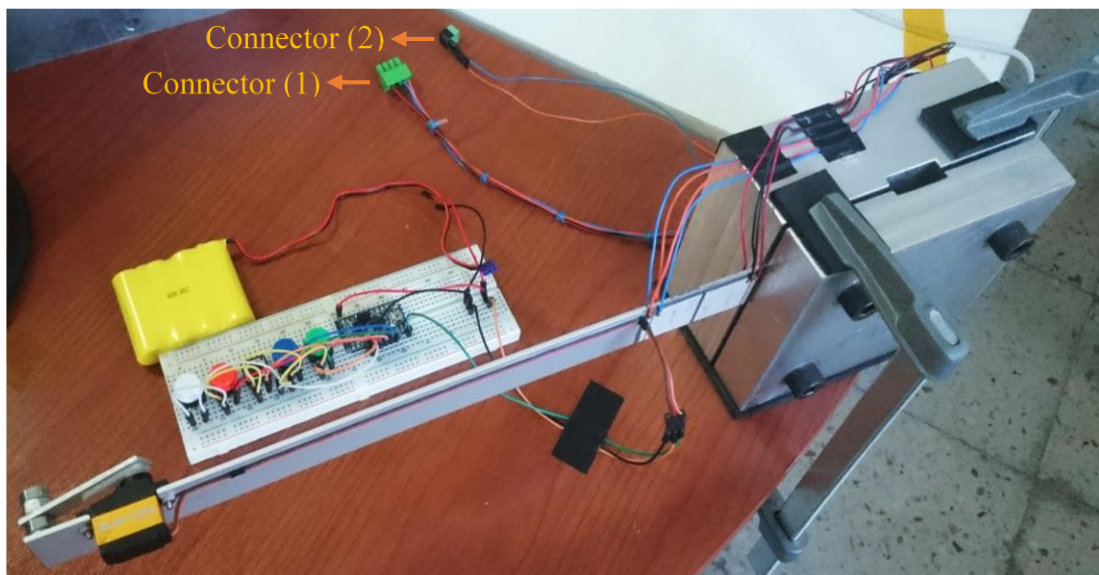
Figure 2.13 Smart Beam

2.4.2 Data Acquisition System

The data acquisition system includes a host pc and a target machine which are connected to each other with an Ethernet cable (TCP/IP Protocol). The host pc is HP Pro 3400MT and has MATLAB, Simulink software and Toolboxes installed on it. A Simulink model is created on the host pc and then, code is generated from the model and executed in real time on the target machine. The target machine is "Speedgoat Education Real-Time Target Machine" [43] which is high-performance real-time simulation and testing platform. A monitor for the target machine is used to observe the signals in real-time. They are shown in Figure 2.14(a). The target machine has a built-in input/output module (Speedgoat I/O 102). There are 32 single-ended or 16 differential analog inputs (16-bit resolution) and 4 single-ended analog outputs and digital channels. In the experimental setup, only analog inputs and outputs (single-ended) are used. There are $\pm 10V$, $\pm 5V$ and $\pm 2.5V$ voltage ranges which are selectable for analog inputs and outputs. Because of the high voltage generation of the piezoelectric patch and to apply as high voltage as possible to the amplifiers, $\pm 10V$ is selected for both analog inputs and outputs. The terminal board of the input/output module are shown in Figure 2.14(b).

Figure 2.14 Data Acquisition System (a) Host PC and xPC Target Machine (b) Terminal Board

In Simulink software, input and output channel blocks are used and shown in Figure 2.15. The analog input channel is used for the piezoelectric sensor (S). First analog output channel (1) is connected to disturbance piezoelectric patch (D) and the other analog output channel (2) is connected to bimorph piezoelectric actuators (A1, A2).
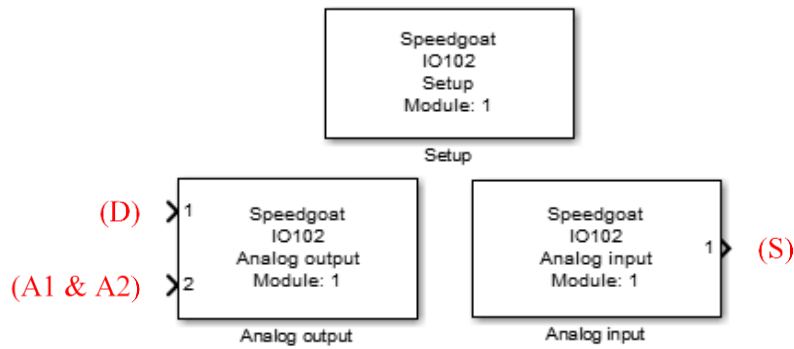
Figure 2.15 I/O102 Blocks

2.4.3 Amplification System

Piezoelectric materials need high voltage for effective usage in active vibration control field. In this experimental setup, one high-voltage amplifier (Sensor Technology SA10 Figure 2.16(a) is installed to use both for disturbance and bimorph actuator signals as the SA10 high-voltage amplifier can be used as two individual amplifiers [44]. In order to power the amplifiers, a high-voltage power supply (Sensor Technology SA21) which can be seen in Figure 2.16(b), is used. In the experiments, SA10 is used in single mode that provides to use it's both channels separately. These amplifiers have voltage gain of 15. The signals that comes from the xPC Target Machine to the inputs of the amplifiers are in the voltage range of ±10V. But, the maximum input voltage of the SA10 amplifier is ±9V [44]. So, a saturation block in Simulink is added not to pass this voltage range. As the amplifiers voltage gain is 15 and the maximum input voltage is ±9V, the output range of the each amplifier channel is ±135 V.

Figure 2.16 Amplification System (a) SA10 Power Amplifier (b) SA21 Power Supply

2.4.4 Sensor System

In order to monitor the voltage of the piezoelectric patch (S) successfully, inverting voltage amplifier is used as piezoelectric materials have high impedance at low frequencies [45]. In addition, the voltage that the sensor piezoelectric patch (S) creates, is higher than the input voltage range of the data acquisition system. To get the voltage in the range of the input (i.e. ±10 V), a voltage amplifier circuit, shown in Figure 2.17, is designed. The op-amp in the figure is one of the four op-amps of LM324N IC and it is supplied with ±10 V. The resistors are RIN = 4.7 MΩ and RF = 1MΩ. The circuit board is shown in Figure 2.18(a) and the power supply which can be seen in Figure 2.18b) is used to power the circuit board.
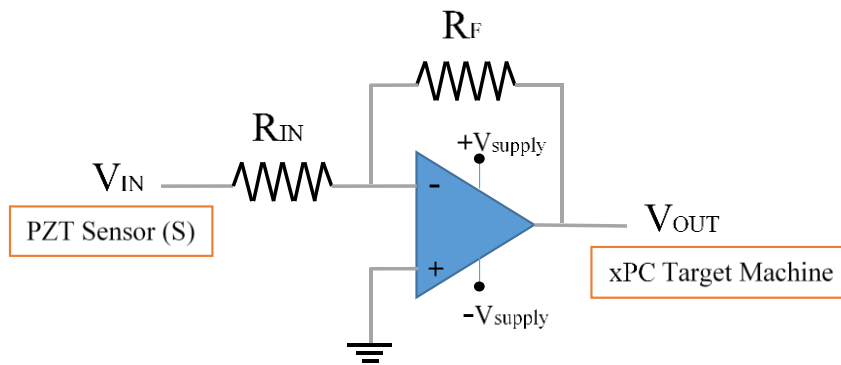
Figure 2.17 Sensor Amplifier Circuit

The gain of an inverted op-amp is calculated by dividing the R_F with R_{IN}.

$$Gain = \frac{R_F}{R_{IN}} = \frac{1}{4.7} = 0.2128$$

Thus, as the range of the input module is ±10 V, maximum allowed voltage that generates by the sensor piezoelectric patch (S) is ±47 V.
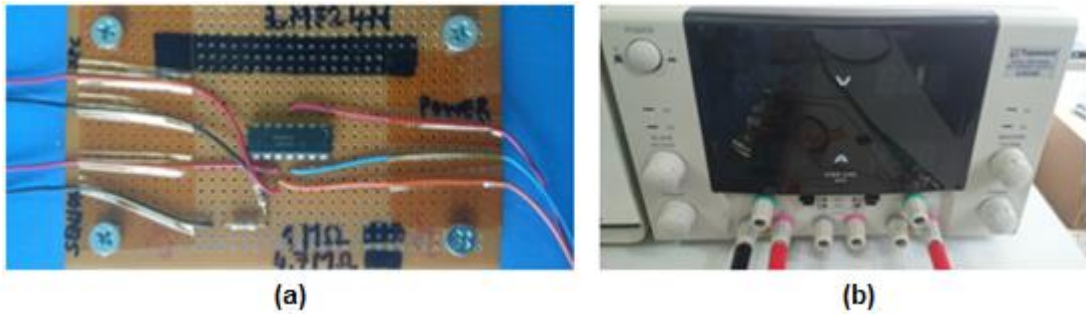
Figure 2.18 Sensor System (a) Sensor Amplifier Circuit
(b) Power Supply for the Circuit

2.4.5 Schematic Diagram of the Experimental Setup

The experimental setup is described in Figure 2.19 below.
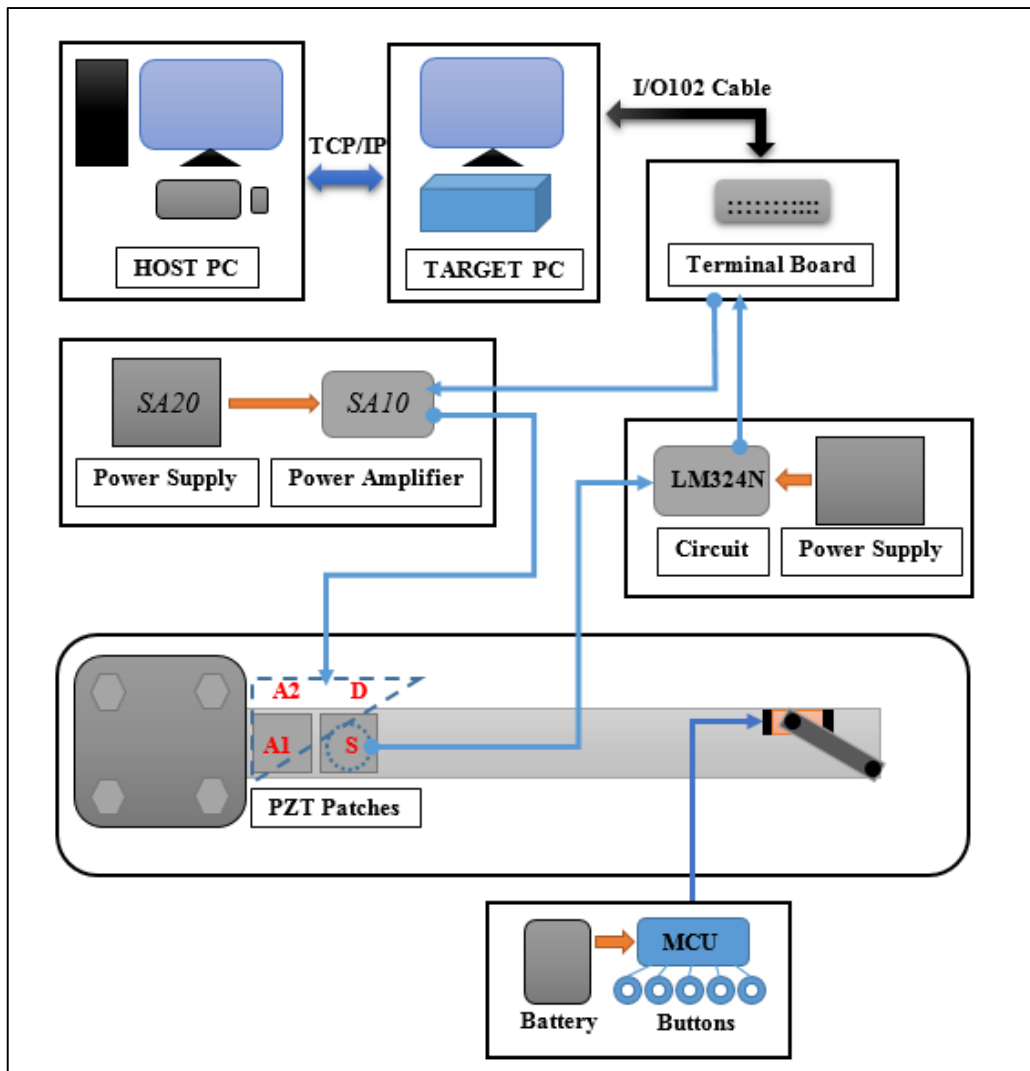
Figure 2.19 Schematic Diagram of the Experimental Setup

2.5 Conclusion

In this chapter, a smart beam having four piezoelectric patches which are used for controlling, creating disturbance and sensing purposes is designed and built. A servomotor mechanism for changing the FRFs of the smart beam is designed and five different arm angle configurations are defined. Changing from one configuration to another is also possible through a simple computing platform and by simply pushing the associated button.

CHAPTER 3

SYSTEM IDENTIFICATION OF THE SMART BEAM

3.1 Introduction

In this chapter, FRFs of the smart beam by using the piezoelectric patches (D – S) and by using the piezoelectric patches (A1&A2 – S) are investigated separately. By changing the servomotor arm to different angle positions, variation of the FRFs are observed. Also, analytical models of the smart beam around its first resonance frequency region for different arm angle configurations are obtained by using the experimental obtained FRFs.

3.2 Excitation of the Smart Beam

The smart beam is excited both by the disturbance piezoelectric patch (D) and by the actuator piezoelectric patches (A1 & A2) separately for different servomotor arm angle configurations. The excitation signal consists of the same swept-frequency cosine signals which are added to each other. Parameters of one of the same added swept-frequency cosine signals are given in Table 3.1.

The swept-frequency signal data is sampled at 10 kHz and total number of samples is chosen as power of two (2^18=262144) to make the Fast Fourier Transform (FFT) computation faster. Hence, the target time is 26.2144 seconds.

Table 3.1 Properties of the swept-frequency cosine (chirp) signal

Frequency Sweep	Logarithmic
Sweep Mode	Unidirectional
Initial Frequency	1 Hz
Target Frequency	Variable
Target Time	26.2144 s
Sample Frequency	10 kHz
Voltage Range	±1V

3.3 Frequency Response Functions

In order to get the FRF of the smart beam for a specific servomotor arm configuration, an excitation signal *x(t)* is applied to the system and the response signal *y(t)* of the system is recorded. It is difficult to identify the frequency content of the signals by looking at the time domain signals. So, by taking FFT of the input and the output time domain signals separately, the discrete Fourier transforms of the input *X(ω)* and the output *Y(ω)* signals are calculated. Then, by dividing the Fourier transform of the output signal with the Fourier transform of the input signal, the FRF is obtained. For all arm configurations, in order to get better FRFs, chirp signals are repeated and response signals are recorded. Then, frequency response function of a specific servomotor arm configuration is obtained by averaging each FRFs linearly. Table 3.2 presents these details.

Table 3.2 Total Excitation Signal and Averaging Mode

Number of Added Sweep Signals	5
Total Time	131.072 s
Averaging Mode	Linear

3.3.1 Frequency Response Functions btw Piezoelectric Patches (D) and (S)

First of all, in order to have a look at the resonance frequency values and the relations between the dB levels in the FRF in the first two out of plane resonance frequencies, an experiment is conducted. Simulink model in Figure 3.1 is made to observe and log input/output data of the smart beam. The target frequency of the excitation signal is chosen as 100 Hz and the excitation signal is applied to analog output 1 which corresponds to the piezoelectric patch (D).
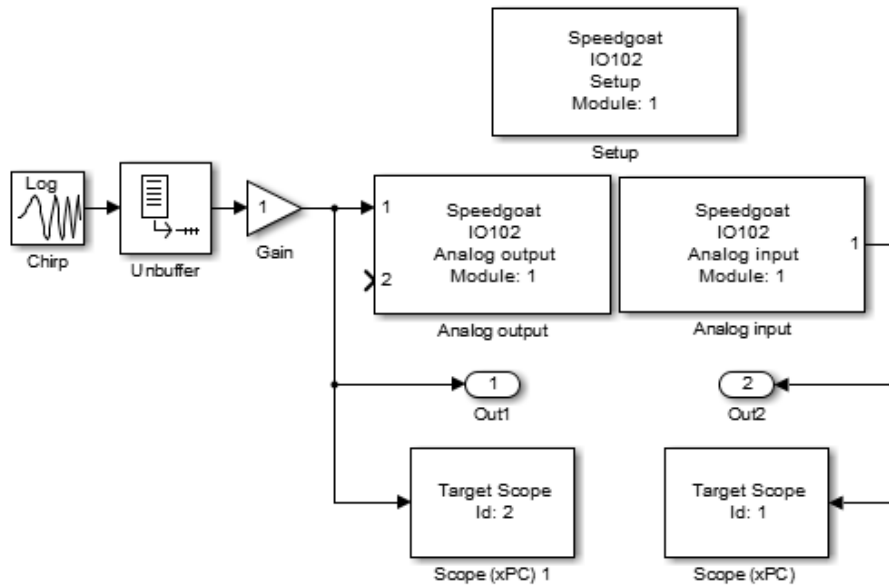
Figure 3.1 Simulink Model of (D)-(S) PZT Configuration

The excitation and the response signals (Figure 3.2) of the smart beam are observed and recorded by the xPC Target Machine for Case 1 (+64° arm angle configuration) to calculate FRF in 1-100 Hz range.
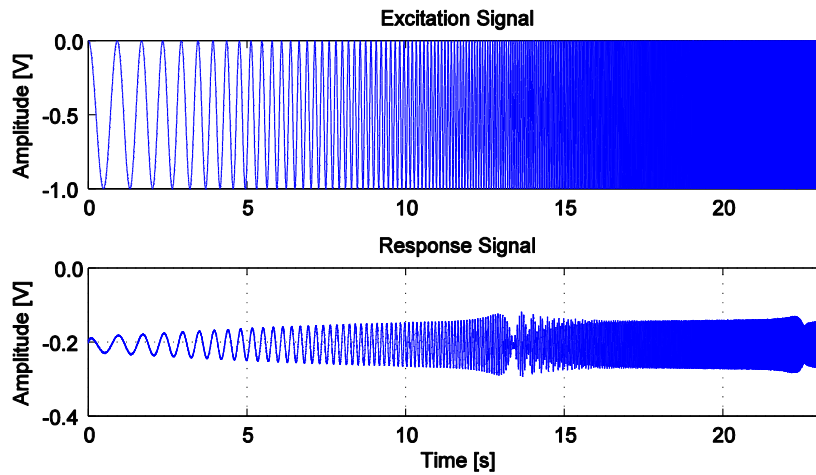
Figure 3.2 Time Domain Input-Output Signals (D)-(S)
PZT Configuration (1-100Hz)
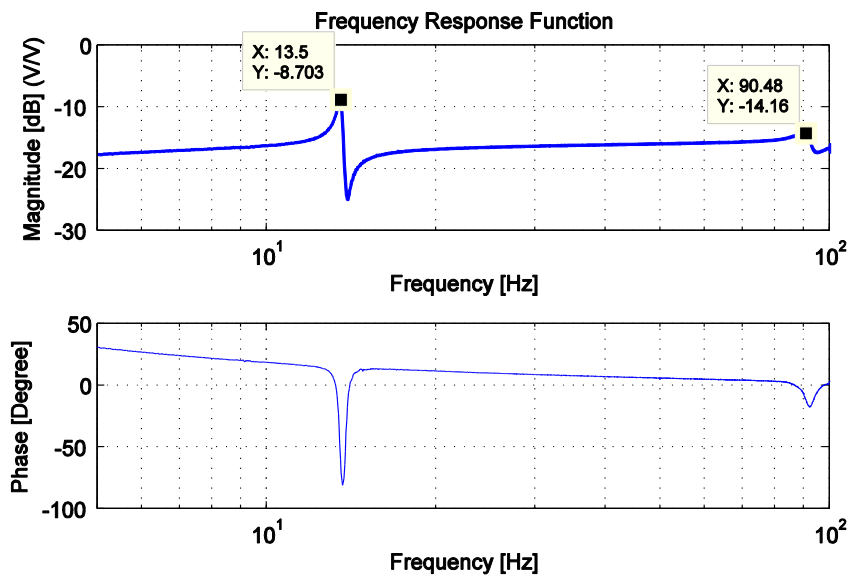
Figure 3.3 Frequency Response Function (5-100 Hz)

As shown in Figure 3.3, the first two resonance frequencies (13.50 Hz, 90.48 Hz) are obtained after analyzing the time domain data of this experimental study. An analysis is performed to obtain theoretical results in order to compare them with the experimental results. A model is created and analyzed by omitting piezoelectric patch and cables on the smart beam, by considering the total attached mass on the beam as a single mass. The analysis can be seen in Appendix A. The difference between the theoretical and experimental results are due to the effects of the nonmodeled parts of the smart beam as PZT patches, cables etc. In this thesis, only the first resonance frequency region is considered and analyzed for servomotor arm angle variations.

Therefore, the target frequency of the excitation signal is changed to 40 Hz and experiments are conducted for all arm angle cases. After that, by using recorded input/output data, Figure 3.4 is plotted. It shows one of the repeated swept-frequency excitation signals and the response signals in time domain. The excitation signals are the same for all arm angle configurations.
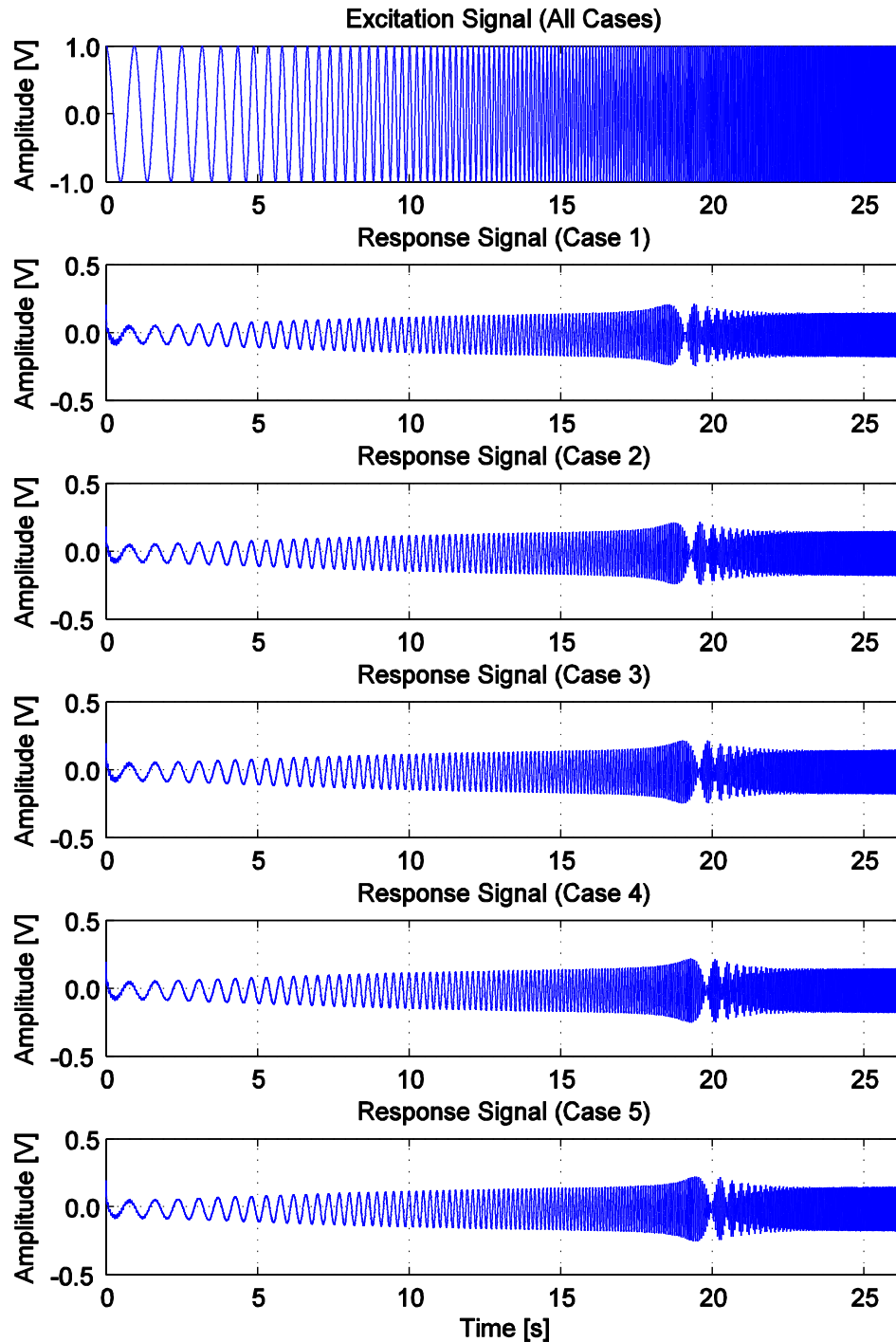
Figure 3.4 Excitation and Response Signals of (D)-(S) PZT Configuration

By analyzing the time domain data in MATLAB, frequency response functions of (D)-(S) PZT configuration for all arm angles are obtained. The frequency response functions are plotted in the range of 5-40 Hz. In the following Figure 3.5 to 3.9, the FRFs of (D)-(S) PZT configuration of the smart beam are shown for the all arm angle cases (i.e. +64°, +32°, 0°, -32° and -64°, respectively).
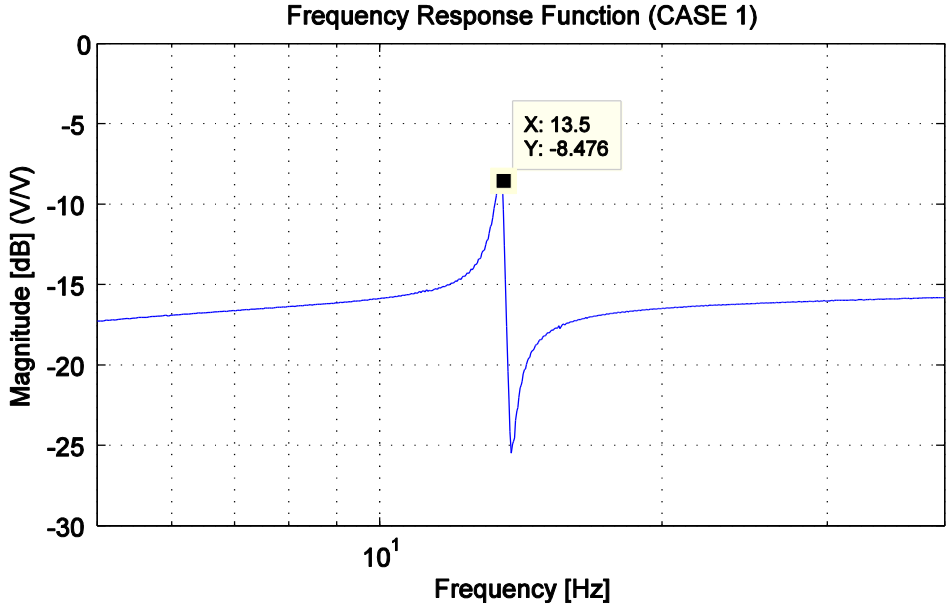
Figure 3.5 Frequency Response Function of (D)-(S) PZT Configuration (Case 1:+64° Arm Configuration)
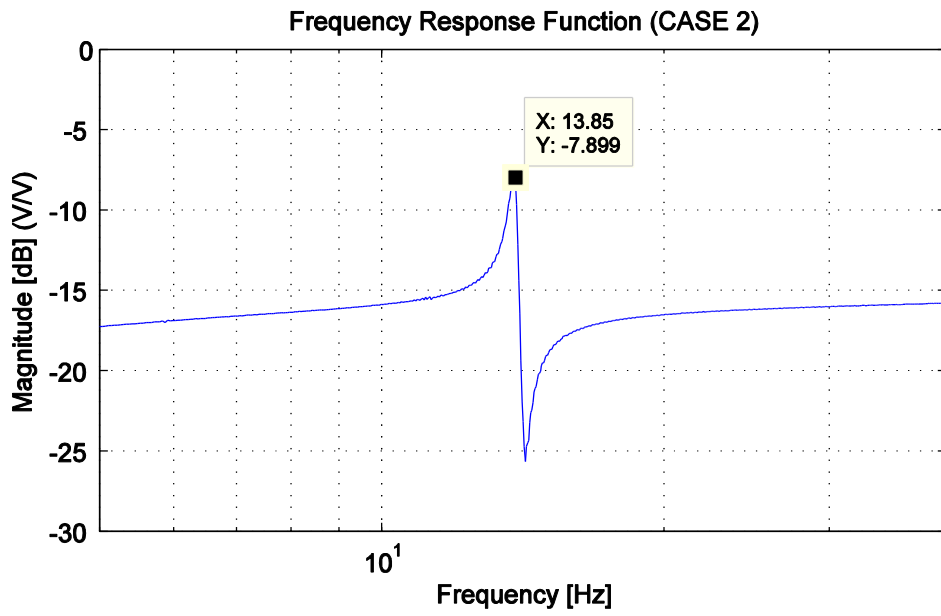
Figure 3.6 Frequency Response Function of (D)-(S) PZT Configuration
(Case 2:+32° Arm Configuration)
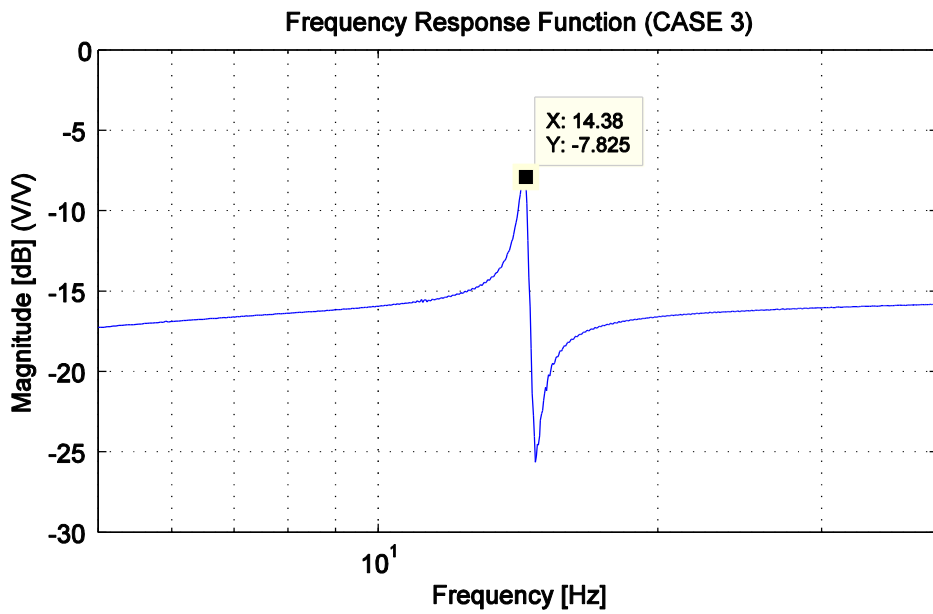
Figure 3.7 Frequency Response Function of (D)-(S) PZT Configuration
(Case 3: 0° Arm Configuration)
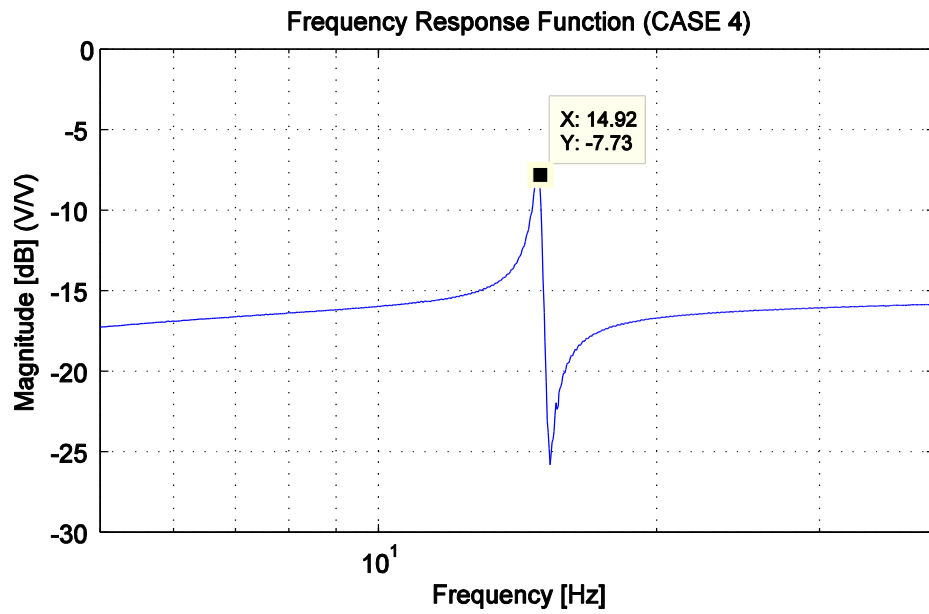
Figure 3.8 Frequency Response Function of (D)-(S) PZT Configuration
(Case 4: -32° Arm Configuration)
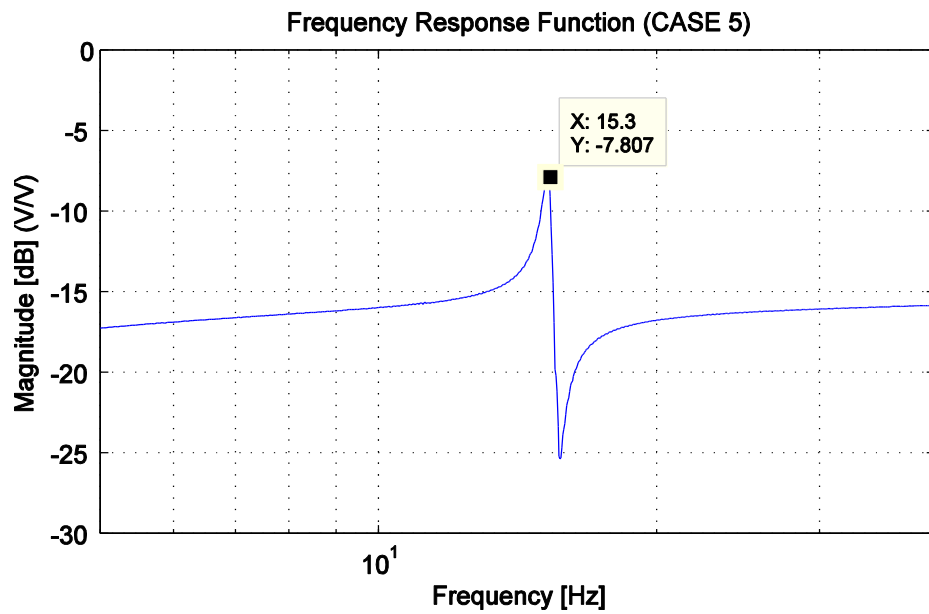
Figure 3.9 Frequency Response Function of (D)-(S) PZT Configuration
(Case 5: -64° Arm Configuration)

As it can be seen from Table 3.3, the first resonance frequency of the smart beam increases as the mass attached arm moves towards to the root of the beam (From +64° to -64° arm angle). Figure 3.10 shows the variation of the frequency response function of (D)-(S) PZT configuration of the smart beam.

Table 3.3 The First Resonance Frequencies and Corresponding Magnitudes of (D)-(S) PZT Configuration of the Smart Beam for the Different Arm Angle Cases

Arm Angle Cases	Resonance Frequency [Hz]	Magnitude at the Resonance Frequency [dB]
Case 1: +64°	13.50	-8.476
Case 2: +32°	13.85	-7.899
Case 3: 0°	14.38	-7.825
Case 4: -32°	14.92	-7.730
Case 5: -64°	15.30	-7.807
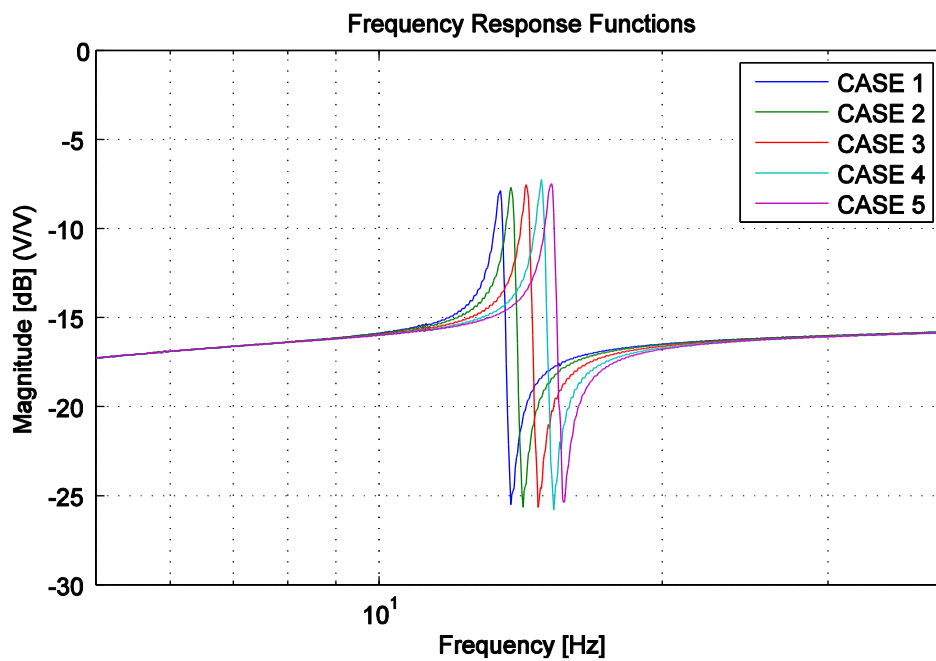
Figure 3.10 FRFs of (D)-(S) PZT Configuration (All Cases)

3.3.2 Frequency Response Functions btw Piezoelectric Patches (A1 & A2) and (S)

In this section, (A1 & A2) piezoelectric patches in bimorph configuration as an actuator and piezoelectric patch (S) as a sensor are used to obtain FRFs. The excitation signal which changes 1 to 40 Hz, is applied to the channel 2 of the analog output. Designed Simulink model can be seen in Figure 3.11.
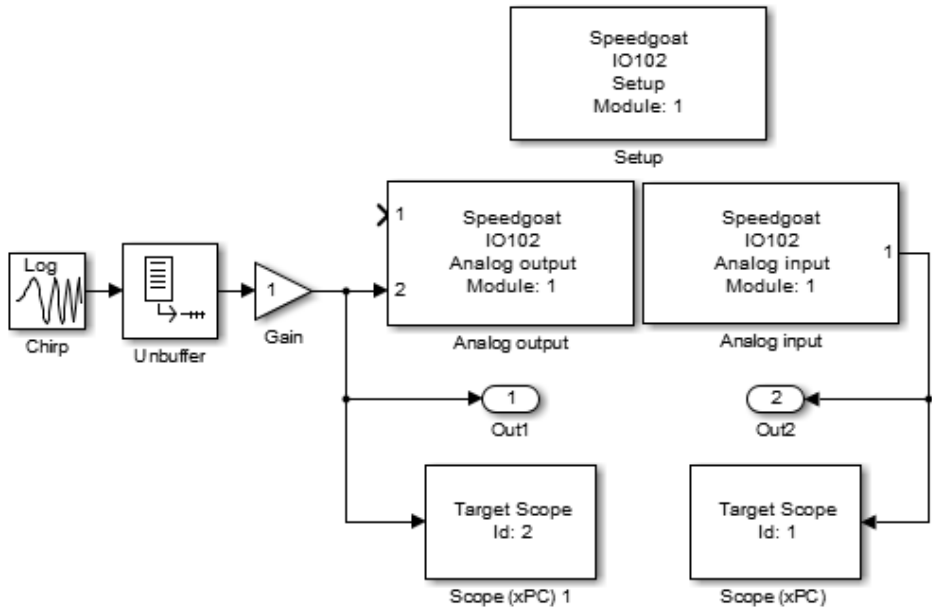
Figure 3.11 Simulink Model of (A1&A2)-(S) PZT Configuration

The procedure for obtaining (A1 & A2)-(S) PZT configuration FRFs of the smart beam is same as in Section 3.3.1. The only difference is the analog output used for the application of the excitation signal. One of the swept frequency excitation signals and the response signals in time domain are shown in Figure 3.12.
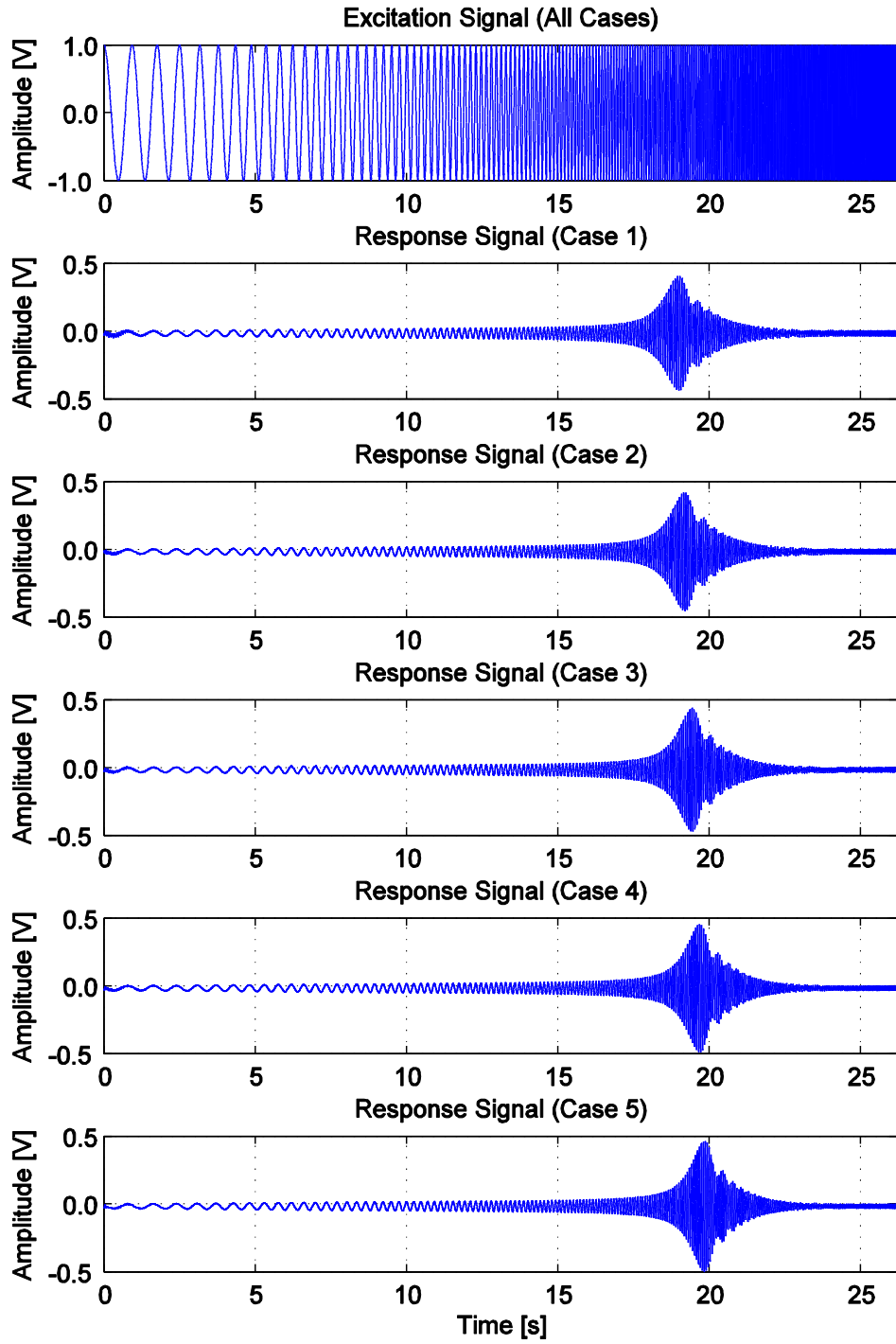
Figure 3.12 Excitation and Response Signals of (A1 & A2)-(S) PZT Configuration

Experimental FRFs of (A1 & A2) – (S) PZT configuration for all arm angles are obtained by analyzing the time domain data in MATLAB. The experimental frequency response functions are converted to analytical models to be used as plants in designing controllers for vibration suppression of the smart beam. Analytical models of the experimental results are obtained by using MATLAB's commands "fitfrd" and "frd". Transfer functions of the smart beam with different servomotor arm angle configurations are estimated in the range of 5.04 Hz - 30.02 Hz which includes first resonance frequency region. To get accurate models, orders of the estimated transfer functions has to be high but not computationally expensive. For finding the minimum necessary order, one of the arm angle configurations is chosen and different model orders are tested. Figure 3.13-3.16 shows the 1st, 2nd, 3rd, and 4th order estimated models respectively for $+64°$ servomotor arm angle (Case 1).
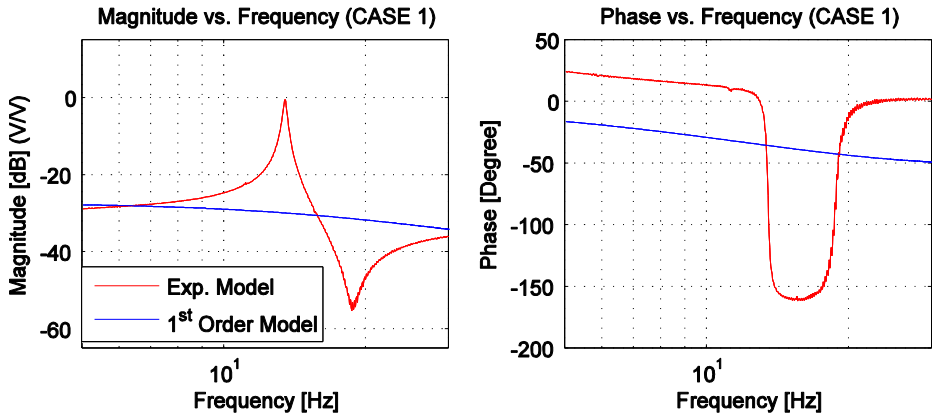
Figure 3.13 Frequency Response of Experimental and 1st Order Analytical Models
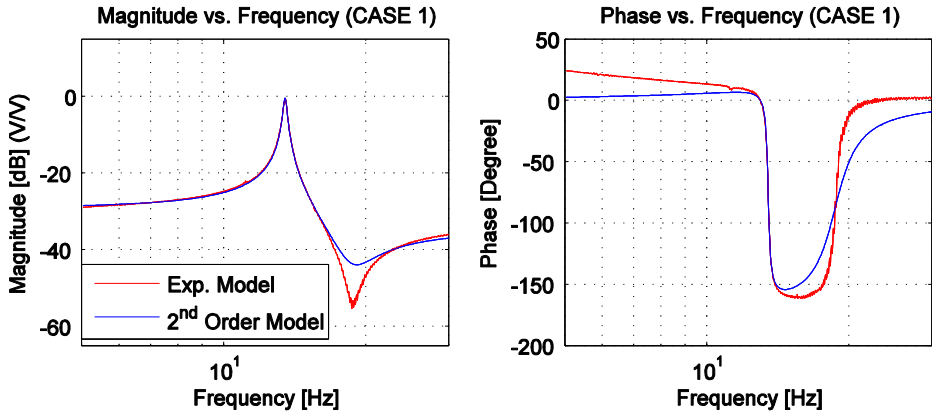
Figure 3.14 Frequency Response of Experimental and 2nd Order Analytical Models
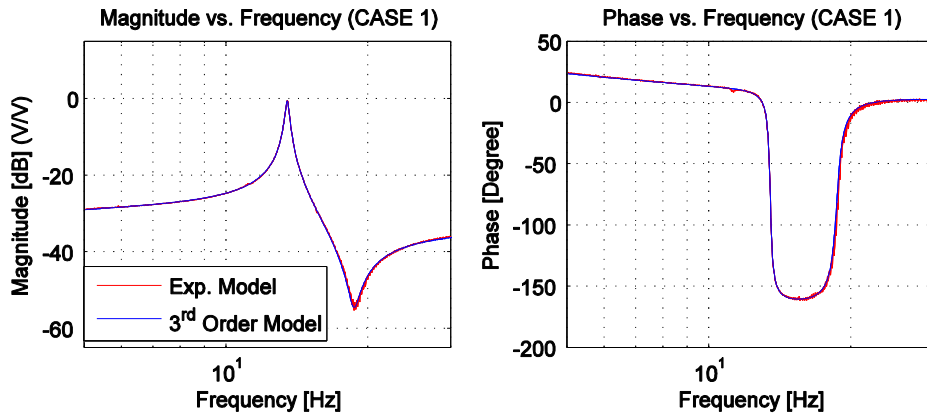
Figure 3.15 Frequency Response of Experimental and 3rd Order Analytical Models
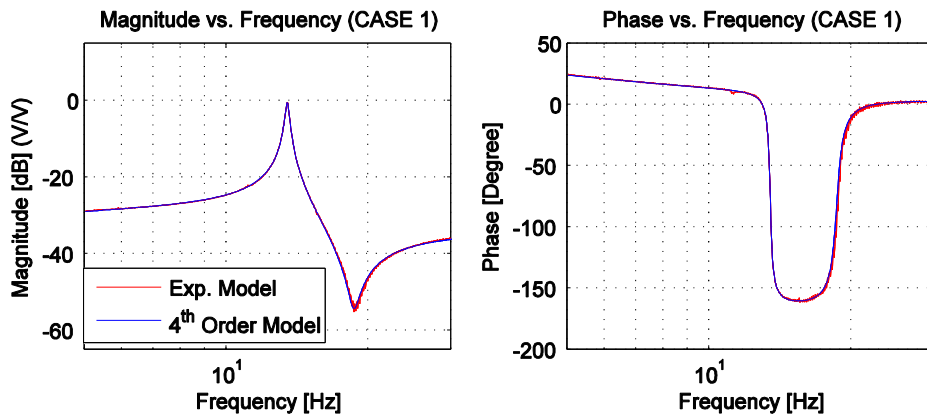
Figure 3.16 Frequency Response of Experimental and 4th Order Analytical Models

It is found that third order is enough for representing the FRF which covers the first resonance frequency of the smart beam. For all servomotor arm angle configurations, 3rd order estimated continuous transfer functions are obtained. The following figures (Figure 3.17 to 3.21) show frequency response functions both experimental and analytical models of (A1 & A2)-(S) PZT configuration of the smart beam for +64°, +32°, 0°, -32° and -64° arm angles respectively. The first resonance frequencies and corresponding magnitudes are shown in Table 3.4 and the estimated transfer functions for each servomotor arm angle are listed in the Table 3.5.
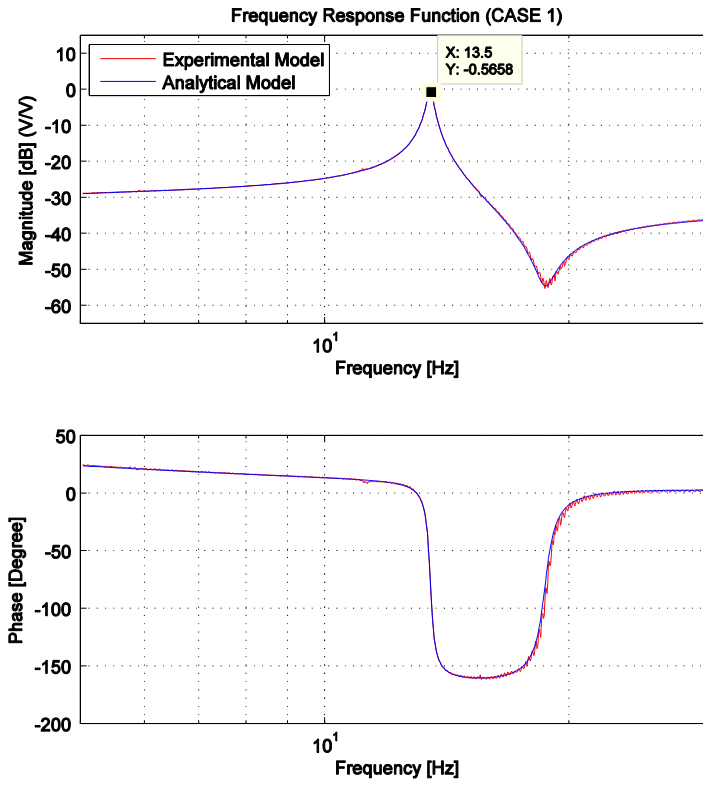
Figure 3.17 FRF of (A1&A2)-(S) PZT Configuration (Case 1: +64°)
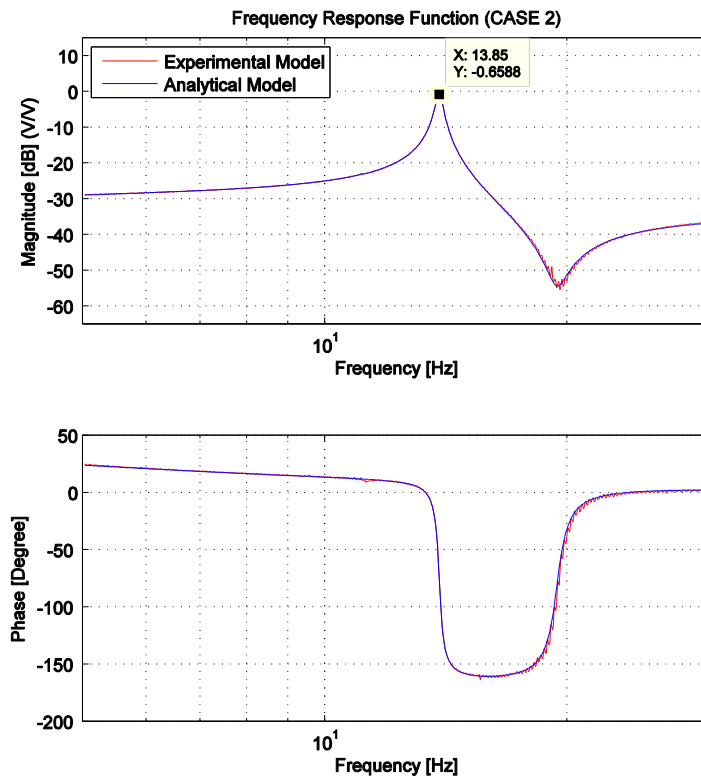
Figure 3.18 FRF of (A1&A2)-(S) PZT Configuration (Case 2: +32°)
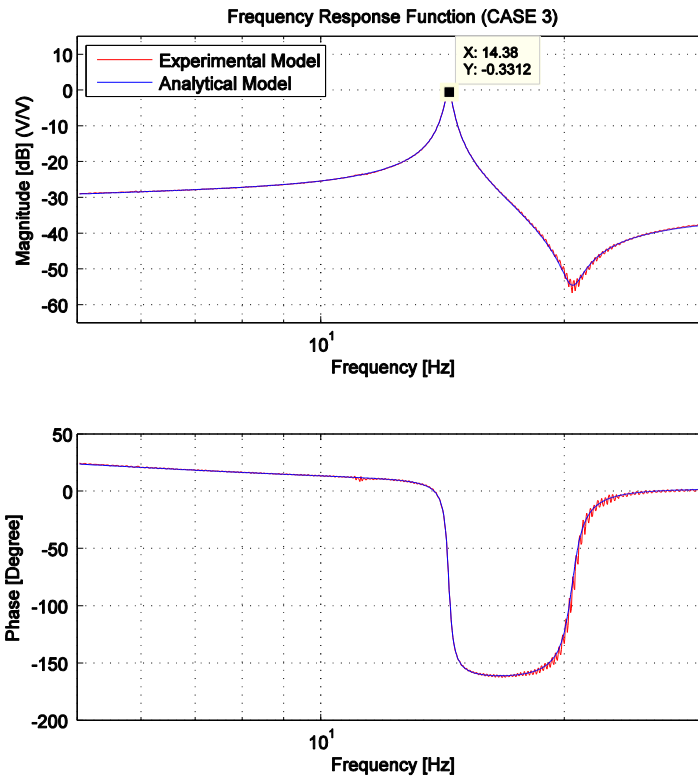
Figure 3.19 FRF of (A1&A2)-(S) PZT Configuration (Case 3: 0°)
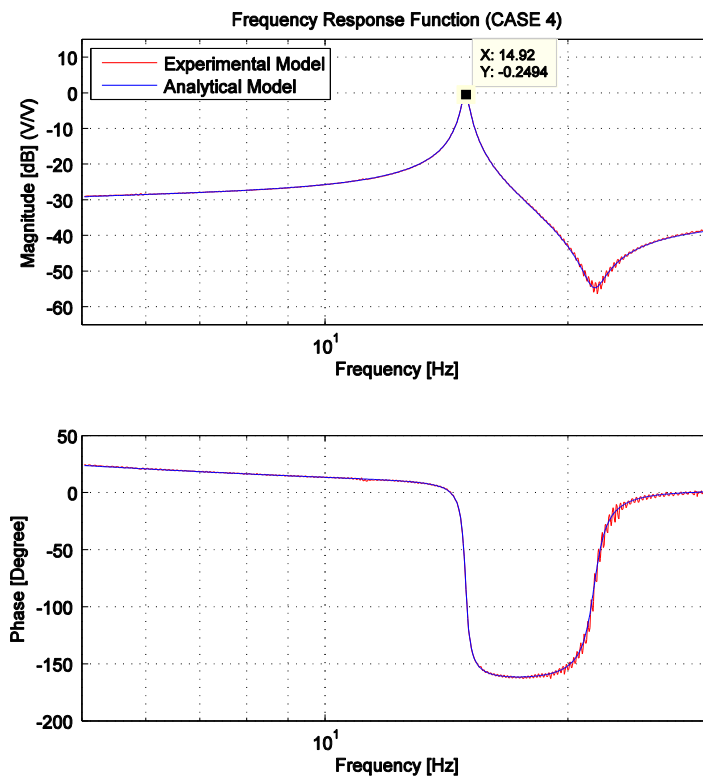
Figure 3.20 FRF of (A1&A2)-(S) PZT Configuration (Case 4: -32°)
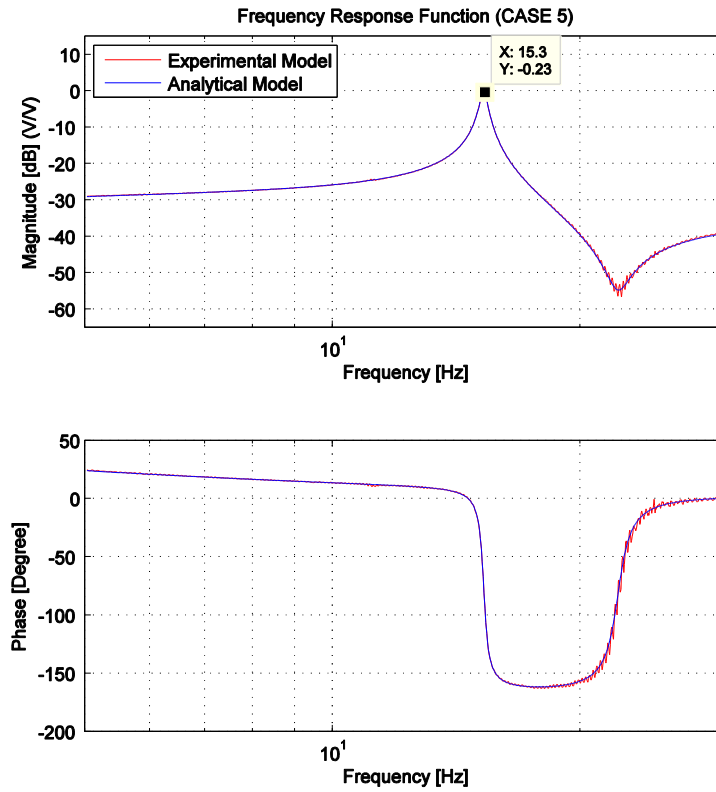
Figure 3.21 FRF of (A1&A2)-(S) PZT Configuration (Case 5: -64°)

Table 3.4 The First Resonance Frequencies and Corresponding Magnitudes of (D)-(S) PZT Configuration of the Smart Beam for the Different Arm Angle Cases

Arm Angle Cases	Resonance Frequency [Hz]	Magnitude at the Resonance Frequency [dB]
Case 1: +64°	13.50	-0.5858
Case 2: +32°	13.85	-0.6588
Case 3: 0°	14.38	-0.3312
Case 4: -32°	14.92	-0.2494
Case 5: -64°	15.30	-0.2300

Table 3.5 Analytical Models of the (A1 & A2)-(S) Configuration of the Smart Beam
for the Different Arm Angle Cases

Arm Angle Cases	Continuous-Time Transfer Functions
Case 1: +64°	$G_1(s) = \dfrac{0.01996\,s^3 + 0.2001\,s^2 + 275.7\,s + 1291}{s^3 + 21.11\,s^2 + 7228\,s + 1.403e05}$
Case 2: +32°	$G_2(s) = \dfrac{0.01943\,s^3 + 0.1975\,s^2 + 290.1\,s + 1231}{s^3 + 20.64\,s^2 + 7641\,s + 1.443e05}$
Case 3: 0°	$G_3(s) = \dfrac{0.01879\,s^3 + 0.1993\,s^2 + 310.7\,s + 1269}{s^3 + 20.58\,s^2 + 8214\,s + 1.539e05}$
Case 4: -32°	$G_4(s) = \dfrac{0.01816\,s^3 + 0.2039\,s^2 + 333.4\,s + 1326}{s^3 + 20.54\,s^2 + 8838\,s + 1.644e05}$
Case 5: -64°	$G_5(s) = \dfrac{0.01784\,s^3 + 0.2058\,s^2 + 349.1\,s + 1380}{s^3 + 20.63\,s^2 + 9260\,s + 1.725e05}$

The experimental frequency response function of the smart beam in the range of 5-30 Hz moves to the right as the servomotor arm angle changes from +64 to -64 degrees. Figure 3.22 shows the variation of the experimentally obtained frequency response functions of (A1&A2)-(S) PZT Configuration of the smart beam.
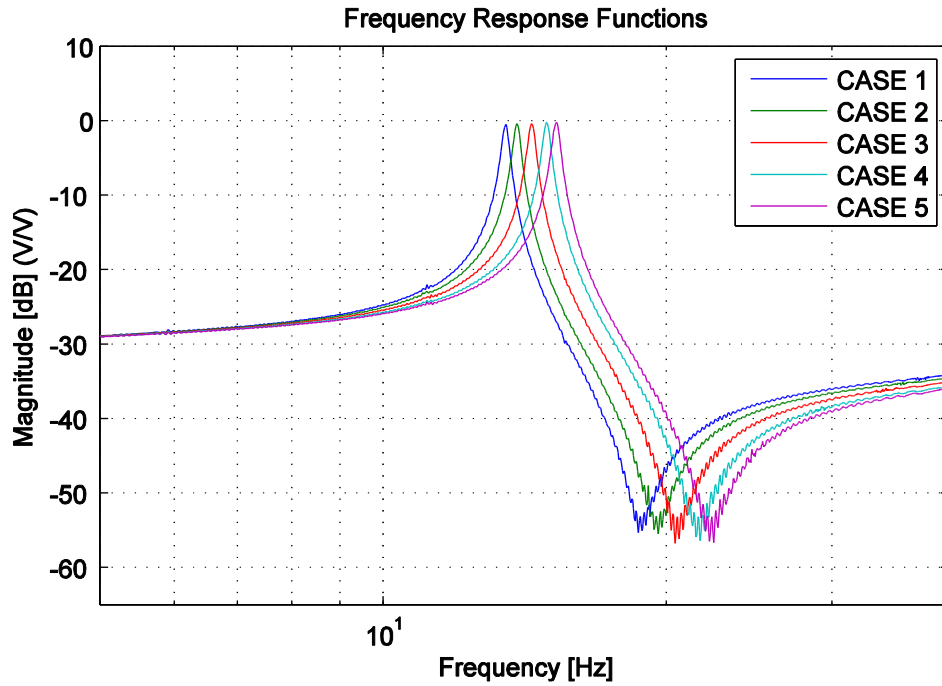
Figure 3.22 FRFs of (A1&A2)-(S) PZT Configuration (All Cases)

3.4 Conclusion

In this chapter, the investigations of the FRFs of the smart beam between the piezoelectric patches (D – S) and (A1 & A2 – S) are presented for all arm angle cases. The excitation and response signals are recorded by the data acquisition system and then FRFs are obtained. For each arm angle cases, resonance frequencies are obtained and compared with each other. The difference between the first resonance frequencies is found as 1.8 Hz for the maximum clockwise and counterclockwise rotations of the servomotor arm angle. The lowest first resonance frequency is obtained as 13.50 Hz at +64° arm angle and the highest first resonance frequency is obtained as 15.30 Hz at -64° arm angle. In this section, the analytical models of the smart beam for all servomotor arm angles are also investigated by using the experimentally obtained FRFs of the smart beam for (A1 & A2 – S) PZT configuration. For different orders and the transfer functions of the smart beam in each case are obtained to be used in the coming control design studies.

44

CHAPTER 4

ACTIVE VIBRATION SUPPRESSION OF THE SMART BEAM BY USING LINEAR QUADRATIC REGULATOR (LQR) METHOD

4.1 Introduction

In this chapter, a controller is designed to be used in free and forced vibration suppression simulations, and therefore, analyses are performed both in time and frequency domain. Then, experiments are conducted to observe the closed loop behavior of the smart beam for free and forced vibrations in time domain. Furthermore, the closed loop system FRF is obtained experimentally and compared with the simulation result. The effect of the plant variation on the closed loop system behavior is also investigated.

4.2 Block Diagram Representation of the State-Space Form of the Smart Beam

Mathematical description of a dynamic system which is used for designing a controller is called as plant. In linear time-invariant (LTI) state-space model of the plant representation, there are two equations. One of them is Equation 4.1 which is the state equation of the system and the other one is Equation 4.2 which is the output equation of the system.

$$\dot{x} = Ax(t) + Bu(t) \tag{4.1}$$
$$y = Cx(t) + Du(t) \tag{4.2}$$

In the Equation 4.1, x defines the state vector and u defines the input vector of the system. The notation $\dot{x}$ defines the first derivative of the state vector. The matrix A is

called as the system matrix and the matrix B is called as the control matrix. In the Equation 4.2, y defines the output vector which is the measurement of the system. The matrix C is called as the output matrix and the matrix D is called as the feed-forward matrix. Simulink block and the detailed block diagram of the plant are shown in Figure 4.1 and Figure 4.2, respectively.
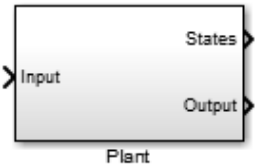
Figure 4.1 Simulink Model of the Dynamic System
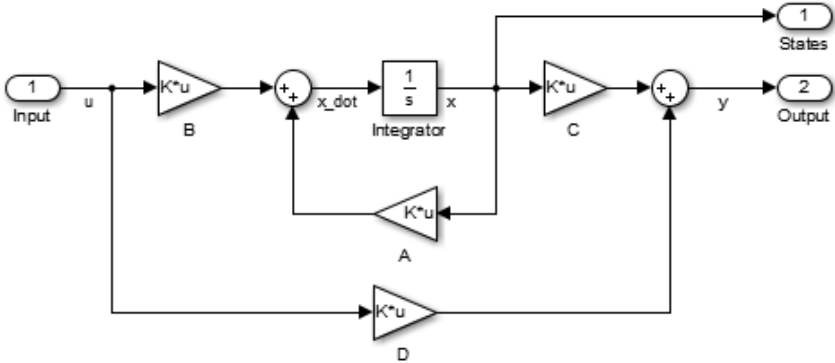
Figure 4.2 Details of the Simulink Model of the Dynamic System

The smart beam is considered as a single input and single output (SISO) system. So, the input u and the output y are not vectors, in fact, they are scalars. The output y is used to simulate data measured from the piezoelectric patch sensor (S) and the input u is used to simulate signal transmission to the piezoelectric patches (A1&A2).

4.3 Linear Quadratic Regulator (LQR) Controller Design

The Linear Quadratic Regulator (LQR) is an optimal controller that uses all the states of the plant and creates a feedback signal as a function of the states. One of the advantages of the LQR controller is that stability is guaranteed if all the states in the system are available and if the model resembles the dynamic system well. Before

designing the controller, controllability of the system has to be verified. If the system is controllable, all the states can be driven. In order to be completely state controllable, the controllability matrix (Equation 4.3) must have rank 'n' which corresponds to the number of state variables of the system.

$$C = [A|AB|A^2B| \dots |A^{n-1}B]$$
(4.3)

The vector of state-feedback control gains represented as K and the control input of the system is shown as in Equation 4.4.

$$u(t) = -Kx(t)$$
(4.4)

Figure 4.3 shows block diagram of the system with full-state feedback controller. Reference is set to 0 which is a desired output value for vibration suppression.
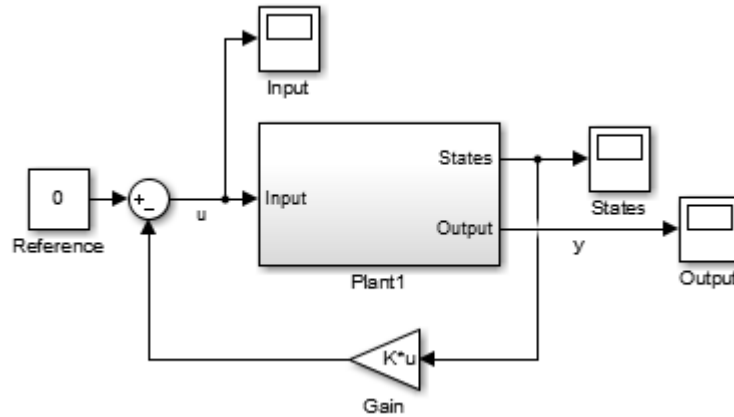
Figure 4.3 Full-State Feedback Control System Simulink Block Diagram

Linear Quadratic Regulator method is used for determining state-feedback control gain vector K. Performance index of the LQR controller is shown in Equation 4.5 where u(t) is input vector and x(t) is state vector of the system in time domain.

$$J = \frac{1}{2} \int_0^\infty [x^T(t)Qx(t) + u^T(t)Ru(t)]dt$$
(4.5)

Here, Q is a positive-semidefinite state variable and R is a positive-definite input variable weighting matrices. In order to achieve an optimal control, the performance index J has to be minimal. After analyzing the performance index equation, the optimal control input which minimizes the performance index is found as in Equation 4.6.

$$u = -R^{-1}B^T P x \qquad (4.6)$$

So, full state-feedback gain vector K is found as in Equation 4.7.

$$K = -R^{-1}B^T P \qquad (4.7)$$

Here, R is a weighting matrix of the LQR controller and B is the control matrix of the plant. The parameter P is calculated by using algebraic Riccati equation which can be seen in Equation 4.8.

$$A^T P + PA - BPR^{-1}B^T P + Q = 0 \qquad (4.8)$$

Thus, to achieve a desired response of the dynamic system, the required gain vector K can be calculated by tuning Q and R parameters. Q is a matrix and R is a scalar value as there is only one control input to the system. Regarding the performance index function, Q and R parameters balance "the relative importance of the state of the system" and "the control input", respectively. In this thesis, Q is chosen as an identity square matrix size of which depends on the number of states of the system and R is chosen as a variable scalar value.

After obtaining the full state-feedback gain vector K, closed loop state-space form of the system is calculated as shown below in Equations 4.9 and 4.10 where 'd' defines the disturbance signal.

$$\dot{x} = Ax + B(d - Kx) \qquad (4.9)$$
$$y = Cx + D(d - Kx) \qquad (4.10)$$

Equations 4.9 and 4.10 are changed into a form shown in Equations 4.11 and 4.12 and the closed loop state-space A_{cl} and C_{cl} matrices are found as in Equations 4.13 and 4.14.

$$\dot{x} = A_{cl}x + Bd \qquad (4.11)$$
$$y = C_{cl}x + Dd \qquad (4.12)$$

where,

$$A_{cl} = A - BK \qquad (4.13)$$
$$C_{cl} = C - DK \qquad (4.14)$$

In experimental studies, in order to control the vibrations of the smart beam via LQR controller, all the states have to be measurable. But, only the output 'y' which is measured from the sensor piezoelectric patch (S) of the smart beam is available. Observability of the system is checked. Hence, one way of dealing with this problem is designing an observer for the states of the dynamic system. In this thesis, instead of designing an observer, desired closed loop behavior of the system is obtained by using MATLAB and Simulink platforms and after obtaining the desired closed loop transfer function of the system and by using the transfer function of the plant, a controller transfer function is calculated to be used in an output feedback control system (Figure 4.4).
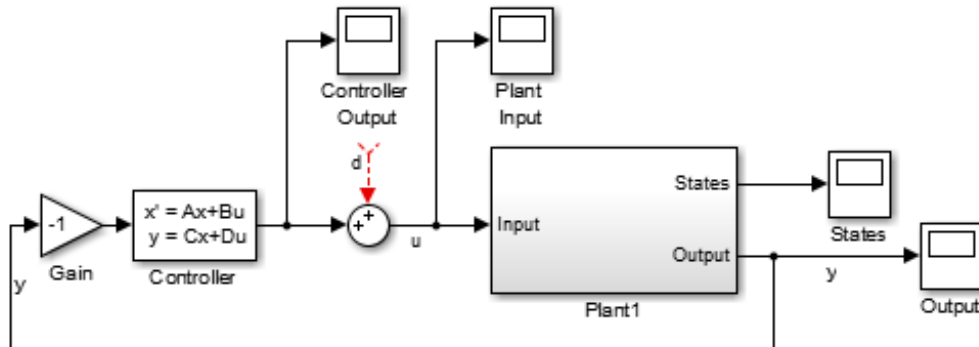
Figure 4.4 Output Feedback Control System Simulink Block Diagram

The desired closed loop transfer function of the system is,

$$\frac{y(s)}{d(s)} = G_{closed\ loop}(s) \qquad (4.15)$$

From the Figure 4.4,

$$y(s) = \left(-y(s) \times G_{controller}(s) + d(s)\right) \times G_{plant}(s) \qquad (4.16)$$

By using the Equation 4.16, the following (Equation 4.17) closed loop transfer function of the system can be calculated.

$$\frac{y(s)}{d(s)} = \frac{G_{plant}(s)}{\left(G_{plant}(s) \times G_{controller}(s)\right) + 1} \qquad (4.17)$$

Thus, the controller transfer function can be written in terms of the transfer function of the plant and the closed loop transfer function of the system as in the Equation 4.18.

$$G_{controller}(s) = \frac{G_{plant}(s) - G_{closed\ loop}(s)}{G_{closed\ loop}(s) \times G_{plant}(s)} \qquad (4.18)$$

Then, the transfer function of the controller is converted into a space-state form. Finally, for the experimental studies, the obtained continuous state-space form of the controller is converted into discrete form.

4.4 Performance Analysis of the Controller

By considering the output range of the xPC Target Machine input/output module and the deflection range of the tip of the smart beam at the first mode, a controller is designed for maximum performance when the servomotor arm angle is fixed at a particular angle. In the study, only the first resonance frequency region of the smart beam is considered.

4.4.1 Active Vibration Control Simulations

In this part, simulations of active vibration control of the smart beam for both free and forced vibrations are conducted. The state-space matrices of the 0° arm angle case is calculated by using the transfer function obtained in Chapter 3 (Table 3.5).

$$A = \begin{bmatrix} -20.5771 & -64.1702 & -37.5772 \\ 128.0000 & 0 & 0 \\ 0 & 32.0000 & 0 \end{bmatrix}$$

$$B = \begin{bmatrix} 1 \\ 0 \\ 0 \end{bmatrix}$$

$$C = \begin{bmatrix} -0.1875 & 1.2215 & -0.3964 \end{bmatrix}$$

$$D = 0.0188$$

By using MATLAB command 'pzplot', open loop poles and zeros of the system are plotted (Figure 4.5) and the eigenvalues of the system are found as,

$$\lambda_1 = -18.8$$
$$\lambda_2 = -0.881 + 90.4i$$
$$\lambda_3 = -0.881 - 90.4i$$

As all the eigenvalues have negative real part, the system is stable.
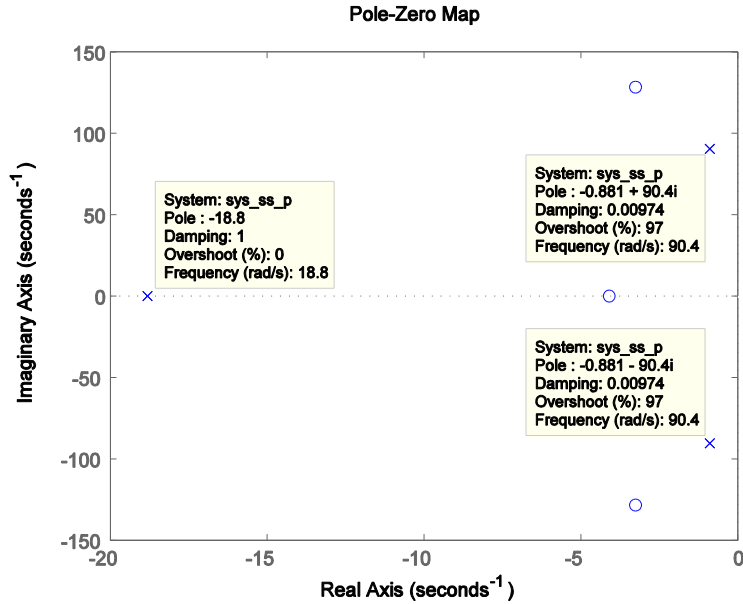
Figure 4.5 Open Loop Pole-Zero Map of the Plant (Case 3)

Controllability matrix is generated by using 'ctrb' command of the MATLAB and then 'rank' command is used to find the rank of the controllability matrix. The result is obtained as 3 which is the same as the number of n=3 (A is n by n matrix). Therefore, controllability of the system is verified.

In order to simulate free vibration of the smart beam by giving a tip displacement and letting the beam vibrate freely, an initial condition vector is needed for the plant model. First, ±0.5 Volt sine wave is applied to the input of the plant model and when the output voltage of the plant model is reached to a constant amplitude vibration, the voltage range of the output observed as ±0.48 V and at the time, when the output voltage of the plant model is measured as the peak voltage +0.48 V, states are recorded and are shown in Equation 4.19.

$$x_0 = \begin{bmatrix} -4.5930 \times 10^{-4} \\ 0.0031 \\ 5.6389 \times 10^{-8} \end{bmatrix} \tag{4.19}$$

For forced vibration suppression, ±0.5 Volt sine wave with 14.38 Hz frequency is applied to the input of the system and then when the output of the plant model is

reached to a constant amplitude vibration (±0.48 V), the controller signal is applied to the system.

The matrix Q (Equation 4.20) is chosen as a 3 by 3 identity matrix multiplied by a parameter α. For the scalar R value (Equation 4.21), symbol β is used. Here, only the relative value of Q and R parameters matters, not their absolute values. So, in this study, α is chosen as 1 and β is used as a variable and is changed to obtain maximum vibration suppression performance.

$$Q = \alpha \times \begin{bmatrix} 1 & 0 & 0 \\ 0 & 1 & 0 \\ 0 & 0 & 1 \end{bmatrix} \tag{4.20}$$

$$R = \beta \tag{4.21}$$

By using the MATLAB function "lqr" (Equation 4.22) which requires Q, R and the system (SYS) for the inputs, the full state feedback gain vector K is obtained as an output.

$$[K, S, e] = lqr (SYS, Q, R) \tag{4.22}$$

After obtaining the K vector, frequency response functions, pole-zero maps, free vibration responses and forced vibration responses are plotted for different β values.
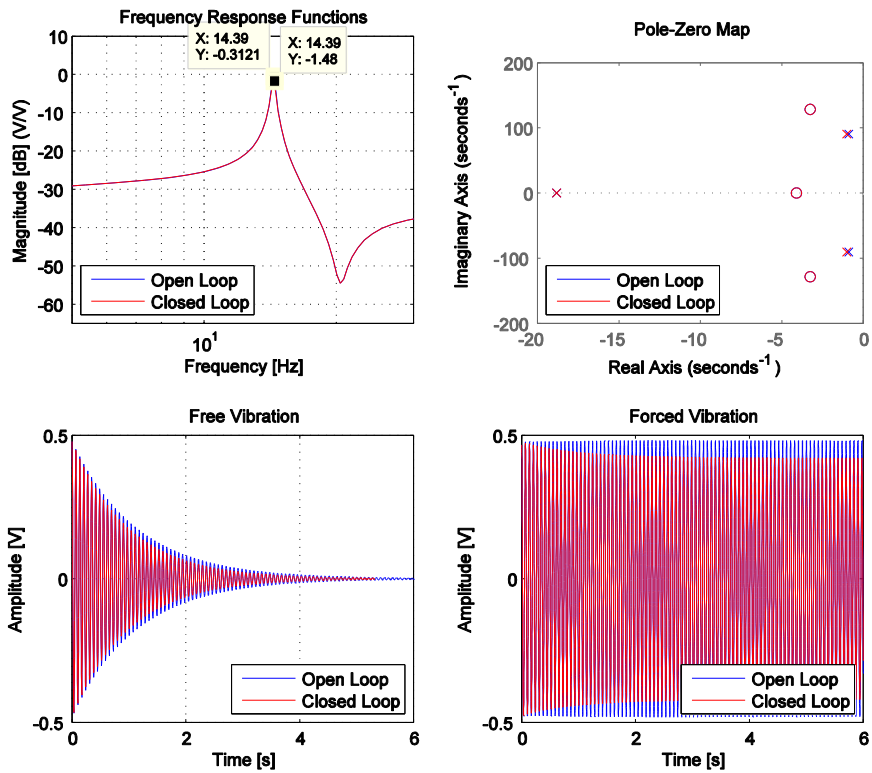
Figure 4.6 Simulation Results for β=1
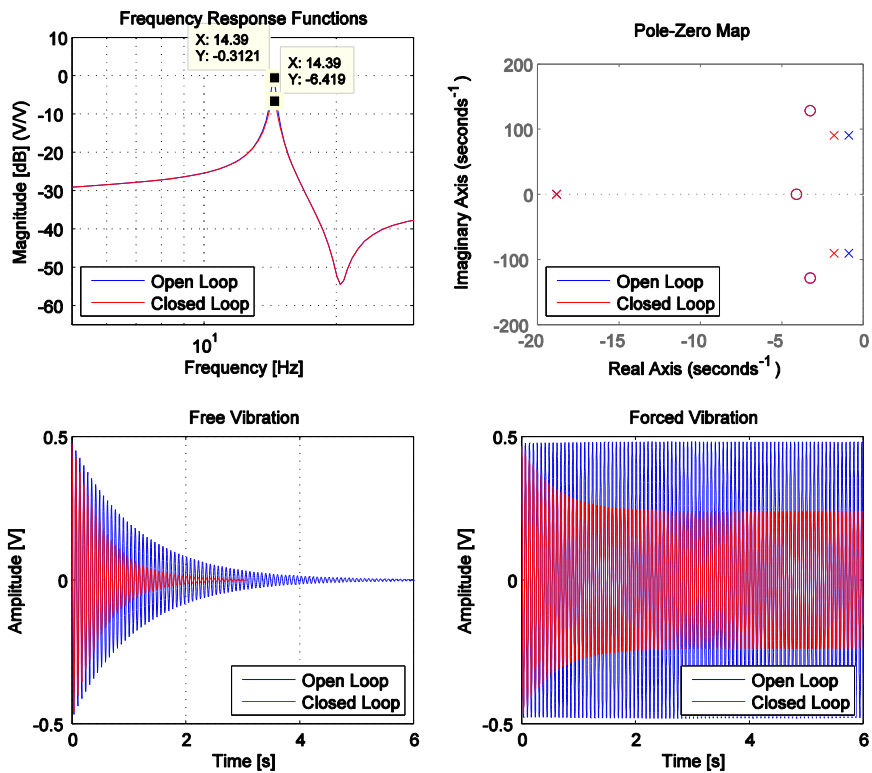
Figure 4.7 Simulation Results for β=0.1
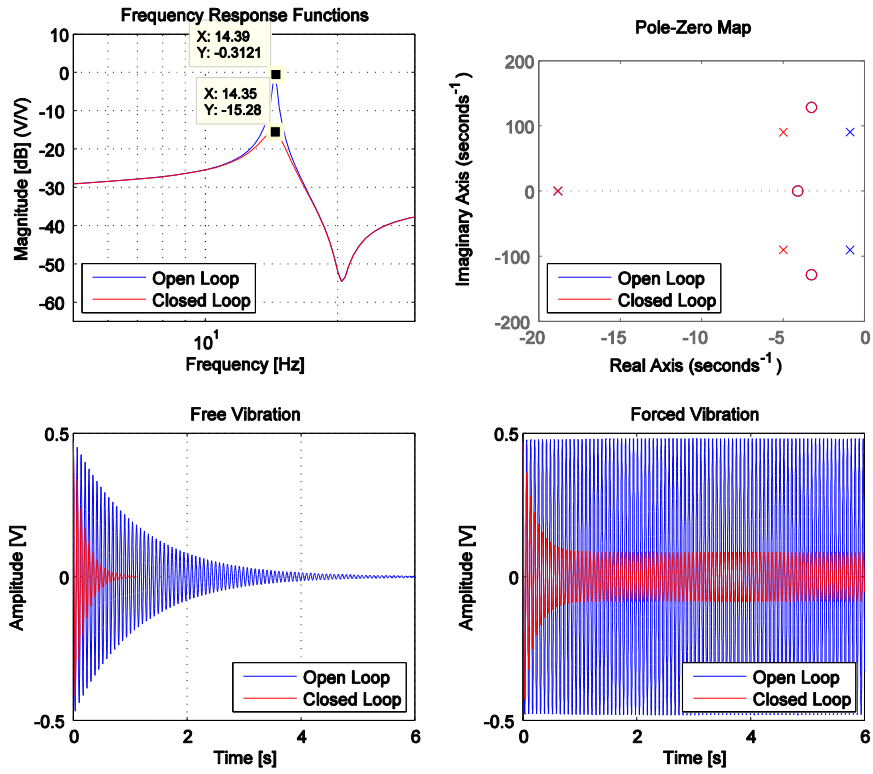
Figure 4.8 Simulation Results for β=0.01
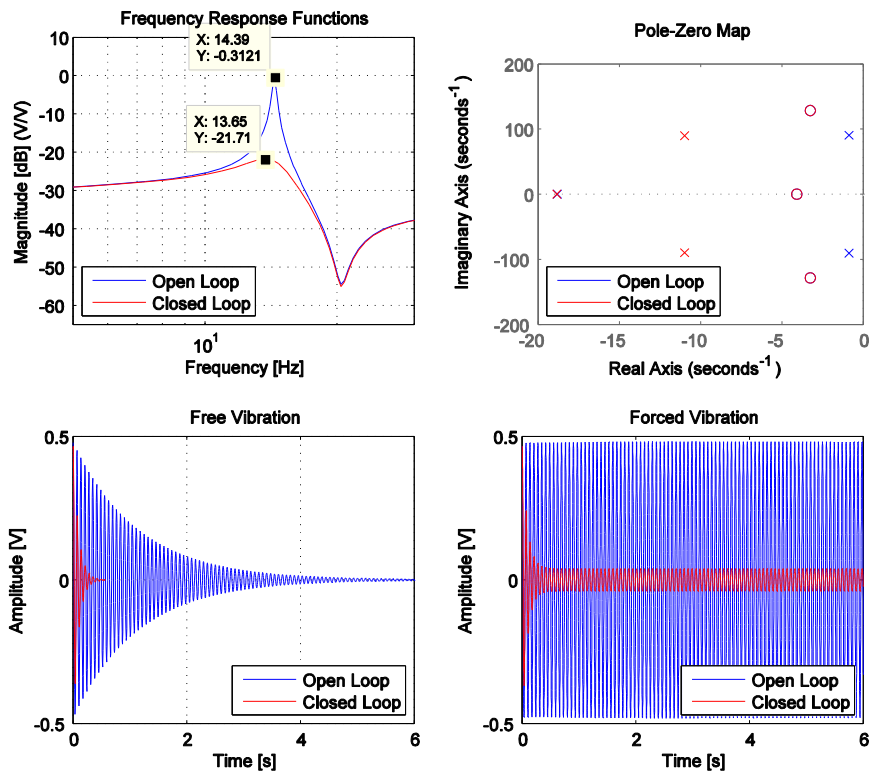
Figure 4.9 Simulation Results for β=0.002
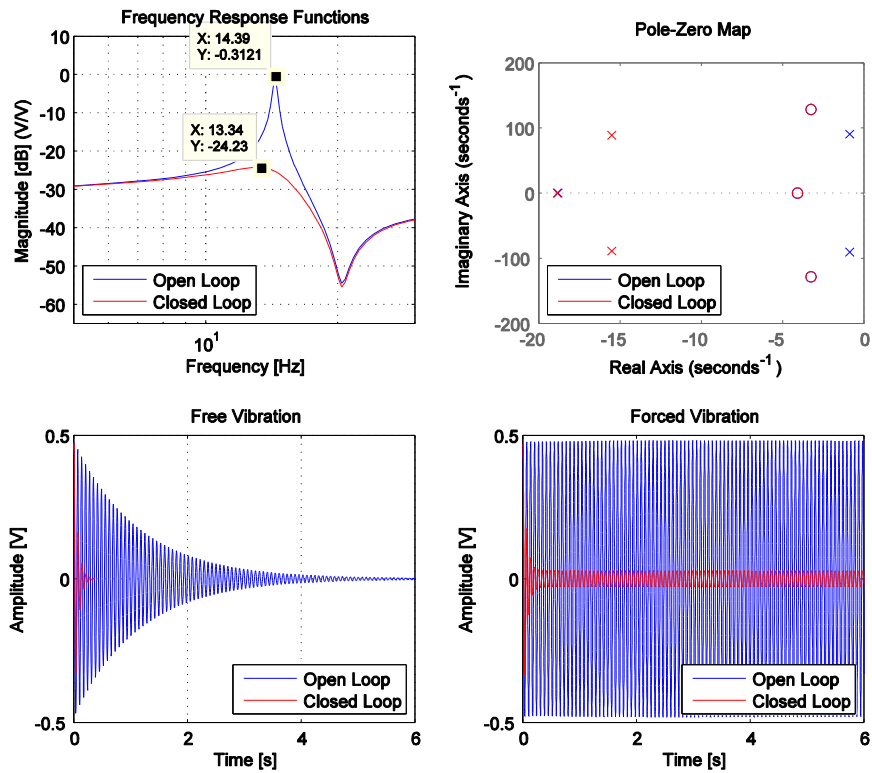
Figure 4.10 Simulation Results for β=0.001

Without the controller, the settling time for the initial condition x_0 is approximately 5.2 seconds with an error band of ±0.005 V. The variable β is decreased until the maximum voltage of the controller output is passed the maximum allowed input voltage of the system (i.e. ±9V).

Table 4.1 Results of the LQR Controller Simulations

Parameters	Gain [dB]	Controller Output [V] (Maximum)	Settling Time [s]	Forced Vibration Suppression
α=1, β=1	-1.17	0.14	4.5	12 %
α=1, β=0.1	-6.11	0.96	2.57	50 %
α=1, β=0.01	-14.97	3.93	0.95	82 %
α=1, β=0.002	-21.40	8.40	0.42	92 %
α=1, β=0.001	-23.92	10.80	0.30	94 %

56

From the Table 4.1, it can be seen that the controller having maximum performance for the initial condition is obtained for α=1, β=0.002 values. The following Table 4.2 shows the eigenvalues of the system with the best controller shown in Figure 4.9.

Table 4.2 Eigenvalues of the Open Loop and Closed Loop System

Open Loop	Closed Loop
$\lambda_1 = -18.8$	$\lambda_1 = -18.8$
$\lambda_2 = -0.881 + 90.4i$	$\lambda_2 = -11 + 89.7i$
$\lambda_3 = -0.881 - 90.4i$	$\lambda_3 = -11 - 89.7i$

This, so called the best performance controller decreased the settling time of the system from 5.2 seconds to 0.42 seconds for the given initial condition. It also decreased the forced vibration amplitude by approximately 92 %.

4.4.2 Active Vibration Control Experiments

In this part, the experimental studies are conducted to analyze the free and forced vibration suppression performance of the designed controller. Without giving any disturbance and control signal to the system, to analyze noise level and DC offset of the sensor signal, an experiment is performed by using the Simulink model shown in Figure 4.11. The signal measured from the sensor piezoelectric patch is recorded and plotted (Figure 4.12). As a result, the maximum noise level is found as 12 mV and the DC offset of the sensor is obtained as -0.0175 V. This value is subtracted from the input module Simulink block of the xPC Target Machine.
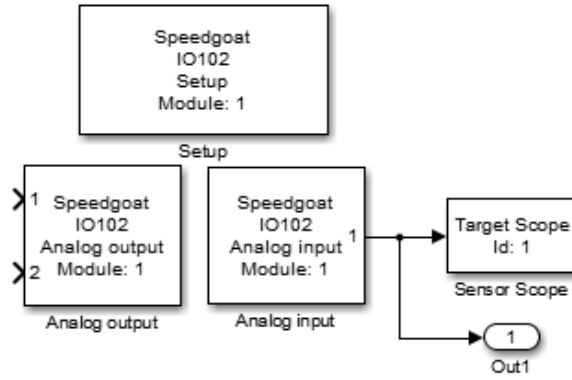
Figure 4.11 Simulink Model for Sensor Measurement
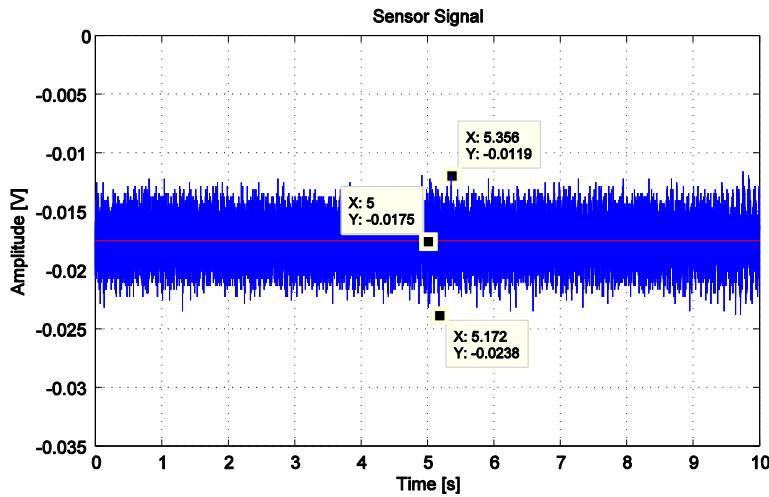
Figure 4.12 Noise Level and DC Offset of the Sensor Signal

The closed loop transfer function of the smart beam with 0° servomotor arm angle configuration is calculated by using the Equation 4.23 where α=1, β=0.002.

$$G_{closed\ loop}(s) = \frac{0.01879\ s^3 + 0.1993\ s^2 + 310.8\ s + 1269}{s^3 + 40.8\ s^2 + 8584\ s + 1.539e05} \qquad (4.23)$$

Transfer function of the plant model is known and therefore the transfer function used for a controller in the experimental studies can be calculated by using the Equation 4.18. This transfer function is then converted into a discrete state-space form by using 10 kHz as the sample rate in MATLAB.

$$G_{controller}(s) = \frac{1076\ s^2 + 1.972e04\ s + 0.08642}{s^3 + 10.6\ s^2 + 1.653e04\ s + 6.752e04} \qquad (4.24)$$

58

4.4.2.1 Free Vibration Suppression

Analysis of the free vibration of the smart beam is performed by giving a displacement to the tip of the smart beam which makes the initial measured sensor value approximately ±0.48V. In the first bending mode, displacement at the tip of the smart beam corresponds to the maximum curvature at the root of the smart beam. The displacement range at the tip of the smart beam is measured as approximately 1 mm when the measured value from the analog input of the target machine is observed as ±0.48V.

To measure the response of the smart beam to the initial condition without applying a controller (i.e. Open loop system), the Simulink model in Figure 4.11 is used. The following Simulink block diagram (Figure 4.13) is created to record controller output and the sensor signal for free vibration suppression analysis with controller (i.e. Closed loop system). The previously obtained DC offset value of the sensor signal is used by adding bias block and a saturation block is also added for the maximum allowed input voltage range of the system. In Figure 4.14, open and closed system time responses to the initial condition and the corresponding controller signal is shown. Zoomed plot of the free vibration suppression experiment can be seen in Figure 4.15.
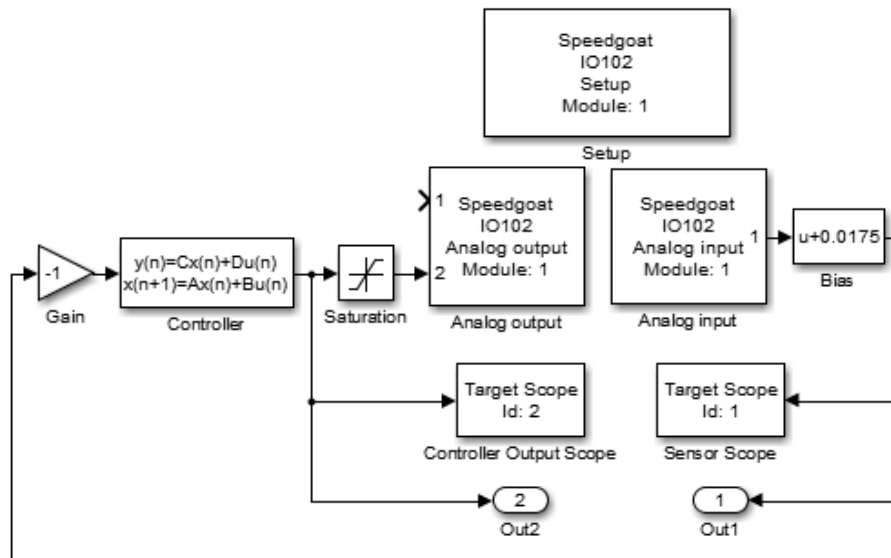
Figure 4.13 Simulink Model for Free Vibration Suppression Experiment
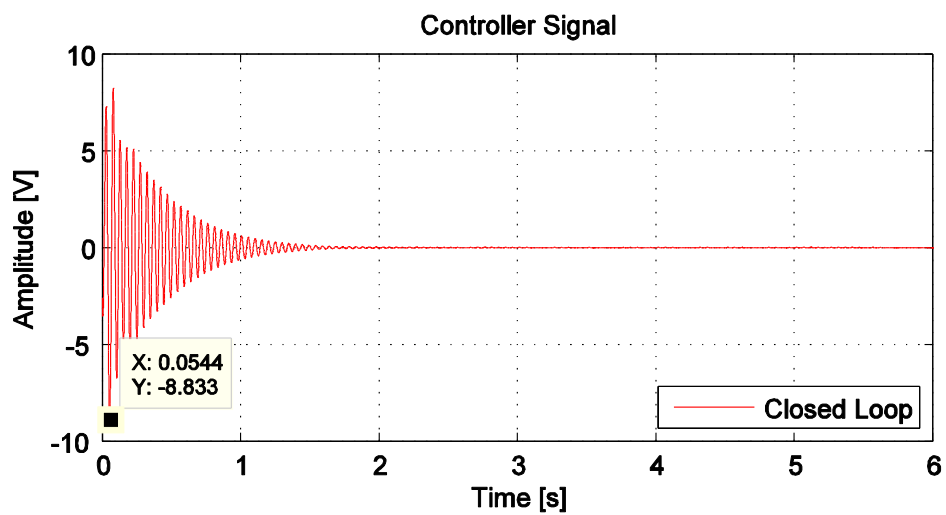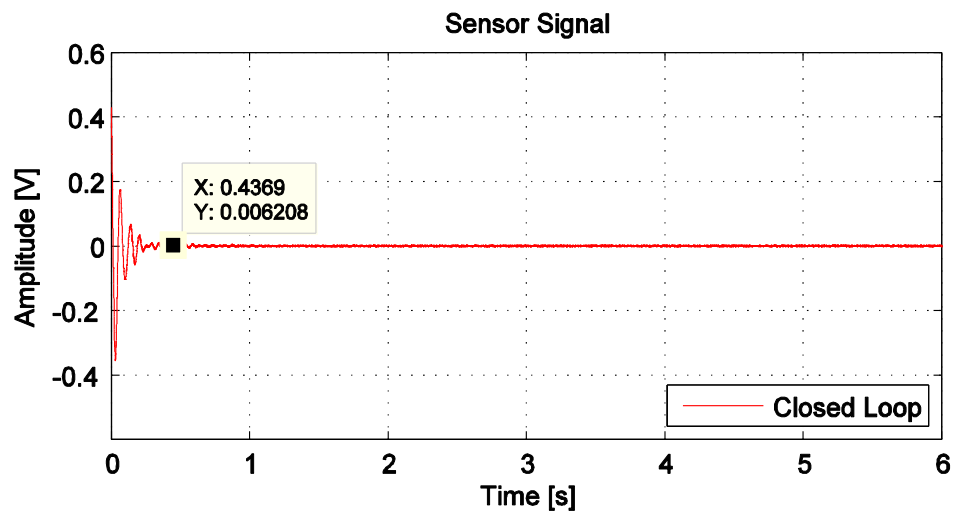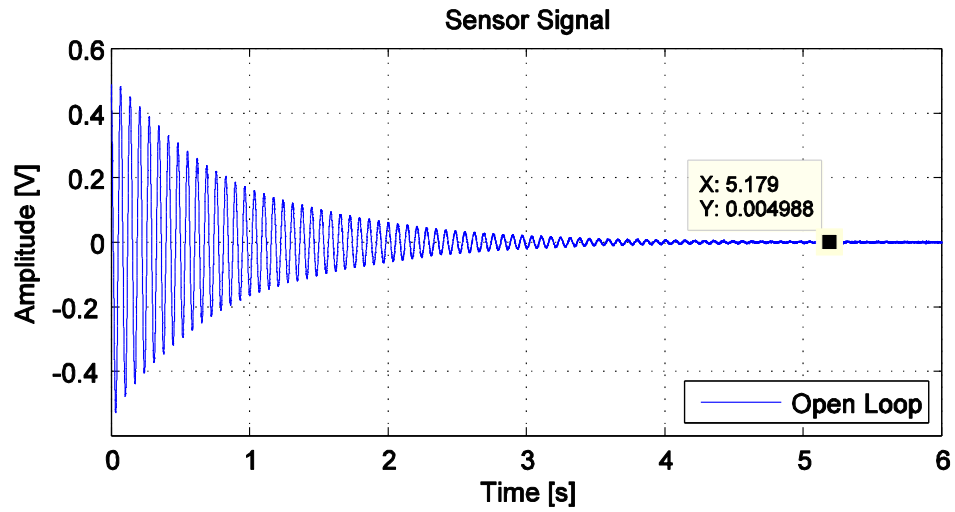
Figure 4.14 Plots of the Free Vibration Suppression Experiments
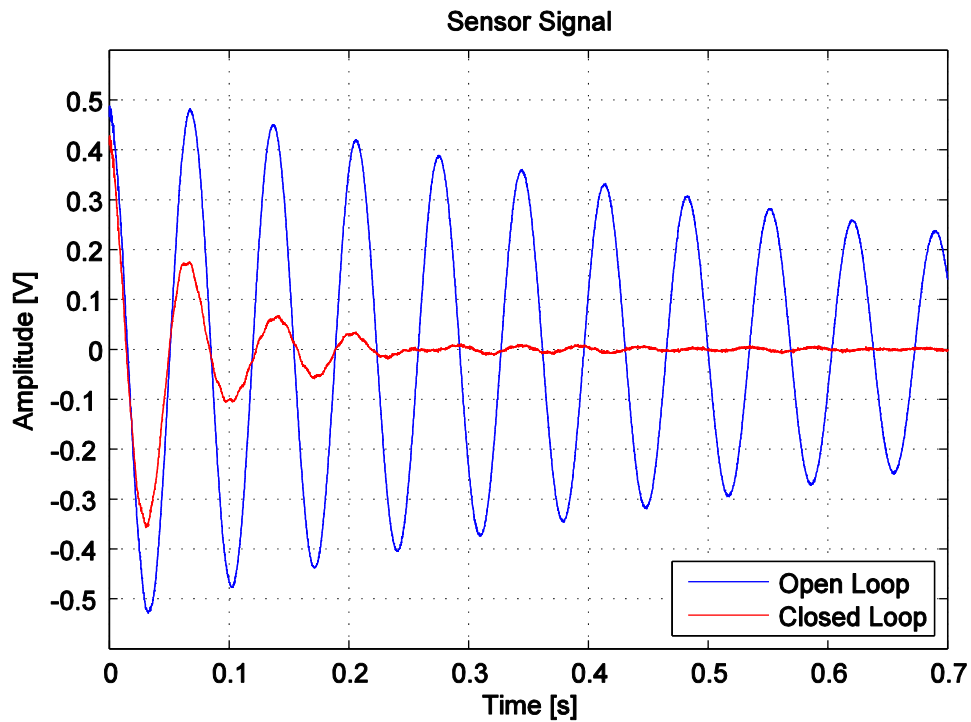
Figure 4.15 Zoomed Plot of the Free Vibration Suppression Experiment

As a result, the settling time values are measured approximately as 5.18 and 0.44 seconds for open loop and closed loop systems respectively. Table 4.3 shows the comparison of the free vibration suppression simulation and experiment results of the smart beam to the given the initial condition.

Table 4.3 Free Vibration Suppression Simulation and Experiment Results

	Settling Time [s]		Controller Output [V]
	Open Loop	**Closed Loop**	**(Maximum Absolute)**
Simulation	5.20	0.42	8.40
Experiment	5.18	0.44	8.83

61

4.4.2.2 The First Resonance Forced Vibration Suppression

Analysis of the first resonance forced vibration suppression is performed by applying a sine wave at 14.38 Hz frequency to the disturbance piezoelectric patch (D) and applying a controller signal to the actuator piezoelectric patches (A1&A2). Forced vibration simulations were made for the vibrating beam when the sensor amplitude shows ±0.48V. This was obtained by applying ±0.5V sine wave to the plant which is (A1&A2 and S) PZT configuration model. However, in the experimental study, the signal at the first resonance frequency of the smart beam is applied to the disturbance piezoelectric patch (D). So, in order to find the amplitude of this sine wave, the magnitude (-7.825 [dB]) at the resonance frequency in (D-S) PZT configuration (Figure 3.7) and the magnitude (-0.3312 [dB]) at the resonance frequency in (A1&A2-S) PZT configuration (Figure 3.19) are used. Voltage ratios for -7.825 [dB] and -0.3312 [dB] level are calculated as 0.41 and 0.96 respectively. Equation 4.26 shows the amplitude of the sine wave at 14.38 Hz frequency to get the vibration when the sensor amplitude shows ±0.48V. For the first resonance forced vibration suppression experiment, a Simulink model is designed and it can be seen in Figure 4.16.

$$0.41 \times Amplitude = (0.96) \times (0.50 \, [V]) \tag{4.25}$$

$$Amplitude = 1.17 \, [V] \tag{4.26}$$
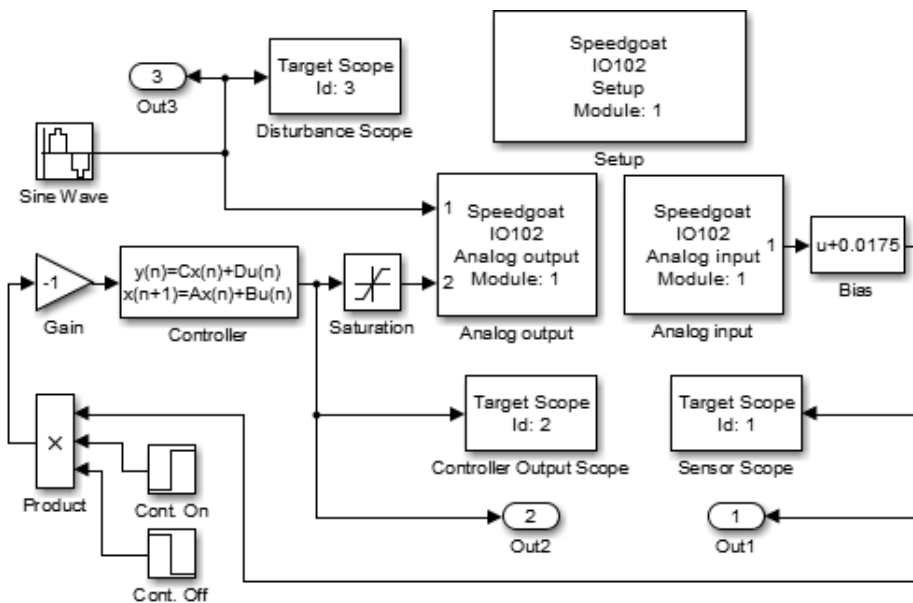
Figure 4.16 Simulink Model for Forced Vibration Suppression Experiment

This experiment lasts 30 seconds. First, a sine wave at the smart beam's resonance frequency is applied to the Channel 1 for 10 seconds (i.e. Open loop system). After that the controller is applied to the system from Channel 2 for again 10 seconds (i.e. Closed loop system) and then, the controller is removed to let the smart beam vibrate at its first resonance frequency again (i.e. Open loop system). Figure 4.17 shows the recorded sensor and controller signals of the first resonance forced vibration suppression experiment. The open and the closed loop response plots of the forced vibration experiments of the smart beam can also be seen in Figure 4.18.
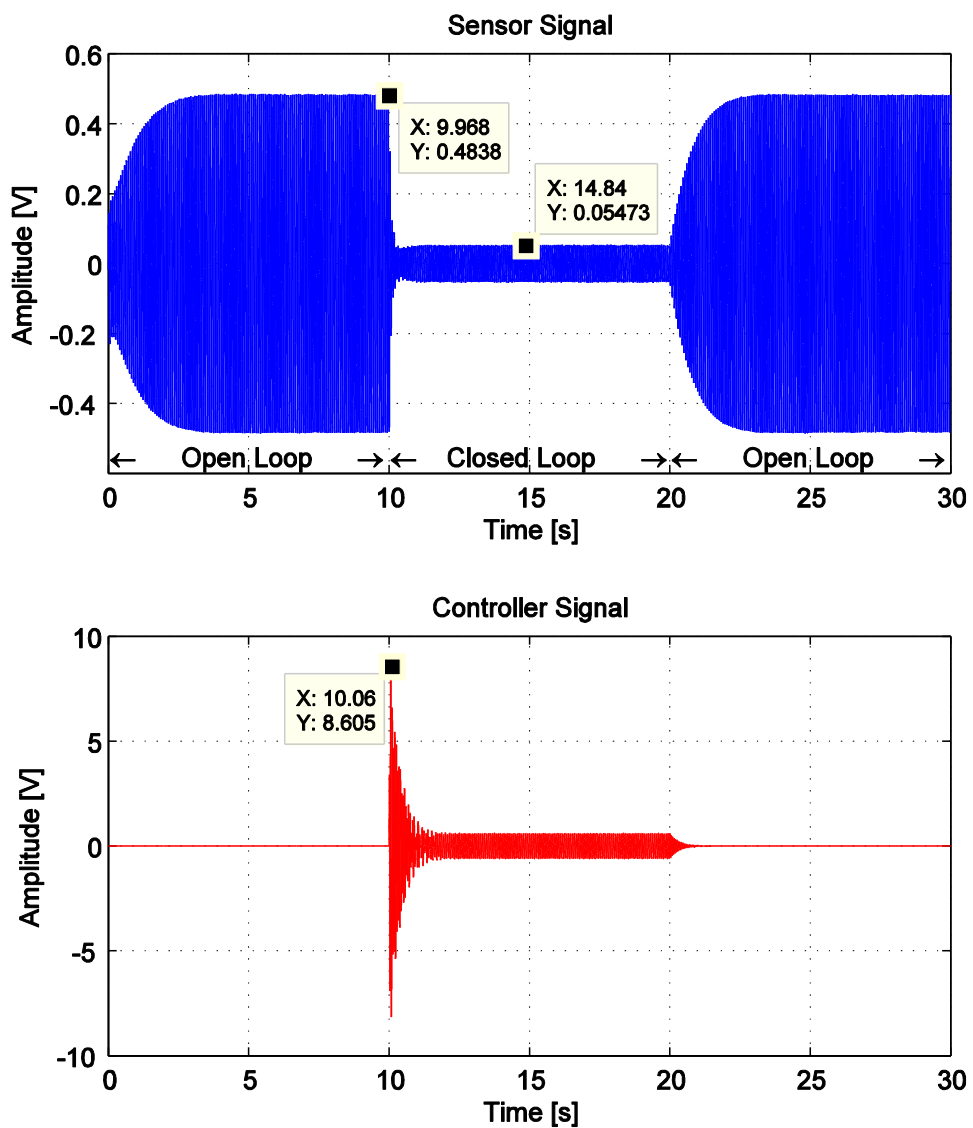
Figure 4.17 Plots of the Forced Vibration Suppression Experiment
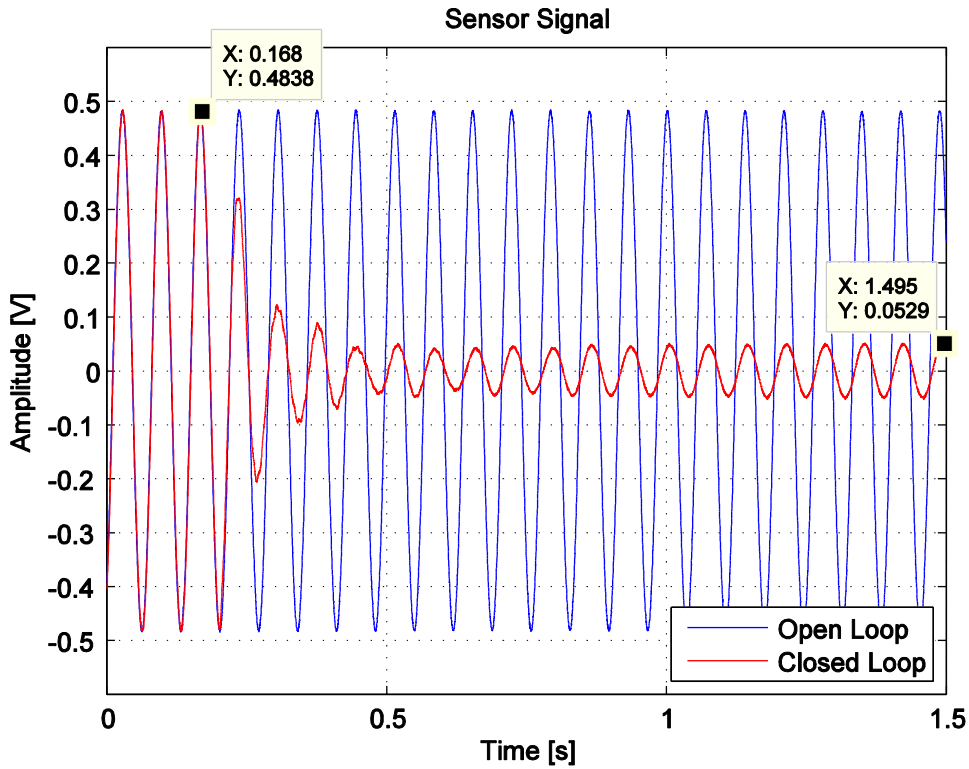
Figure 4.18 Open and Closed Loop Plots of the Forced Vibration Experiments

The forced vibration suppression performance of the controller is calculated as 89 % which is very close to the percentage value obtained by the simulations. Table 4.4 shows the comparison of the forced vibration suppression simulation and experiment results of the smart beam.

Table 4.4 Forced Vibration Suppression Simulation and Experiment Results

	Suppression Performance (Percentage)	Controller Output [V] (Maximum Absolute)
Simulation	92 %	8.40
Experiment	89 %	8.60

4.4.2.3 Experimentally obtained Frequency Response Functions

Experiments are performed in order to obtain the frequency response functions for both open and closed loop systems. The smart beam is excited with piezoelectric patches (A1&A2) by applying a chirp signal (1-40 Hz) and the response of the smart beam is measured with sensor piezoelectric patch (S). The following Simulink block diagram (Figure 4.19) is designed to perform the experiments.
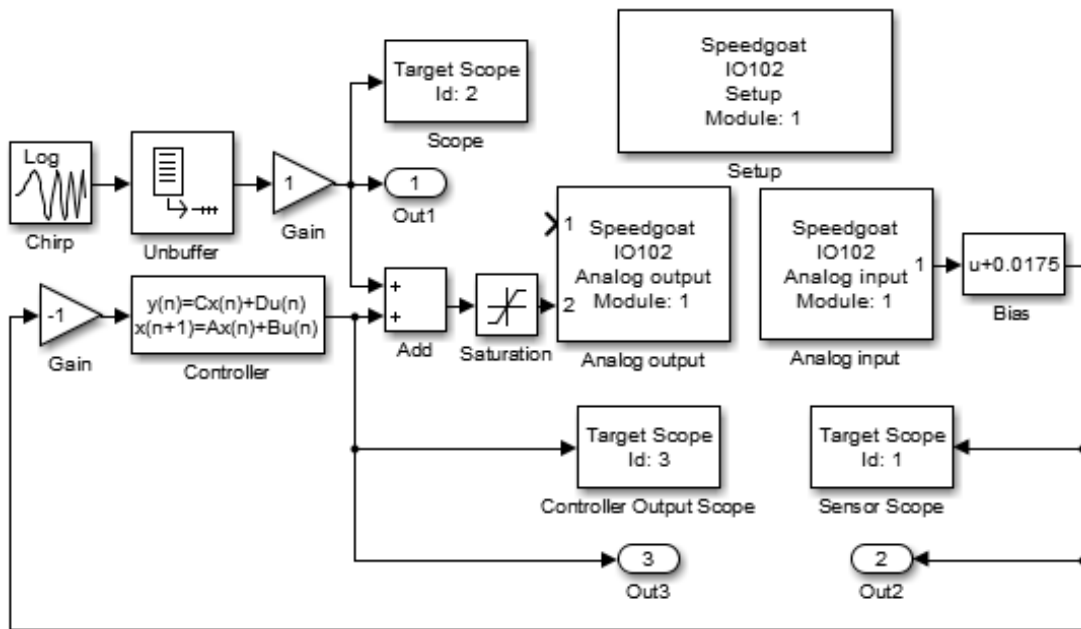
Figure 4.19 Simulink Model for Experimental Frequency Response Functions

Two different experiments are conducted to get time domain excitation, response and controller output signals for both open and closed loop systems. By using these recorded signals for one of the repeated swept-frequency excitation signal, the system responses and controller signal are plotted (Figure 4.20). After analyzing the time domain data in MATLAB, the frequency response functions (Figure 4.21) are obtained and plotted in the range of 5-30 Hz. The obtained closed loop experimental results are observed to be in good agreement with the simulation results (Table 4.5).
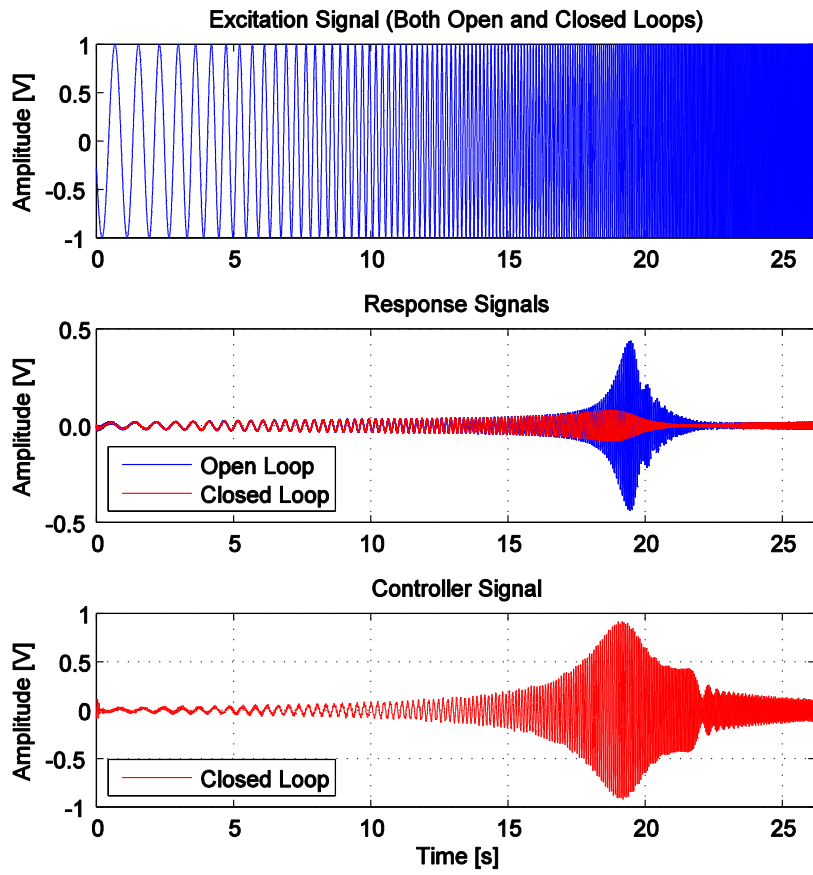
Figure 4.20 Excitation, Response and Controller Output Signals
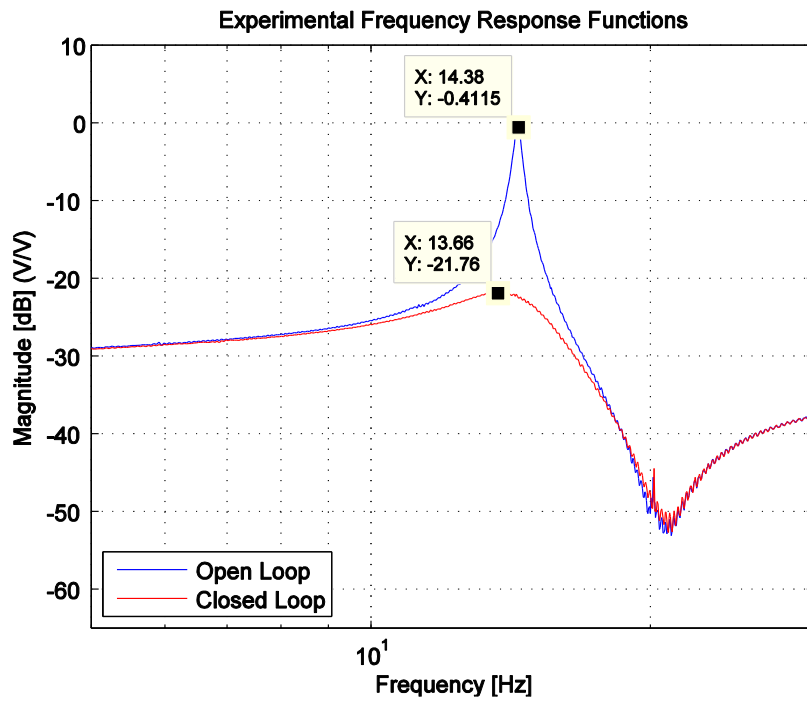
Figure 4.21 Experimental Open and Closed Loop Frequency Response Functions

66

Table 4.5 Closed Loop Peak Frequency and Magnitude

	Frequency [Hz]	**Magnitude [dB]**
Simulation	13.65	-21.71
Experiment	13.66	-21.76

4.4.3 Effect of Plant Variation to the Closed Loop System

The designed controller (Equation 4.24) is used to control the vibrations of the smart beam for the Case 3 (0° arm angle configuration) successfully. In this part, the controller is kept the same and the arm angle of the smart beam is changed to various configurations and the corresponding behavior of the closed loop system is observed. The closed loop pole-zero plots of the systems are plotted (Figure 4.22) and it is observed that the controller and the plant combinations (i.e. For Case 1, Case 2, Case 4) are stable except the Case 5. The particular case has poles on the right half plane of the complex plane and these poles are corresponding to the frequency of 20.7 Hz making the system unstable. Closed loop FRFs for different cases are shown in Figure 4.23 and the undesired peak can also be seen for the Case 5. For each case, maximum peak value and its corresponding frequency value for the closed loop system is found (from Figure 4.23) and listed in the Table 4.6. The obtained values for the Case 3 is also added to this table for comparison purposes and the maximum peak value is also taken for the resonance frequency region except the undesired peak value occurred at 20.7 Hz (see in Figure 4.23, Case 5).
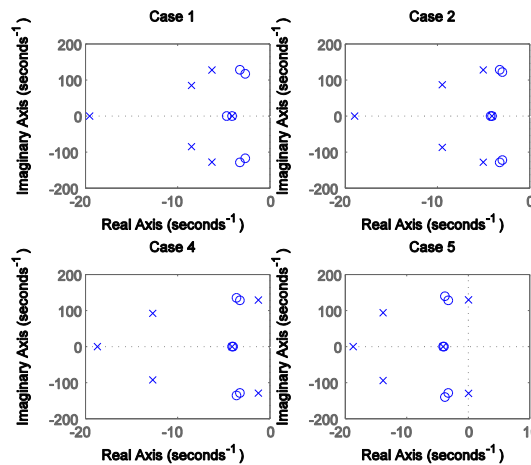
Figure 4.22 Closed Loop Pole-Zero Maps for Different Plants
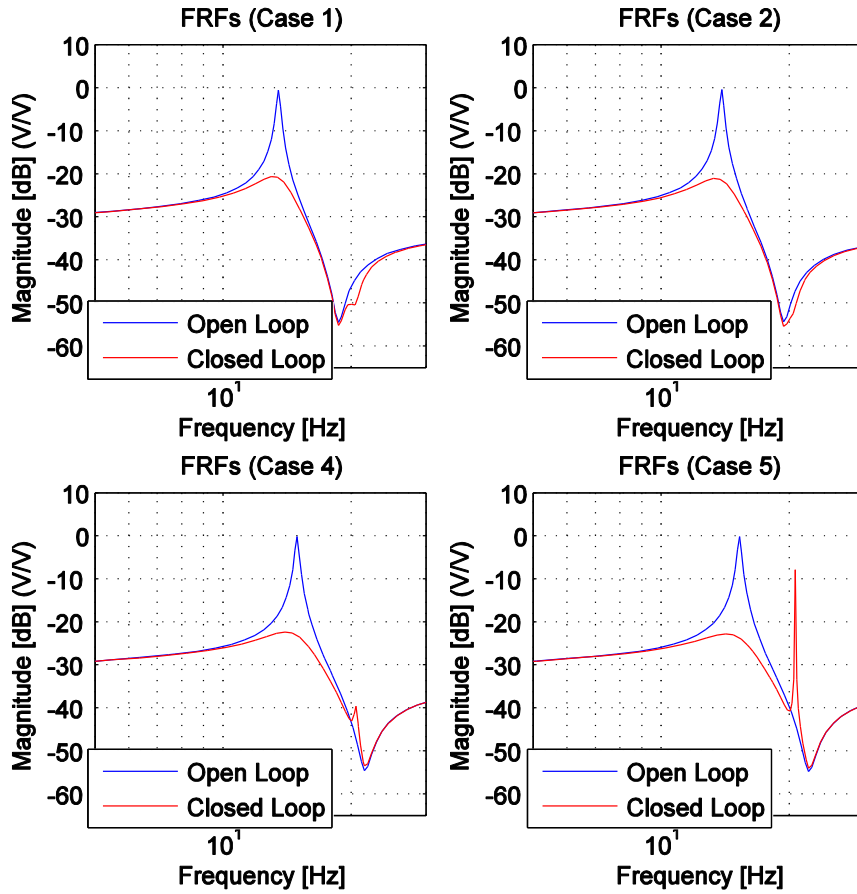
Figure 4.23 FRFs for Different Closed Loop Systems

Table 4.6 Closed Loop System Maximum Peak Frequencies and Magnitudes at
Corresponding Frequencies for Different Plant Cases

Arm Angle Cases	Frequency [Hz]	Magnitude at the Frequency [dB]
Case 1: +64°	12.98	-20.63
Case 2: +32°	13.28	-21.08
Case 3: 0°	13.68	-21.71
Case 4: -32°	13.99	-22.37
Case 5: -64°	14.19	-22.79

It can be seen from the Table 4.6 that as servomotor arm moves to the tip of the smart beam, the forced vibration suppression performance decreases at the corresponding frequencies. On the contrary, the forced vibration suppression performance increases as the arm moves towards to the root of the smart beam. The dB levels are close to each other for all the cases.

However, using the designed controller (i.e. the control designed for Case 3) to the plant in Case 5 making the closed loop system unstable which is a problem to be considered. For this particular case, an experiment is conducted to observe the unstable behavior of the closed system. As in the free vibration experiments, the Simulink block diagram shown in Figure 4.13 is used. There is not a specific sine wave disturbance in this experiment but there is a disturbance which is externally applied in a short time at the tip of the smart beam. Then, the response of the smart beam is recorded as shown in the Figure 4.24 and the divergent signal frequency is found as approximately 20.7 Hz as expected.
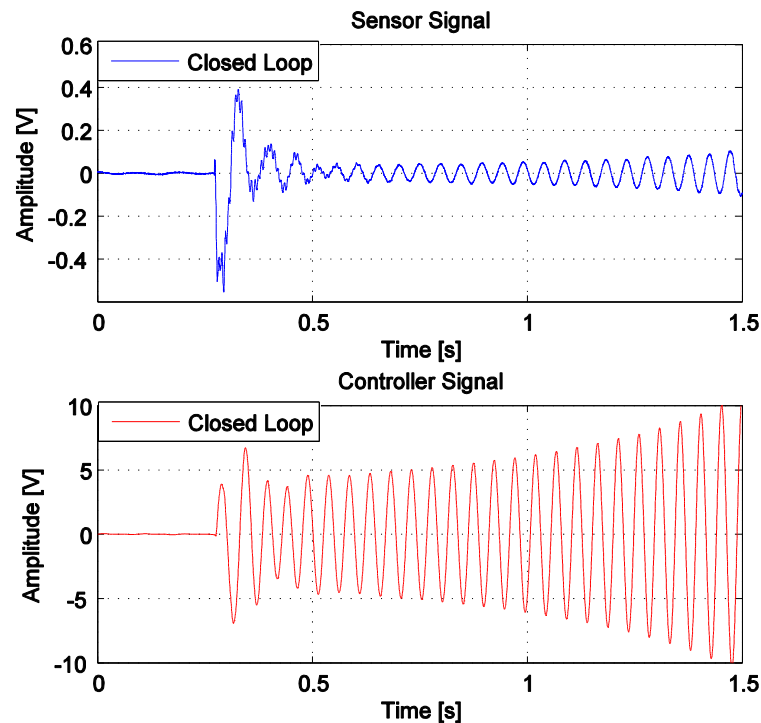
Figure 4.24 Experimental Results for Case 5 (-64° Arm Angle)

4.5 Conclusion

In this chapter, full state feedback controller is designed by using linear quadratic regulator (LQR) method. The LQR gains are calculated for different parameters and by considering the tip deflection range of the smart beam (i.e. initial condition) and the maximum voltage range of the analog output of the IO102 module, the best LQR gain is also decided. Simulations are performed for free and forced vibration suppression. In the free vibration simulation study, it is found that the designed controller decreases the settling time of the system from 5.2 seconds to 0.42 seconds. In the forced vibration simulation study, it is found that the performance of the controller is approximately 92%. For the experimental studies, in the free vibration suppression, the designed controller decreases the settling time of the smart beam from 5.18 to 0.44. Furthermore, by applying a sine wave at the smart beam's resonance frequency, the forced vibration suppression experiments are performed and the performance of the controller is obtained as approximately 89%. Considering the time domain, experimental results are in good agreement with the results obtained from the simulations. Additional experiments are performed in order to observe the closed loop behavior of the smart beam in the frequency domain and the FRF of the smart beam is found almost the same with the results obtained through the simulations. Moreover, effect of the plant variation to the closed loop behavior of the system is observed by using the designed controller. It is found that the variation of the plant causes performance change and also it may affect the stability of the system when excessive variation occurs.

CHAPTER 5

ACTIVE VIBRATION SUPPRESSION OF THE SMART BEAM WITH A NEURAL NETWORK BASED ADAPTIVE ELEMENT

5.1 Introduction

In this chapter, design and test of a neural network based adaptive element are presented. Firstly, design of a multilayer feedforward neural network with back propagation algorithm is described. Then, a neural network based adaptive element is designed and added to the system and training of the neural network is performed. Following this, forced and free vibration simulations are investigated to observe the behavior of the closed loop system in case of a plant variation. Finally, forced and free vibration suppressions of the plant is achieved experimentally.

5.2 Multilayer Feedforward Neural Network with Back-Propagation Algorithm

An artificial neural network is a computing system inspired by the structure and functions of neural networks in biological systems. It is presented as interconnected processing elements called as neurons. The block diagram in Figure 5.1 shows the model of a neuron which is a fundamental unit in the neural network.

Mathematical model of the neuron k shown in Figure 5.1 is described as follows [46]:

$$y_k = \varphi \left(\sum_{j=1}^{m} \omega_{kj} x_j + b_k \right) \qquad (5.1)$$

where, $x_1, x_2, x_3 \ldots x_m$ are the input signals, $\omega_{k1}, \omega_{k2}, \omega_{k3} \ldots \omega_{km}$ are the respective weights of the neuron k, ω_{k0} is the bias, φ is the activation function, and y_k is the output signal of the neuron.
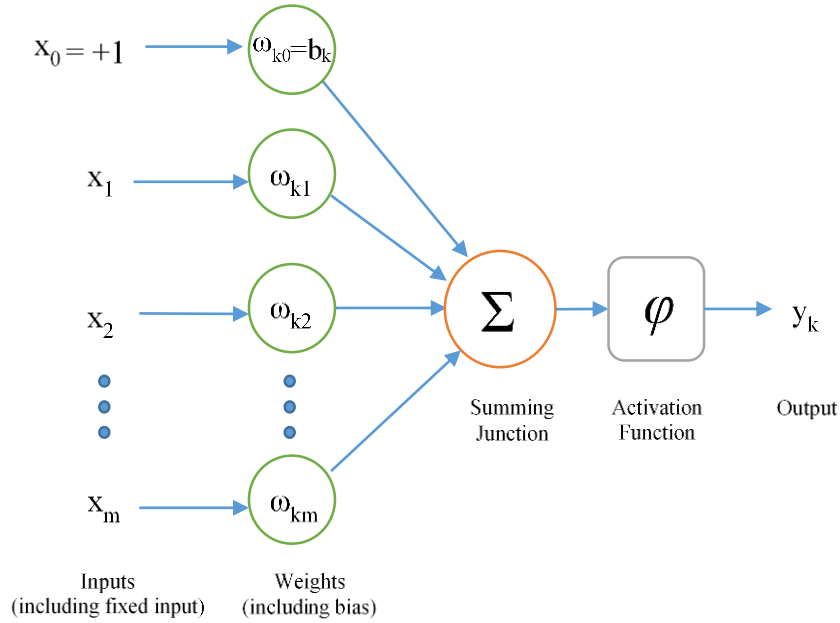
Figure 5.1 Model of a Neuron Labeled as (k)

One of the most common artificial neural networks used in control field is the multilayer perceptron which is constructed by ordering the neurons in layers. A multilayer perceptron consists of an input layer, one or more hidden layers and an output layer. A multilayer feedforward neural network with one hidden layer (containing a sufficient number of units) is capable of approximating any continuous function to any degree of accuracy [47].

For the activation function, hyperbolic tangent sigmoid defined in Equation 5.2 is used. Because of its differentiability, it is commonly used in multilayer networks which are trained by using back-propagation algorithm. Derivative of the transfer function is required for computation of the local gradients.

$$\varphi(x) = \frac{1 - e^{-x}}{1 + e^{-x}} \tag{5.2}$$

The activation function φ limits the output of the neuron. The hyperbolic tangent sigmoid takes the input value between plus and minus infinity and gives an output value between -1 and 1. It is possible to use different activation functions for different neurons, but in this thesis, the hyperbolic tangent sigmoid is used for all neurons in the neural network. The output voltage range between -1 to 1 is suitable for vibration control signals but to apply signal within the voltage range of the smart beam system, scaling factor is applied to the neural network.

Learning is one important property of neural networks. Supervised learning methods are commonly used in active vibration control field [48] . In supervised learning neural networks, weights are adjusted to get a desired response. However, in unsupervised learning neural networks, there is no teacher to provide a desired response. It is used for finding patterns or grouping in data.

There are two different methods used in supervised learning of the multilayer perceptron. They are namely batch learning and online learning. In the batch method of supervised learning, weights of the multilayer perceptron are adjusted after the presentation of all examples in the training sample. This training sample data constitute one epoch of training. In the online method of supervised learning, weights of the multilayer perceptron are adjusted after presentation of each individual input vector. For batch learning, the cost function is defined by the average error energy. However, for online learning, the cost function is the total instantaneous error energy. In this thesis, online learning which is also called as incremental learning is used as the neural network training method.

The backpropagation algorithm is a popular method for training the neural network. The training proceeds in two propagations as forward and backward. In the forward propagation, the input signal propagates layer by layer until it reaches the output of the network. The weights remain unchanged throughout the network and outputs of each neuron in the first layer are computed by using the input vector. Then, they are forwarded to the next layer to be used for the next layer's neurons.

As an example, a graphical description of neural network with back-propagation is given in Figure 5.2. Top part of the figure (i.e. black color) is the forward pass and the bottom part of the figure (i.e. blue color) is the backward pass. There are 2 inputs, 2 hidden neurons and 2 output neurons.
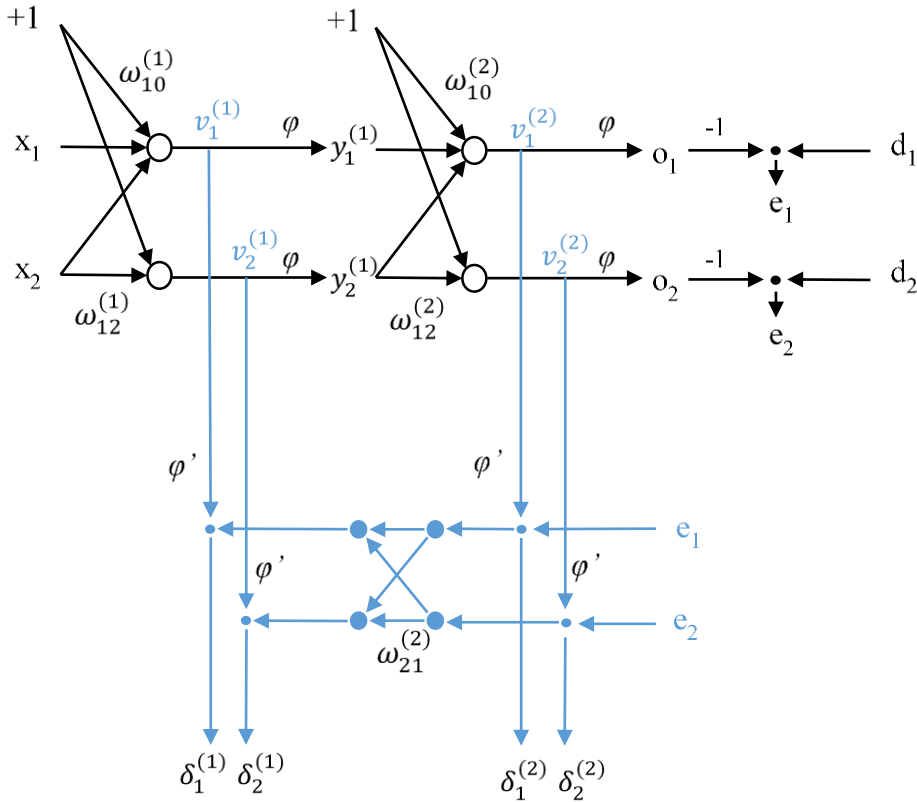
Figure 5.2 Graphical Description of a Back-Propagation Learning

The induced local field $v_j^{(l)}$ for neuron j in layer l is calculated as;

$$v_j^{(l)} = \sum_i \omega_{ji}^{(l)} y_i^{(l-1)} \tag{5.3}$$

where, $y_i^{(l-1)}$ is the output signal of neuron i in the previous layer $l-1$ and $\omega_{ji}^{(l)}$ is the weight of neuron j in layer l that is fed from neuron i in layer $l-1$.

For $i = 0$, the fixed input and the weights of its connections applied to neuron j in layer l are shown as;

$$y_0^{(l-1)} = +1 \tag{5.4}$$

$$\omega_{j0}^{(l)} = b_j^{(l)} \tag{5.5}$$

The output signal of neuron j in layer l is,

$$y_j^{(l)} = \varphi_j(v_j) \tag{5.6}$$

For the jth element of the input vector and j^{th} element in the output vector respectively are shown as,

$$y_j^{(0)} = x_j \tag{5.7}$$

$$y_j^{(L)} = o_j \tag{5.8}$$

where, L is referred to the depth of the network which is 2 for the multilayer perceptron with one hidden layer.

The error signal which is obtained by subtracting the output of the network from the desired output is shown as,

$$e_j = d_j - o_j \tag{5.9}$$

where d_j is the jth element of the desired response vector. For vibration control of the smart beam, the output of the neural network is a scalar value and the desired output value is zero.

Matrix form of the forward calculation is obtained from individual variable form of the equations and the Simulink block diagram of the forward calculation which is shown in Figure 5.3, is created.
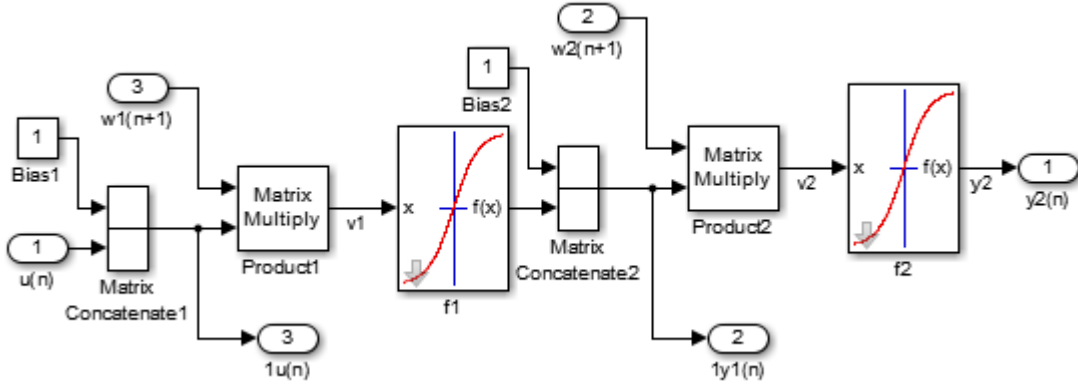
Figure 5.3 Forward Calculation Simulink Block Diagram

For backward propagation, computation of the local gradients are defined as [46];

$$\delta_j^{(l)} = \begin{cases} e_j^{(L)} \; \varphi_j{}'(v_j^{(L)}) \\ \varphi_j{}'(v_j^{(l)}) \sum_k \delta_k^{(l+1)} \; \omega_{kj}^{(l+1)} \end{cases} \tag{5.10}$$

where $\varphi_j{}'$ is differentiation of the transfer function.

According to generalized delta rule, adjustment of the weights of the neural network in layer l is [46],

$$\omega_{ji}^{(l)}(n+1) = \omega_{ji}^{(l)}(n) + \alpha \left[\Delta\omega_{ji}^{(l)}(n-1) \right] + \eta \delta_{ji}^{(l)}(n) y_i^{(l-1)} \tag{5.11}$$

where, η is the learning rate parameter and α is the momentum constant.

Learning rate parameters can be different for each neuron but in this neural network design study, they are chosen as the same for all the neurons. If the learning rate parameter is chosen too large in order for fast learning, the network may become unstable. On the other hand, choosing small parameters for the learning rate is an improvement as there is smoother trajectory but this may cause very slow learning. In addition to the learning rate parameter term, a simple method for increasing the rate of

76

learning, namely momentum term is added to the delta rule. The momentum parameter is used to prevent the network from converging to a shallow local minimum or saddle. By using the equations above for the back propagation, Simulink blocks for output and hidden layers are constructed. Inside of these layer blocks, there are added options for choosing the initialization of the weights as random or previously created. There is also a parameter to make the learning on or off. Simulink block diagram for the backward calculation of the neural network is shown in Figure 5.4.
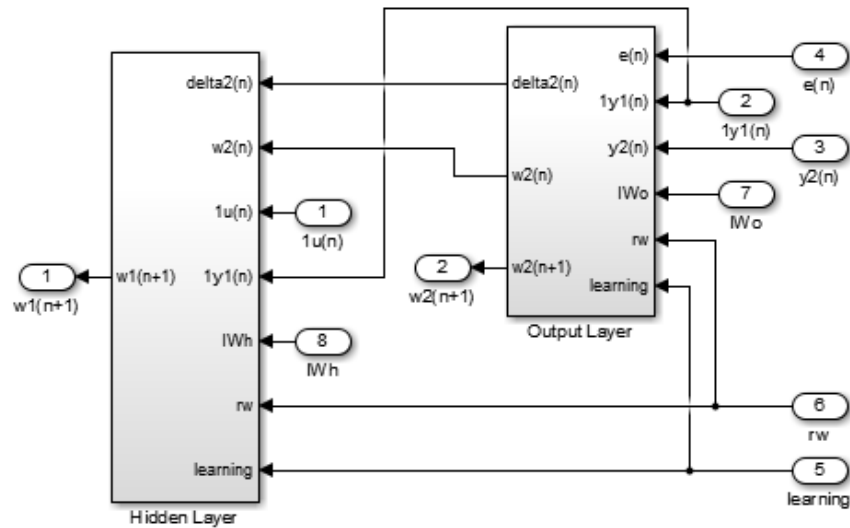
Figure 5.4 Backward Calculation Simulink Block Diagram

After connecting the output and the hidden layers (Figure 5.5), scaling factor is added to the network to make it in the range of the system and instantaneous error energy (Equation 5.12) block is made to observe the behavior of the network.

$$E_j = \frac{1}{2} e_j^2 \qquad (5.12)$$
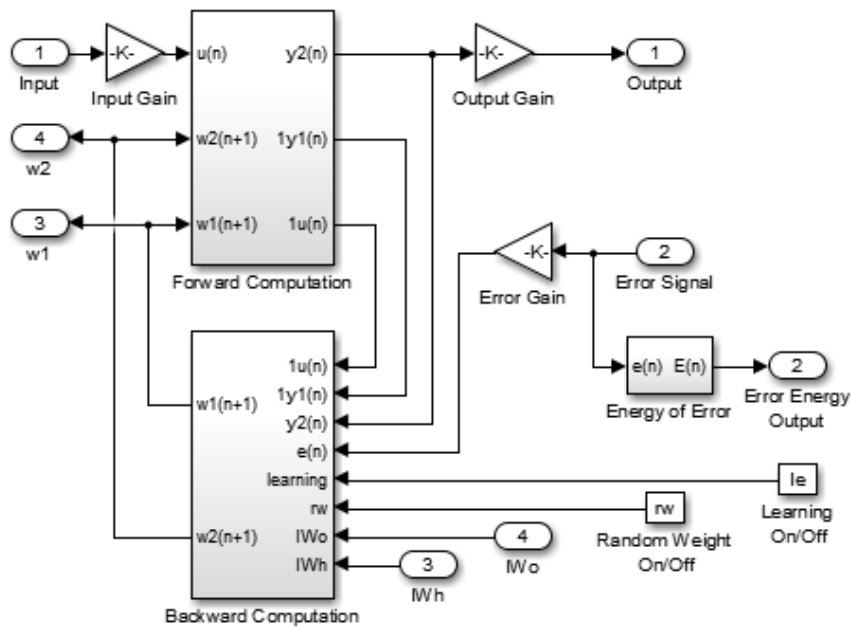
Figure 5.5 Inside of the Neural Network Simulink Block

Figure 5.6 shows the Simulink block which is the final form of the neural network. As a summary, the parameters that can be entered are;

- Number of Inputs
- Number of Hidden Neurons
- Number of Output
- Learning Rate
- Momentum Constant
- Scale Factor

and the options that can be chosen are;

- Learning On/Off
- Initial Random Weights On/Off
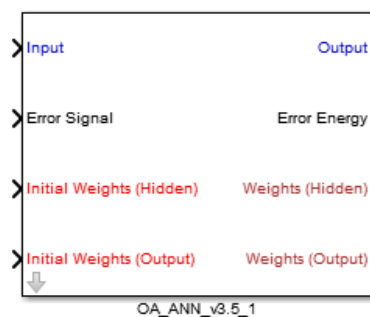
Figure 5.6 Simulink Block of the Neural Network

5.3 Active Vibration Suppression Simulations

There might be a case such as there is a signal source at a specific frequency or combination of frequencies applied to the structure which does not create much problem considering the amplitude of the vibration of the structure. In case of variation of the frequency response function of the structure like change in boundary condition, connections on the structure, mass, crack etc. one of the resonance frequencies of the structure may match with frequency content of the disturbance signal.

As it can be seen in Figure 4.23, using the designed controller to the plant in Case 5 makes the closed loop system unstable. In order to observe this behavior, changing the configuration from Case 4 to 5 is chosen.

It is considered that disturbance signal of the smart beam is the sine wave at a frequency of 15.30 Hz but the smart beam configuration is at the Case 4 (i.e. the resonance frequency of 14.92 Hz and servomotor arm angle of -32°). In this case, the smart beam vibrates at a low vibration level of -9.2 [dB].

In case of a variation in the frequency response function of the smart beam which can be achieved by changing the servomotor arm angle (from Case 4 to Case 5), the smart beam's vibration amplitude starts to increase and reaches to the vibration level of -0.22 [dB]. Figure 5.7 shows the frequency response functions of the smart beam at servomotor arm angles of -32° (Case 4) and -64° (Case 5).
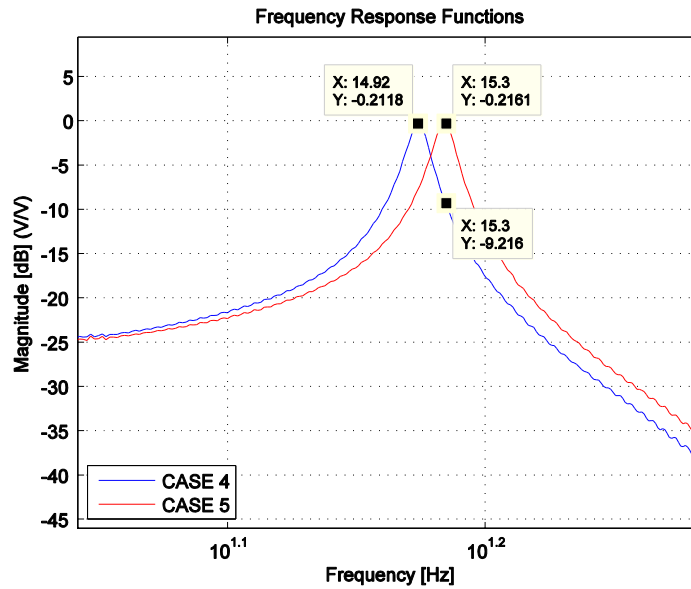
Figure 5.7 Frequency Response Functions at Case 4 (arm angle of -32°) and Case 5 (arm angle of -64°) Configurations

In order to simulate plant variation while the system is operating, a Simulink block namely "variable plant" is designed. It changes the matrices of the state-space form of the smart beam at an arm angle case to another arm angle case's matrices. The sampling frequency is chosen as 200 Hz and the input signal of the plant is kept constant as 15.30 Hz which is the first resonance frequency of the plant in Case 5. Then, the servomotor arm angle is changed from -32° (i.e. Case 4) to -64° (i.e. Case 5) at a time of 2 seconds. The following Figure 5.8 shows the Simulink block diagram and Figure 5.9 presents the result of the variation in the frequency response function of the plant.
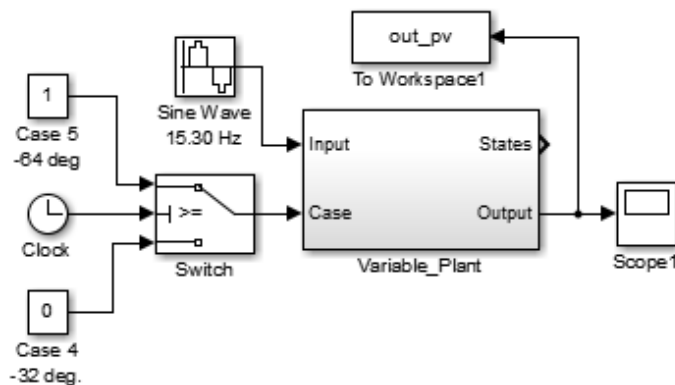
Figure 5.8 Plant Variation Simulink Block Diagram
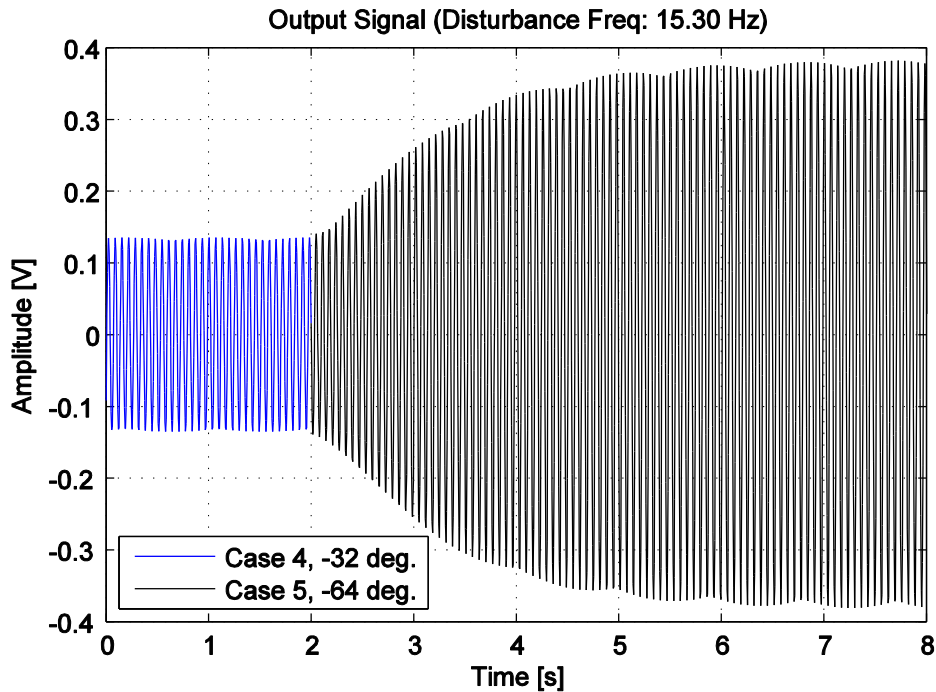
Figure 5.9 Output Signal (Plant Variation)

A neural network controller is desired to be used for suppression of the smart beam via handling the variations in the FRF of the smart beam. In [49], and [50], details of controlling of a flexible system method are described. This method is implemented to the vibration suppression study hence tracking purpose is not used so that the reference is chosen as a zero consideration on the offset of the sensor. The previously designed controller (in Chapter 4) and a reference model (i.e. Case 3) are used in the adaptive controller design. The neural network works as an element to handle the difference between the reference model output and the real system output. This difference depends on the states of the reference model, the states of the real system and the input of the real system. However, states of the real system are not measurable. Only the output of the real system is measured from the piezoelectric sensor patch. As the system is observable, the states of the real system can be obtained by using previously obtained data of the input and the output of the real system. Thus, the inputs of the neural network are taken as the previous values of the output, the input of the real system and the states of the reference model. In order to simulate an active vibration suppression, firstly random weights are chosen to train the neural network and the parameters which are used for the first training simulation are shown in Table 5.1.

Simulations are restarted for several times with random weights until the desired error energy is obtained. The weights obtained after a successful simulation are saved to be used for the further cases (i.e. variations in plant scenarios) as initial weights.

Table 5.1 Parameters of the Neural Network for the First Training Simulation

Number of Inputs	11
Number of Output	2
Learning Rate	0.02
Momentum Constant	0.7
Scale Factor	100
Learning On/Off	On
Initial Random Weights On/Off	On

In section 4.4.3, it was presented that the system with -64° arm angle (i.e. Case 5) is unstable if the controller designed for the Case 3 is used. Firstly, a simulation is performed to observe the instability of the system when the arm changes from Case 4 to Case 5. Then, a neural network based adaptive element is added to the block diagram and another simulation is performed. It is shown that the system with the controller designed by using LQR method and the neural network together can suppress the vibrations without being affected by the plant variation. Figure 5.10 shows the Simulink block diagram used during the simulations. The arm angle is then changed intentionally at particular time (at 2 second) and the results of the simulations are shown in Figure 5.11. After the variation, the system only with the designed controller becomes unstable as expected. With the neural network, the system keeps the vibrations of the plant suppressed by making the system stable. The suppression performance at the first resonance frequency of the plant with Case 5 is obtained approximately as 88 % which is very close to the result obtained from the simulations performed in Chapter 4 for the Case 3.

Figure 5.10 Simulink Block Diagram for Forced Vibration Suppression Simulations
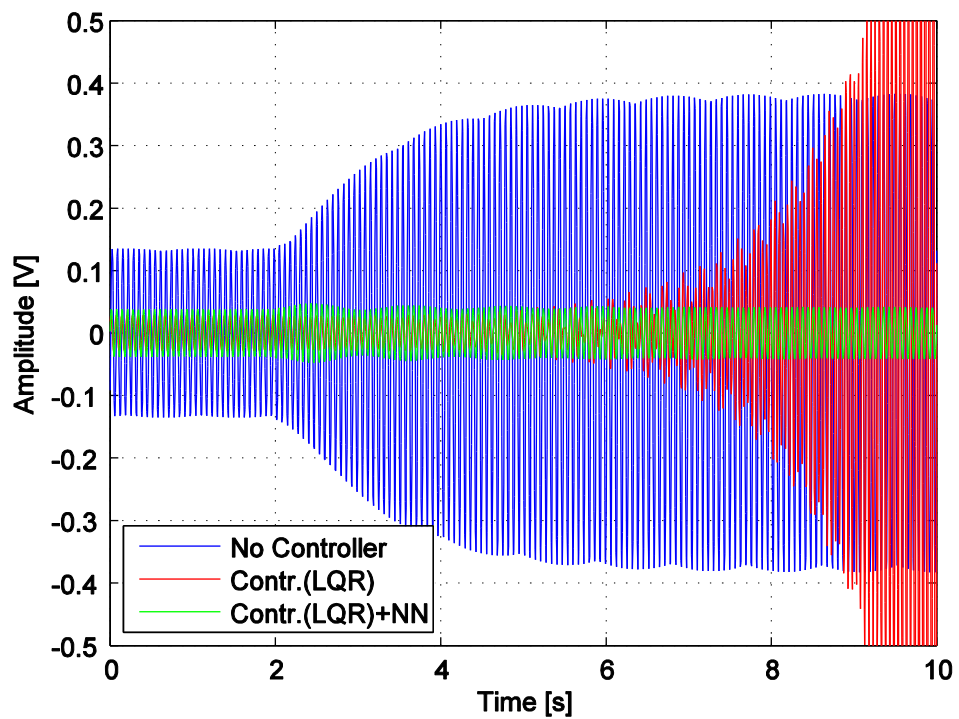
Figure 5.11 Results of Forced Vibration Suppression Simulations

Free vibration suppressions of the plant without controller, with the previously designed controller only and with the neural network added controller for -64° servomotor arm angle (Case 5) are also performed. The Simulink block diagram can be seen in Figure 5.12. The initial states of the plant are obtained by using the same procedure presented in Chapter 4 and used to simulate free vibration of the plant. Figure 5.13 shows the results of the free vibration suppression simulation and as a result, when the initial voltage starts from 0.4, free vibration suppression of the plant lasts for approximately 3.5 seconds without controller. With the controller designed by using LQR method, the settling time is approximately found as 0.5 seconds but as the controller designed for the Case 3 is used for the Case 5, the system starts to vibrate at the frequency of the unstable pole which is at 20.7 Hz. To observe the instability, a noise signal includes 20.7 Hz with relatively very low amplitude is added to the input of the system. Moreover, the neural network based adaptive element is added to the block diagram and the free vibration suppression simulation is also conducted. As a result, the closed loop system is obtained as a stable system and the settling time is found as approximately 0.3 seconds but the suppression of the signal at unstable pole frequency (i.e. 20.7 Hz) lasts more hence the additional suppression time approximately 0.7 seconds is observed.
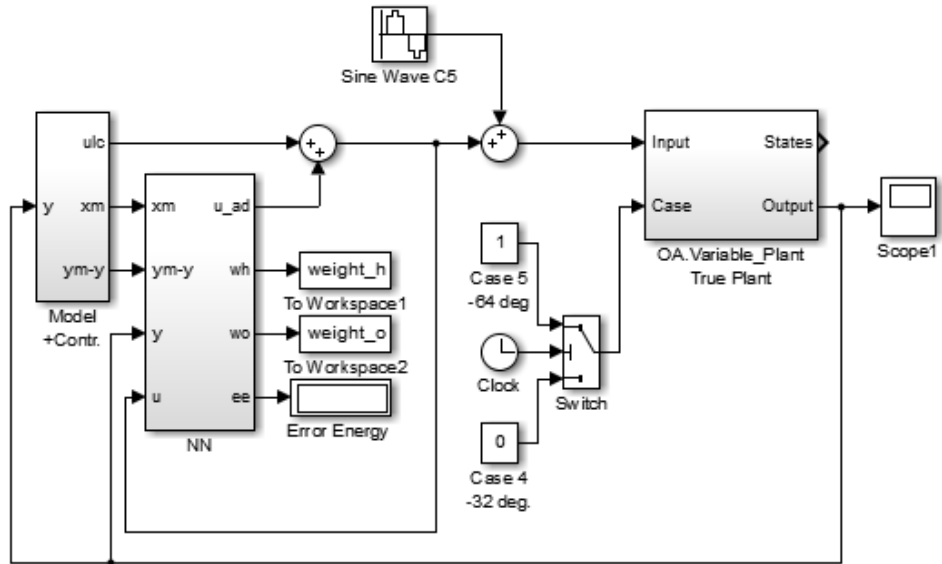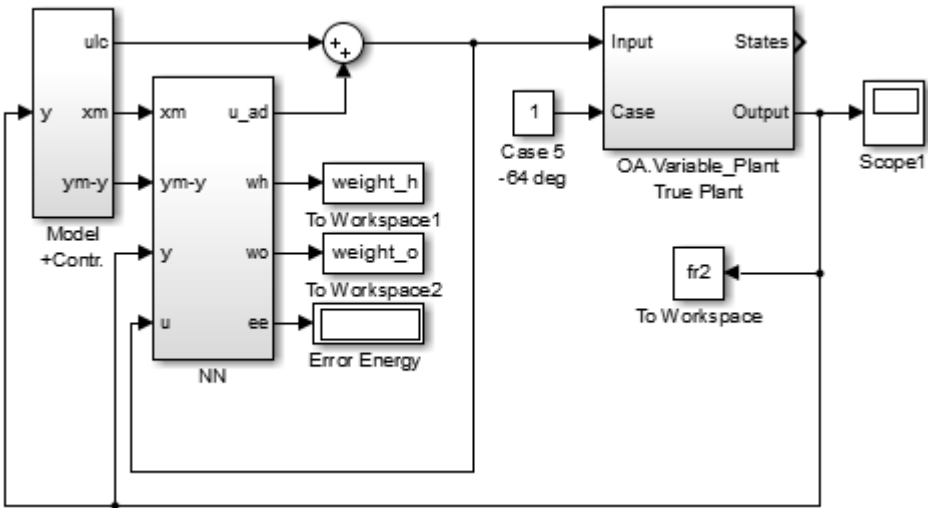

Figure 5.12 Simulink Block Diagram for Free Vibration Suppression Simulations
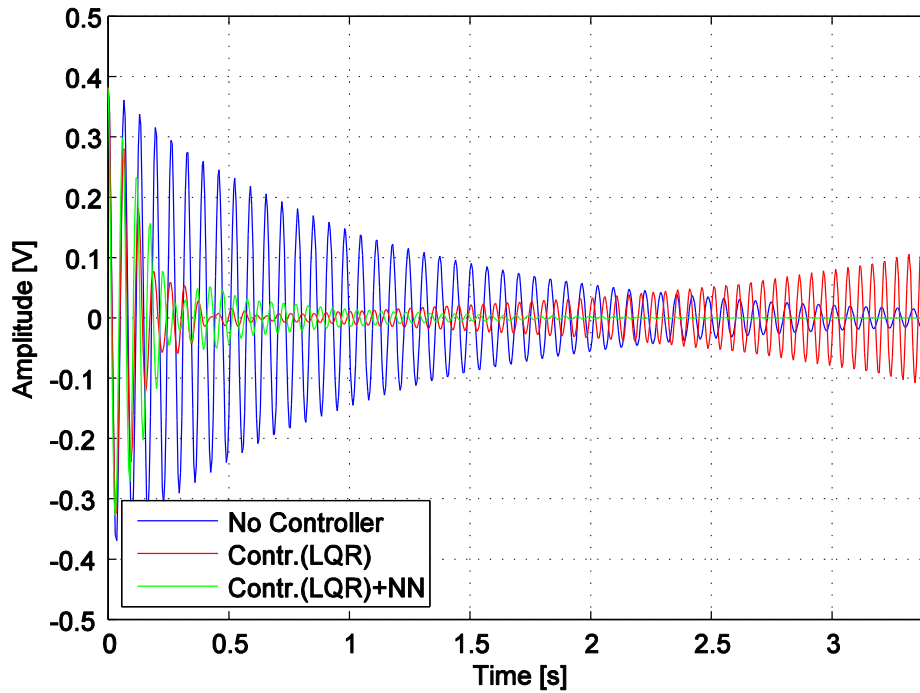
Figure 5.13 Results of Free Vibration Suppression Simulations

5.4 Active Vibration Suppression Experiments

In this section, experimental studies are conducted to analyze the free and forced vibration suppression behaviors of the controller designed in Chapter 4 and the controller with the neural network in case of arm angle variation from -32° (i.e. Case 4) to -64° (i.e. Case 5). Firstly, an experiment is conducted to observe the increase in vibration level of the beam after changing the servomotor arm from -32 to -64°. The disturbance signal's frequency is 15.30 Hz which is the resonance frequency of the plant in the arm configuration of Case 5. The designed Simulink block diagram is shown in Figure 5.14. By only using the input channel 1 where the disturbance signal is applied and by detaching the input channel 2 which is used for control purpose, the block diagram is built. The servomotor arm angle is changed at a particular time (i.e. at 2 second) and the response of the smart beam to the FRF variation without controller is plotted (Figure 5.15). Secondly, by adding the controller which is designed by LQR method to the block diagram, the behavior of the smart beam to the variation of the servomotor arm angle from -32° to the -64° is observed.
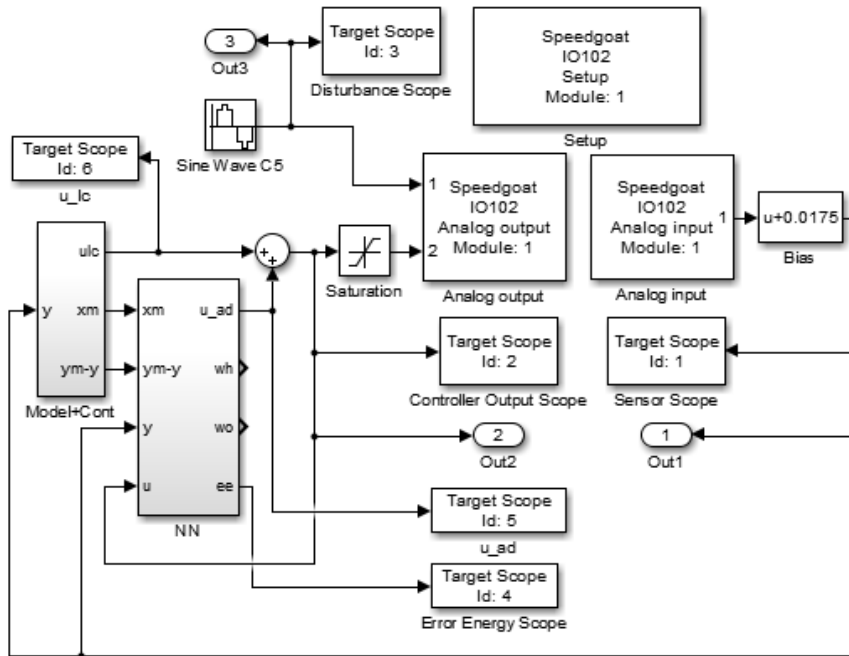
Figure 5.14 Simulink Block Diagram for the Forced Vibration Suppression
Experiments
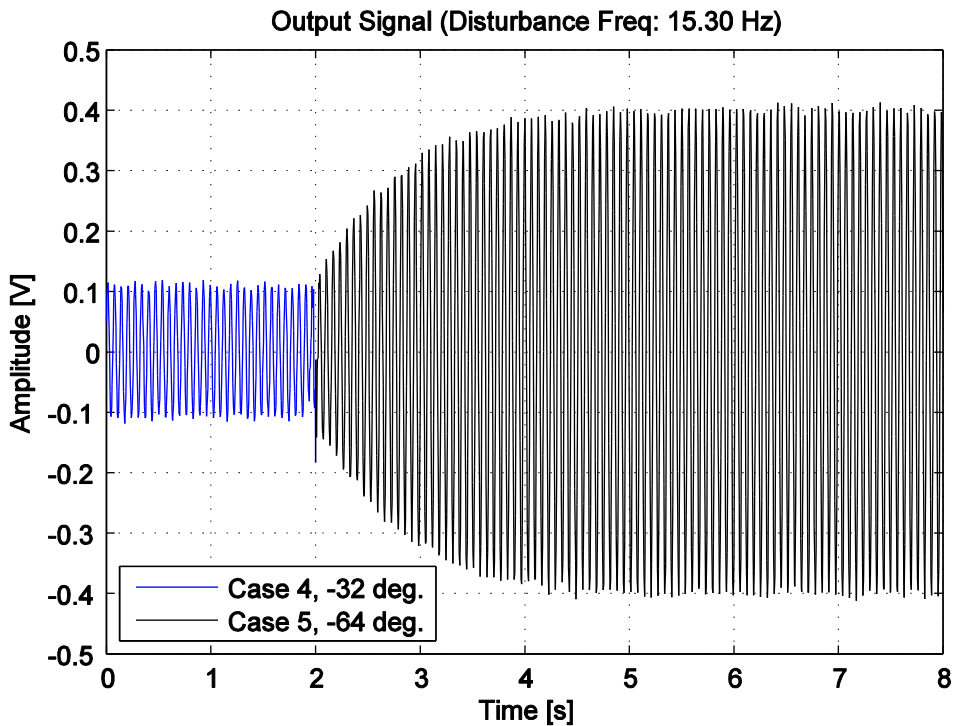
Figure 5.15 Experimental Result of a Plant Variation

86

Then, the neural network is added to the block diagram and an experiment is conducted again. The response of the smart beam is observed as stable and the vibration suppression performance of the system is found as 89 % which is very close to the result obtained in the simulation studies. All these results are presented in Figure 5.16.

Finally, by detaching the disturbance signal in the Simulink block diagram and applying the same procedures followed in the simulation studies, free vibration responses of the smart beam without controller, with the controller designed by using LQR method and with the neural network based adaptive element added system are experimentally obtained and the results are shown in Figure 5.17.
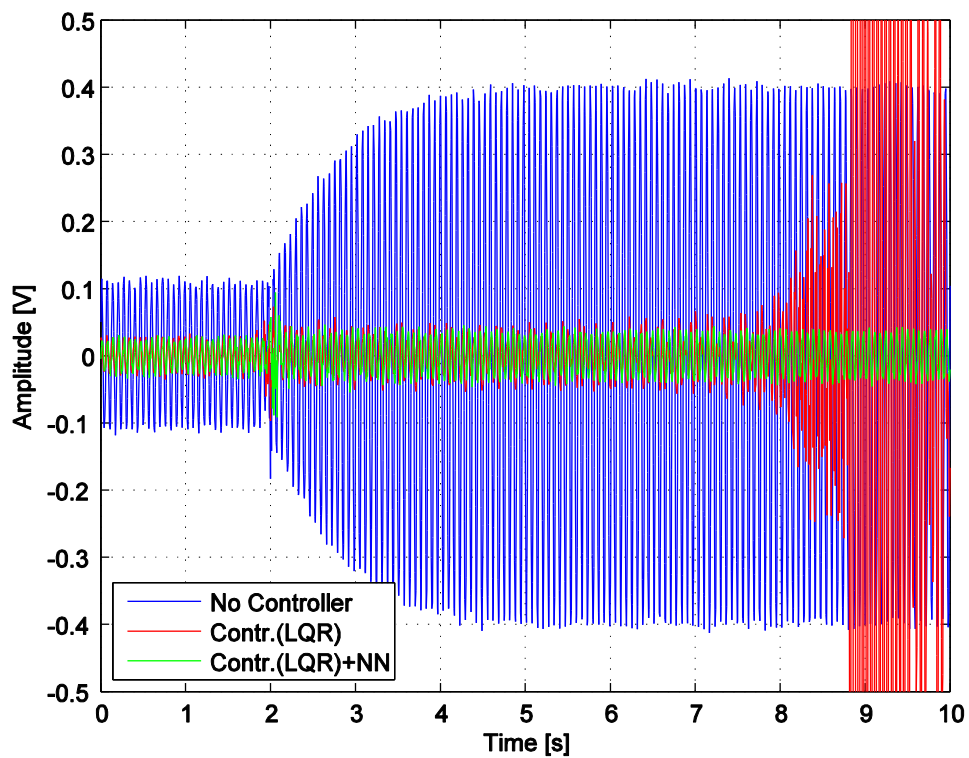
Figure 5.16 Results of the Forced Vibration Suppression Experiments
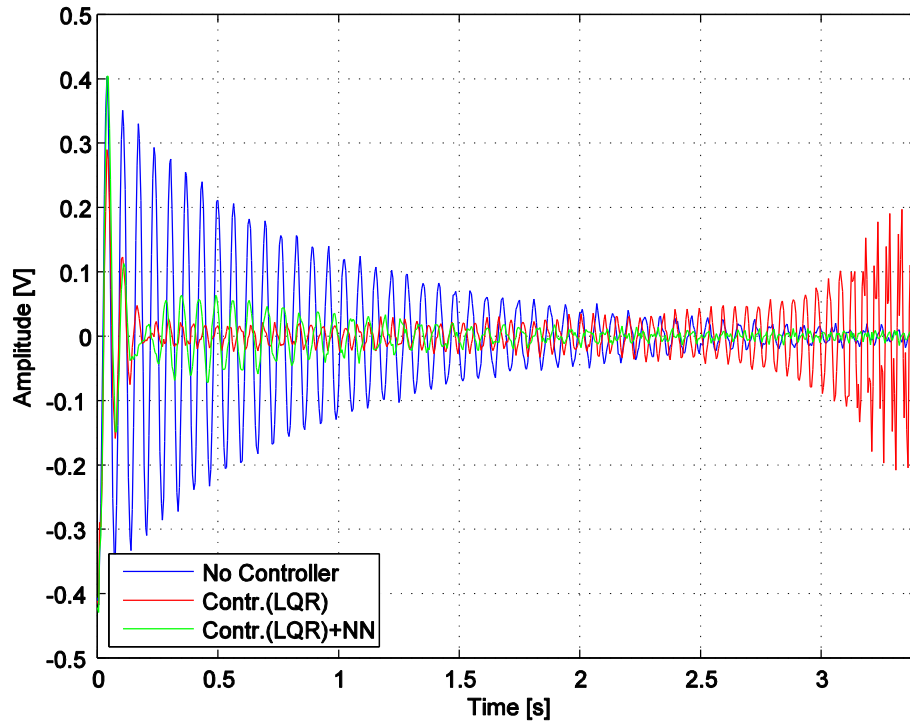
Figure 5.17 Results of the Free Vibration Suppression Experiments

5.5 Conclusion

In this chapter, a multilayer feedforward neural network with back propagation algorithm is designed and created as a Simulink block. Then, a neural network based adaptive element is obtained and trained. By using the previously designed controller with the neural network based adaptive element, simulations are conducted for both free and forced vibration suppressions. For the forced vibration case, the frequency of the disturbance is kept the same and the frequency response function of the plant is changed to match the fundamental resonance frequency with the disturbance frequency. For the free vibration case, the system's behavior for an initial condition is observed after a variation in the FRF of the plant occurs. Following that, the experiments are conducted in order to compare the results with the results obtained in the simulation studies. As a conclusion, it is shown that a linear controller with the neural network based adaptive element is capable of suppressing vibrations of the smart beam by handling the consequences due to variations between the real system and the reference model outputs.

CHAPTER 6

CONCLUSION

6.1 General Conclusions

In this thesis, active vibration suppression of a smart beam with piezoelectric patches which are used for controlling, creating disturbance and sensing purposes is successfully presented through designed controllers comprising a linear quadratic regulator and a neural network based one.

Initially, a smart beam having four piezoelectric patches is designed and built. A servomotor mechanism for changing the FRFs of the smart beam is also adapted and five different arm angle configurations are defined and changing from one configuration to another is achieved via a computing platform and an associated button.

The investigations of the FRFs of the smart beam between different piezoelectric patch combinations are presented for all arm angle cases. Those FRFs are also obtained experimentally and by using them, analytical models of the smart beam for all servomotor arm angles are investigated by considering the PZT configuration used for the control purposes. It is found that piezoelectric patches are effective smart materials for both sensing and actuating purposes. Moreover, it is observed that the servomotor mechanism can be used effectively for creating noticeable variations in the frequency response functions of the smart beam around its first resonance frequency.

A full state feedback controller is designed by considering the tip deflection range of the smart beam (i.e. for an initial condition) and the maximum voltage range of the input of the system. The best LQR gain is decided and then the simulations are performed for the suppression of the free and the forced vibrations. It is found that the designed controller decreases the settling time of the system (i.e. considering the free vibration of the smart beam) and decreases the amplitude of the first resonance frequency vibration (i.e. considering the forced vibration of the smart beam) significantly through the simulation studies. Additionally, it is observed that the experimental results are in good agreement with that of obtained from the simulations. In addition to these, the effect of the plant variation to the closed loop behavior of the system is observed by using the designed controller and it is realized that this variation in the smart beam causes performance change and it may possibly affect the stability of the system when excessive variations occur.

Finally, a feedforward back propagation neural network algorithm is designed and used as an adaptive element and it is observed that a linear controller with a neural network based adaptive element is an effective solution for suppressing the vibrations of the smart beam even if there are variations in the frequency response function of the smart beam.

6.2 Recommendations for Further Studies

In this thesis, the frequency range of interest covers only the first out-of-plane bending mode of the smart beam with different arm angle configurations. Since FRF variation also affects the higher modes, as a future work, suppression of the higher modes of the smart beam can also be investigated with the existence of this arm angle variation.

In addition, the maximum initial tip deflection for the free vibration suppression analysis is chosen and the controller is designed by using LQR method. This range may be decreased to the level that the controller can suppress the free vibration without oscillation. The behavior of this system can be investigated (i.e. overshoot, rise time…)

In the neural network study, it is assumed that the controller output voltage is in the range of the system. The output voltage of the controller can easily pass the limits when excessive disturbance is applied to the system. It may affect online learning of the neural network in a negative way. Hence as a future work, this problem can be investigated.

REFERENCES

[1] W. Belgacem, A. Berry, and P. Masson, "Active vibration control on a quarter-car for cancellation of road noise disturbance," *J. Sound Vib.*, vol. 331, no. 14, pp. 3240–3254, 2012.

[2] H. Yamada, M. Sasaki, and Y. Nam, "Active Vibration Control of a Micro-Actuator for Hard Disk Drives using Self-Sensing Actuator," *J. Intell. Mater. Syst. Struct.*, vol. 19, no. 1, pp. 113–123, 2007.

[3] U. Schonhoff, A. Klein, and R. Nordmann, "Attitude control of the airborne telescope SOFIA: mu-synthesis for a large scaled flexible structure," in *Proceedings of the 39th IEEE Conference on Decision and Control (Cat. No.00CH37187)*, 2000, vol. 4, pp. 3576–3581.

[4] E. Foo and R. M. Goodall, "Active suspension control of flexible-bodied railway vehicles using electro-hydraulic and electro-magnetic actuators," *Control Eng. Pract.*, vol. 8, no. 5, pp. 507–518, 2000.

[5] S. Daley, F. a. Johnson, J. B. Pearson, and R. Dixon, "Active vibration control for marine applications," *Control Eng. Pract.*, vol. 12, no. 4, pp. 465–474, 2004.

[6] D. J. Mead, *Passive Vibration Control*, 1st ed. Chichester, New York: Wiley, 1998.

[7] M. Ciminello, a. Calabro, S. Ameduri, and a. Concilio, "Synchronized Switched Shunt Control Technique Applied on a Cantilevered Beam: Numerical and Experimental Investigations," *J. Intell. Mater. Syst. Struct.*, vol. 19, no. 9, pp. 1089–1100, 2008.

[8] M. V. Gandhi and B. S. Thompson, *Smart Materials and Structures*. Springer Netherlands, 1992.

[9] "History of Piezoelectricity." [Online]. Available: http://www.piezo.com/tech4history.html. [Accessed: 09-Jul-2015].

[10] S. W. Or, "Overview of Smart Materials Technology." [Online]. Available: http://resources.edb.gov.hk/physics/articleIE/smartmaterials/SmartMaterials_e .htm. [Accessed: 09-Jul-2015].

[11] A. Y. Koma, "Active Vibration Control of Smart Structures Using Piezoelements," Carleton University, Ottawa, Ontario, 1997.

[12]   C.-K. Soh, Y. Yang, and S. Bhalla, *Smart Materials in Structural Health Monitoring, Control and Biomechanics*, 1st ed. Springer-Verlag Berlin Heidelberg, 2012.

[13]   W. Heywang, K. Lubitz, and W. Wersing, *Piezoelectricity: Evolution and Future of a Technology*. Springer, 2008.

[14]   F. K. Straub, V. R. Anand, T. S. Birchette, and B. H. Lau, "Smart Rotor Development and Wind Tunnel Test," in *35th European Rotorcraft Forum*, 2009.

[15]   T. Bailey and J. E. Hubbard, "Distributed piezoelectric-polymer active vibration control of a cantilever beam," *J. Guid. Control. Dyn.*, vol. 8, no. 5, pp. 605–611, 1985.

[16]   E. F. Crawley and J. De Luis, "Use of piezoelectric actuators as elements of intelligent structures," *AIAA J.*, vol. 25, no. 10, 1987.

[17]   J. L. Fanson and T. K. Caughey, "Positive position feedback control for large space structures," *AIAA J.*, vol. 28, no. 4, pp. 717–724, 1990.

[18]   G. Song, S. P. Schmidt, and B. N. Agrawal, "Active vibration suppression of a flexible structure using smart material and a modular control patch," *Proc. Inst. Mech. Eng. Part G-Journal Aerosp. Eng.*, vol. 214, no. G4, pp. 217–229, 2000.

[19]   W. J. Manning, A. R. Plummer, and M. C. Levesley, "Vibration control of a flexible beam with integrated actuators and sensors," *Smart Mater. Struct.*, vol. 9, pp. 932–939, 2000.

[20]   T. Çalışkan, "Piezoelectric ceramics and their applications in smart aerospace structures," Middle East Technical University, 2002.

[21]   S. P. Singh, H. S. Pruthi, and V. P. Agarwal, "Efficient modal control strategies for active control of vibrations," *J. Sound Vib.*, vol. 262, no. 3, pp. 563–575, 2003.

[22]   M. Sahin, F. M. Karadal, Y. Yaman, O. F. Kircali, V. Nalbantoglu, F. D. Ulker, and T. Caliskan, "Smart structures and their applications on active vibration control: Studies in the Department of Aerospace Engineering, METU," *J. Electroceramics*, vol. 20, no. 3–4, pp. 167–174, 2008.

[23]   M. Itik, M. Salamci, D. Ulker, and Y. Yaman, "Active Vibration Suppression of a Flexible Beam via Sliding Mode and Hinf control," in *Proceeding of the 44th IEEE Conference on Decision and Control, and the European Control Conference*, pp. 1240–1245.

[24] C. M. a. Vasques and J. Dias Rodrigues, "Active vibration control of smart piezoelectric beams: Comparison of classical and optimal feedback control strategies," *Comput. Struct.*, vol. 84, no. 22–23, pp. 1402–1414, 2006.

[25] I. Z. M. Darus and M. O. Tokhi, "Genetic algorithm active vibration control of flexible plate structures," in *Proceedings of the 51st Annual Meeting of the ISSS*, 2007.

[26] Q. Wenzhong, S. Jincai, and Q. Yang, "Active control of vibration using a fuzzy control method," *J. Sound Vib.*, vol. 275, no. 3–5, pp. 917–930, Aug. 2004.

[27] H. Kawabe, N. Tsukiyama, and K. Yoshida, "Active vibration damping based on neural network theory," *Mater. Sci. Eng. A*, vol. 442, no. 1–2 SPEC. ISS., pp. 547–550, 2006.

[28] Y. Yaman, F. D. Ulker, V. Nalbantoglu, T. Çalışkan, S. E. Prasad, D. Waechter, and B. Yan, "Application of H∞ Active Vibration Control Strategy in Smart Structures," in 3rd International Conference on Advanced Enginnering Design, 2003.

[29] Y. Yaman, T. Çalışkan, V. Nalbantoglu, S. E. Prasad, D. Waechter, and B. Yan, "Active Vibration Control of a Smart Beam," *Canada-US CanSmart Workshop on Smart Materials and Structures*. Montreal, Canada, 2001.

[30] F. M. Karadal, "Active Flutter Suppression of a Smart Fin. Master's thesis," Middle East Technical University, 2008.

[31] Y. Yaman, T. Çalışkan, V. Nalbantoglu, F. D. Ulker, S. E. Prasad, D. Waechter, and B. Yan, "Active Vibration Control of Smart Plates by Using Piezoelectric Actuators," *6th Biennial Conference on Engineering Systems Design and Analysis*. Istanbul, Turkey, 2002.

[32] F. D. Ulker, "Active Vibration Control of Smart Structures. Master's thesis," Middle East Technical University, 2003.

[33] O. F. Kircali, Y. Yaman, V. Nalbantoglu, M. Sahin, F. M. Karadal, and F. D. Ulker, "Spatial control of a smart beam," *J. Electroceramics*, vol. 20, no. 3–4, pp. 175–185, 2008.

[34] Ö. F. Kircali, Y. Yaman, V. Nalbantoglu, and M. Sahin, "Active Vibration Control of a Smart Beam by Using a Spatial Approach," in *New Developments in Robotics, Automation and Control*, A. Lazinica, Ed. I-Tech Education and Publishing, 2008, pp. 377–410.

[35] Ö. F. Kircali, "Active Vibration Control of a Smart Beam: A Spatial Approach. Master's thesis," Middle East Technical University, 2006.

[36] C. Onat, M. Sahin, and Y. Yaman, "Active Vibration Suppression of a Smart Beam via PIλDμ Control," *International Workshop on Piezoelectric Materials and Applications in Actuators*. Antalya, Turkey, 2010.

[37] C. Onat, M. Sahin, and Y. Yaman, "Active Vibration Suppression of a Smart Beam by Using an LQG Control Algorithm," *2nd International Conference of Engineering Against Fracture (ICEAF II)*. Mykonos, Greece, 2011.

[38] C. Onat, M. Sahin, and Y. Yaman, "Active Vibration Suppression of a Smart Beam by Using a Fractional Control," *2nd International Conference of Engineering Against Fracture (ICEAF II)*. Mykonos, Greece, 2011.

[39] C. Onat, M. Sahin, and Y. Yaman, "An Experimental Performance Evaluation for the Suppression of Vibrations of the Second Mode of a Smart Beam," *6. Ankara International Aerospace Conference*. Ankara, Turkey, 2011.

[40] C. Onat, M. Sahin, and Y. Yaman, "Optimal Control of a Smart Beam by Using a Luenberger Observer," in *3rd International Conference of Engineering Against Failure*, 2013.

[41] C. Onat, M. Sahin, and Y. Yaman, "Design of an LPV Based Fractional Controller for the Vibration Suppression of a Smart Beam," *CanSmart2011, International Workshop on Smart Materials & Structures and NDT in Aerospace*. Montreal, Canada, 2011.

[42] "Savöx SH-0253 Micro Digital Servo." [Online]. Available: http://www.savoxusa.com/Savox_SH0253_Micro_Digital_Servo_p/savsh0253.htm. [Accessed: 07-Apr-2015].

[43] "Educational Real-Time Target Machine." [Online]. Available: http://www.mathworks.com/hardware-support/xpc-target-turnkey.html. [Accessed: 10-May-2015].

[44] "Sensor Technology SA10." [Online]. Available: http://www.sensortech.ca/site/index.cfm?DSP=Page&ID=79. [Accessed: 10-May-2015].

[45] Mustafa Uğur Aridoğan, "Performance Evaluation of Piezoelectric Sensor/Actuator on Investigation of Vibration Characteristics and Active Vibration Control of a Smart Beam. Master's thesis," Middle East Technical University, 2010.

[46] S. Haykin, *Neural Networks and Learning Machines*, 3rd ed. Hamilton, Ontario, Canada: Pearson Education, 2008.

[47] J. A. Franklin, T. M. Mitchell, and S. Thrun, *Recent Advances in Robot Learning: Machine Learning*. Springer US, 2012.

[48] N. R. Fisco and H. Adeli, "Smart structures: Part II - Hybrid control systems and control strategies," *Sci. Iran.*, vol. 18, no. 3 A, pp. 285–295, 2011.

[49] A. J. Calise, B.-J. Yang, and J. I. Craig, "Augmenting Adaptive Approach to Control of Flexible Systems," *J. Guid. Control. Dyn.*, vol. 27, no. 3, pp. 387–396, 2004.

[50] A. J. Calise, N. Hovakimyan, and M. Idan, "Adaptive output feedback control of nonlinear systems using neural networks," *Automatica*, vol. 37, no. 8, pp. 1201–1211, 2001.

APPENDIX A

THEORETICAL ANALYSIS

The smart beam can be modelled as a cantilever uniform beam where a mass M is located at position "a" from the left side of the beam. The details of the model can be seen in Figure A.1.
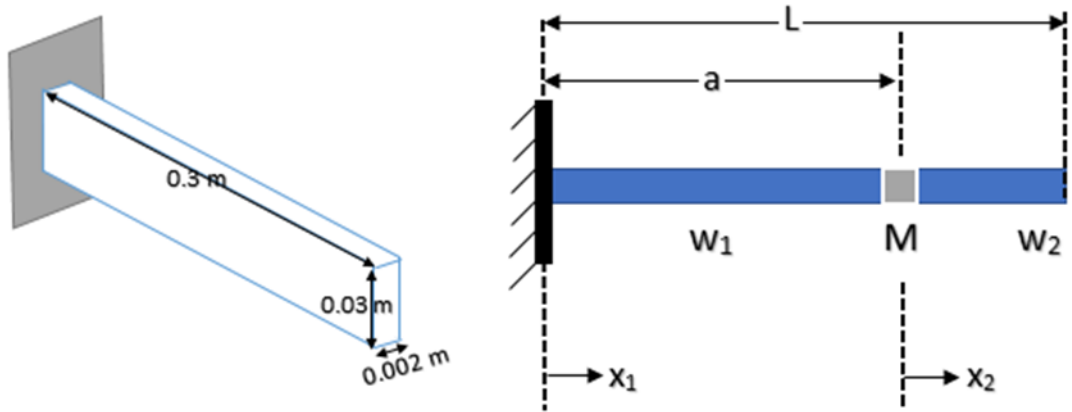

Figure A.1 The details of the model

The equation of motion of a beam (Euler-Bernoulli, $f(x, t) = 0$)* can be written as,

$$\frac{\partial^2}{\partial x^2}\left(EI(x)\frac{\partial^2 w(x,t)}{\partial x^2}\right) + m(x)\frac{\partial^2 w(x,t)}{\partial t^2} = 0$$

For a uniform beam, $I(x) = I \quad and \quad m(x) = m$

$$EI\frac{\partial^4 w(x,t)}{\partial x^4} + m\frac{\partial^2 w(x,t)}{\partial t^2} = 0$$

By using separation of variable method, the solution is assumed to be,

$$w(x,t) = W(x)F(t)$$

* S. S. Rao, *Vibration of Continuous Systems*. J Wiley, Hoboken, NJ, 2007.

Substituting the solution to the equation of motion,

$$EI\frac{\partial^4 W(x)}{\partial x^4}F(t) + m\frac{\partial^2 F(t)}{\partial t^2}W(x) = 0$$

$$\frac{EI}{m}\frac{1}{W(x)}\frac{\partial^4 W(x)}{\partial x^4} = -\frac{\partial^2 F(t)}{\partial t^2}\frac{1}{F(t)} = -\omega^2$$

So, the equation of motion of a cantilever beam is found as,

$$EI\frac{\partial^4 W(x)}{\partial x^4} + \omega^2 W(x)m = 0$$

$$\beta^4 = \frac{\omega^2 m}{EI}$$

Thus, the general solution of a beam is,

$$W(x) = C_1 \sin \beta x + C_2 \cos \beta x + C_3 \sinh \beta x + C_4 \cosh \beta x$$

The general solutions of the system are written separately for each part.

$$W_1(x) = C_1 \sin \beta x + C_2 \cos \beta x + C_3 \sinh \beta x + C_4 \cosh \beta x$$

$$W_2(x) = C_5 \sin \beta x + C_6 \cos \beta x + C_7 \sinh \beta x + C_8 \cosh \beta x$$

And the natural frequency is,

$$\omega = \beta^2 \sqrt{\frac{EI}{m}} = (\beta L)^2 \sqrt{\frac{EI}{mL^4}}$$

For the left boundary, the beam is fixed. That means the displacement and slope are equal to zero.

$$W_1(x_1)|_{x_1=0} = 0$$

$$\frac{dW_1(x_1)}{dx_1}\bigg|_{x_1=0} = 0$$

100

For the right boundary, the beam is free. That means the moment and shear force are equal to zero. Thus,

$$\frac{d^2 W_2(x_2)}{dx_2^2}\bigg|_{x_2=L-a} = 0$$

$$\frac{d^3 W_2(x_2)}{dx_2^3}\bigg|_{x_2=L-a} = 0$$

For the mass on the cantilever beam, there are 4 compatibility equations.

1. The left displacement is equal to the right displacement.

$$W_1(x_1)|_{x_1=a} = W_2(x_2)|_{x_2=0}$$

2. The left slope is equal to the right slope.

$$\frac{d}{dx} W_1(x_1)\bigg|_{x_1=a} = \frac{d}{dx} W_2(x_2)\bigg|_{x_2=0}$$

Shear forces and moments which are shown in Figure A.2 are used to find the other compatibility equations.
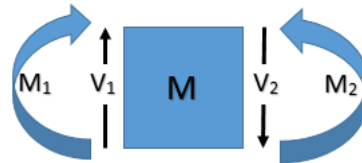

Figure A.2 Shear and Moments

3. The moment equation, (Counterclockwise is positive, I is assumed to be zero)

$$\sum M = I \times \alpha$$

$$-EI \frac{d^2 W_1(x_1)}{dx_1^2}\bigg|_{x_1=a} + EI \frac{d^2 W_2(x_2)}{dx_2^2}\bigg|_{x_2=0} = 0$$

4. The force equation, (Up is positive)

$$\sum F = m \times a$$

$$EI\frac{d^3W_1(x_1)}{dx_1^3}\Bigg|_{x_1=a} - EI\frac{d^3W_2(x_2)}{dx_2^3}\Bigg|_{x_2=0} = -\omega^2 MW_2(x_2)|_{x_2=0}$$

By using the boundary and the compatibility equations, the coefficients of the constants are collected and the coefficient matrix is created symbolically by using Mathcad software. After that, the values $\left(E = 69\ [GPa], I = 2 \times 10^{-11}\ [m^4], m = 0.162\ \left[\frac{kg}{m}\right], a = 0.026\ [m], L = 0.3\ [m], M = 0.027\ kg\right)$ and the relation $\omega^2 = \beta^4\frac{EI}{m}$ are substituted into the matrix. As a result, a matrix which contains only the β and L parameters is obtained. βL is written as "x" to make the computations easily. The coefficient matrix is shown as,

$$\begin{bmatrix} \square & \cdots & \square \\ \vdots & \ddots & \vdots \\ \square & \cdots & \square \end{bmatrix}\begin{pmatrix} C_1 \\ \vdots \\ C_8 \end{pmatrix} = 0$$

$$\begin{pmatrix}
0 & 1 & 0 & 1 & 0 & 0 & 0 & 0 \\
1 & 0 & 1 & 0 & 0 & 0 & 0 & 0 \\
\sin(0.867 \cdot x) & \cos(0.867 \cdot x) & \sinh(0.867 \cdot x) & \cosh(0.867 \cdot x) & 0 & -1 & 0 & -1 \\
\cos(0.867 \cdot x) & -1 \cdot \sin(0.867 \cdot x) & \cosh(0.867 \cdot x) & \sinh(0.867 \cdot x) & -1 & 0 & -1 & 0 \\
-1 \cdot \sin(0.867 \cdot x) & -1 \cdot \cos(0.867 \cdot x) & \sinh(0.867 \cdot x) & \cosh(0.867 \cdot x) & 0 & 1 & 0 & -1 \\
-1 \cdot \cos(0.867 \cdot x) & \sin(0.867 \cdot x) & \cosh(0.867 \cdot x) & \sinh(0.867 \cdot x) & 1 & 0.556 \cdot x & -1 & 0.556 \cdot x \\
0 & 0 & 0 & 0 & -1 \cdot \sin(0.133 \cdot x) & -1 \cdot \cos(0.133 \cdot x) & \sinh(0.133 \cdot x) & \cosh(0.133 \cdot x) \\
0 & 0 & 0 & 0 & -1 \cdot \cos(0.133 \cdot x) & \sin(0.133 \cdot x) & \cosh(0.133 \cdot x) & \sinh(0.133 \cdot x)
\end{pmatrix}$$

In order to calculate the natural frequencies, determinant of the coefficient matrix is obtained and equated to zero. Thus, first three βL values are obtained by solving the equation and then, the natural frequencies are calculated.

$$\omega_1 = 11.5\ Hz\ (\%\ 15), \qquad \omega_2 = 107.4\ Hz\ (\%\ 19)$$

The values in the parenthesis show the percentage difference with respect to the experimentally obtained results.